APPENDICES

APPENDIX A

LIST OF THE CHEMICALS AND INSTRUMENTS

1. Chemicals

All chemicals used as in this study were analytical grade reagents

Chemicals	Source
100X Hypoxanthine Thymidine (HT)	Gibco, Grand Island, NY, USA
10X BM condimed HI	Roche, Mannheim, Germany
50X Hyposanthine Aminopterin Thymidin (HAT)	Gibco, Grand Island, NY, USA
5-bromo-4-chloro-3-indoly-β-Dgalactoside (X-gal)	Invitrogen, San Diego, CA
Acrylamide	Biorad, Hercules, CA, USA
Agarose (electrophoresis grade)	Sigma-Aldrich. St.Louis, MO, USA
Amersham Hybond™-ECL	GE healthcare Bio-Sciences Co. Piscataway, NJ
Ammonium peroxodisulphate	GE healthcare Bio-Sciences Co. Piscataway, NJ
Ampiillin	Sigma-Aldrich. St.Louis, MO, USA
Bac-N-Blue™ transfection kit	Invitrogen, San Diego, CA

Chemicals	Source
BCA Protein Assay	Thermo Fisher Scientific Inc., Rockford, IL, USA
BCML (N,N-bis(carboxymethyl) lysine hydrate)	Sigma-Aldrich. St.Louis, MO, USA
Bis-acrylamide	Biorad, Hercules, CA, USA
BM condimed	Gibco, Grand Island, NY, USA
Bovine Serum Albumin (BSA)	Sigma-Aldrich. St.Louis, MO, USA
Bradford protein assay	Thermo Fisher Scientific Inc., Rockford, IL, USA
Bromphenol blue	Sigma-Aldrich. St.Louis, MO, USA
EDTA	Sigma-Aldrich. St.Louis, MO, USA
Ethanol	Merck, Darmstadt, Germany
Ethidium bromide	Sigma-Aldrich. St.Louis, MO, USA
Fetal bovine serum (FBS)	Gibco, Grand Island, NY, USA
FractionPREP^{TM} Cell Fractionation System	Biovision, Mountain View, CA, USA
GeneJet™ PCR purification kit	Fermentas, Burlington, ON, Canada
Glacial acetic acid	BDH Laboratory Supplies, UK
Glycerol	Sigma-Aldrich. St.Louis, MO, USA
Glycine, Ultrapure	USB Corporation, Cleveland, OH, USA

Chemicals	Source
Grace's insect medium	Gibco, Grand Island, NY, USA
HisTrap column	GE healthcare Bio-Sciences Co. Piscataway, NJ
HiTrap protein G HP column	GE healthcare Bio-Sciences Co. Piscataway, NJ
IMDM medium	Gibco, Grand Island, NY, USA
Imidazole	Sigma-Aldrich. St.Louis, MO, USA
IPTG, dioxan-free	Fermentas, Burlington, ON, Canada
Kanamycin	Sigma-Aldrich. St.Louis, MO, USA
LB Broth Agar	Bio Basic inc., Ontario, Canada
L-glutamine	Gibco, Grand Island, NY, USA
Methanol	Merck, Darmstadt, Germany
NaCl	Sigma-Aldrich. St.Louis, MO, USA
NaOH	Sigma-Aldrich. St.Louis, MO, USA
Non-fat dried milk	Difco Laboratories, Detroit, MI, USA
Penicillin/Streptomycin	Gibco, Grand Island, NY, USA
Polyethylene Glycol 18000, Ultrapure	USB corporation, Cleveland, OH, USA
PVDF membrane	PALI, Esat Hills, NY, USA
ProofStart DNA polymerase	QIAGEN, Hilden, Germany
QIAprep spin Miniprep kit	QIAGEN, Hilden, Germany

Chemicals	Source
QIAquick Gel Extraction kit	QIAGEN, Hilden, Germany
QIAquick PCR purification Kit	QIAGEN, Hilden, Germany
RNeasy Mini Kit	QIAGEN, Hilden, Germany
Serum-free medium, PFHM-II	Gibco, Grand Island, NY, USA
Sucrose	Sigma-Aldrich. St.Louis, MO, USA
Sodium chloride	Merck, Darmstadt, Germany
SureBlue^{TM} TMB Microwell Peroxidase Substrate	KPL, Gaithersburg, MD, USA
T_4 ligase enzyme	Fermentas, Burlington, ON, Canada
TEMED	Biorad, Hercules, CA, USA
Tetracyclin	Sigma-Aldrich. St.Louis, MO, USA
TNM-FH medium	Invitrogen, San Diego, CA, USA
Transcriptor High Fidelity cDNA synthesis kit	
Tris [hydroxymethyl] aminomethane, Ultrapure	USB Corporation, Cleveland, OH, USA
Triton X-100	Sigma-Aldrich. St.Louis, MO, USA
Trypan Blue 0.4%	Sigma-Aldrich. St.Louis, MO, USA
Tryptone water	Merck, Darmstadt, Germany
Tween 20	Fluka, Buchs, Switzerland

Chemicals	Source
Urea	Sigma-Aldrich. St.Louis, MO, USA
Whatman 3MM blotting paper	GE healthcare Bio-Sciences Co. Piscataway, NJ
Yeast extract	Bio Basic inc., Ontario, Canada

2. Instruments

Instruments	Source
27ºC incubator	Shel Lab, Cornelius, OR, USA
37 °C CO2 incubator EG 115 IR	Jouan GmbH, Unterhaching, Germany
37 °C incubator	JP Selecta, Barcelona, Spain
ÄKTA prime™ plus	GE healthcare Bio-Sciences Co. Piscataway, NJ, USA
Amicon Ultra centrifugal filter units	Millipore, Cork, Ireland
BECKMAN L-60 ultracentrifuge	Beckman Coulter, Fullerton, CA, USA
BECKMAN SW41 ultracentrifuge	Beckman Coulter, Fullerton, CA, USA
BD FACSCanyo™ II cytometer	San Diego, CA, USA
Electron microscope JEM 1400 Jeol with Orius-Gatan digitalized camera	Gatan France, 78113 Grandchamp
Electrophoretic power supply 3000Xi	BioRad, Hercules, CA, USA
Shaking incubator (JSSI-100C) JS	JS Research Inc., Gongju-city, Koria
Inverted microscope	Olympus, Japan
Laminar Flow biological safety cabinet	NUAIRE, Plymouth, MN, USA
Microcentrifuge	Eppendorf AG, Hamburg, Germany
Microplate	NUNC, Roskilde, Denmark
MiniVE vertical electrophoresis system	Amersham Pharmacia Biotech, Buckinghamshire, UK

Instruments	Source
MRX-150 Refrigerated microcentrifuge	Tomy Tech USA Inc., CA, USA
MyLab orbital shaker OS-20	BioSan Ltd., Riga, Latvia
RT 6000 D refrigerated centrifuge	Sorvall, Kendro Laboratory Products GmbH, Langenselbold, Germany
UV spectrophotometer	Shimadzu Scientific Instruments Inc, Kyoto, Japan
UV transilluminator	Fotodyne incorporated, Hartland, WI, USA
VersaDoc image analyzer	Biorad, Hercules, CA, USA
Quantity One program	Biorad, Hercules, CA, USA
Vortex-Genie K-550-GE	Scientific Industries Inc, Bohemia, NY, USA

APPENDIX B

LIST OF CELL LINES AND MICROORGANSIMS

1. Cell lines

Name	Type of cell lines
Sf9	Pupal ovarian tissue of *Spodoptera frugiperda*

2. Microorganisms

Escherichi coli XL-1 Blue MRF'

Genotype: Δ(*mcrA*)*183* Δ(*mcrCB-hsdSMR-mrr*)*173 endA1 supE44 thi-1 recA1* gyrA96 *rel*A1 *lac [F'* proAB lacI^{q}*Z⊿*M15 *Tn*10 *(Tet^{r})]*

Escherichi coli HB2151

Genotype: *nalr thi-1 ara lac*-proAB [*F´* proAB lacI^{q} lacZΔM15]

Escherichi coli BL21(DE3)

Genotype: F^{-} *omp*T *gal dcm lon hsd*S$_{B}$ (r_{B}^{-} m_{B}^{-}) λ(DE3 [*lacI lac*UV5-T7 *gene 1 ind1 sam7 nin5*])

APPENDIX C

LIST OF ANTIBODIES AND CONJUGATED ANTIBODIES

Antibody names	Source
Anti-CA (Clone G18)	Generated in this study
Anti-HA tag mAb	Sigma-Aldrich. St.Louis, MO,USA
Anti-His_6 tag antibody	Genscript, Piscataway, NJ, USA
Anti-MA (Clone HB-8975)	Purchased from ATCC
Anti-gpIII mAb	Exalpha Biologicals, Watertown, MA, USA
Anti-GP64 mAb	Santa Cruz Biotechnology, Inc., Santa Cruz, CA USA
Colloidal gold-tagged goat anti-mouse immunoglobulins	British Biocell International Ltd, Cardiff, UK
HRP-conjugated anti-gpVIII antibody	Amersham Pharmacia Biotech, Buckinghamshire, UK
HRP-conjugated anti-HA antibody	Roche, IN, USA
HRP-conjugated anti-mouse immunoglobulins	KPL, Gaithersburg, MD, USA

APPENDIX D

LIST OF ENZYMES

Enzymes	Sources
Accuprime™ Pfx DNA polymerase	Invitrogen, San Diego, CAAnti
Hind III	Fermentas, St. Leon-Rot, Germany
Kpn I	Fermentas, St. Leon-Rot, Germany
Nhe I	Fermentas, St. Leon-Rot, Germany
Sfi I	Fermentas, St. Leon-Rot, Germany
T4 DNA ligase	Fermentas, St. Leon-Rot, Germany

APPENDIX E

REAGENT PREPARATIONS

1. Reagents for gel electrophoresis

1.1 10X Tris-acetate/EDTA electrophoresis buffer (TAE)

Tris-base	48.40	gm
Glacial acetic acid	11.42	ml
0.5 M EDTA, pH 8.0	20	ml

Dissolved all ingredients in deionized distilled water and filled up to 1,000 ml.

Sterilized by autoclave and kept at room temperature.

1.2 1 or 2 % Agarose gel

Agarose	1 or 2	gm
1× TAE	100	ml

Melted by microwave oven until the agarose was completely dissolved.

1.3 Ethidium bromide working solution (10 mg/ml)

Ethidium bromide	1.0	gm
Distilled water	100	ml

Dissolved and kept in dark bottle at 4 °C.

1.4 6X gel loading buffer

Bromphenol blue	0.25	%
Glycerol	30	%

Mixed thoroughly and stored at -20 °C.

2. Medium for bacteria culture

50% glucose

D-glucose	5.0	gm

Added distilled water to 10 ml and boiled in boiling water.

Filtered through 0.2 µm Millipore filter and store at 4 ºC

LB broth

Yeast extract	5.0	gm
Tryptone	10.0	gm
NaCl	10.0	gm

Dissolved all ingredients in 1,000 ml distilled water.

Sterilized by autoclave and kept at 4 °C.

2.3 LB agar

LB agar	15	gm

Dissolved all ingredients in 1,000 ml distilled water.

Sterilized by autoclave, poured on Petri dish (plate) and stored at 4 °C.

2.4 2XTY broth

Tryptone	16	gm
Yeast extract	10	gm
NaCl	5	gm

Dissolved in 1,000 ml distilled water.

Sterilized by autoclave and kept at 4 °C.

2.5 Terrific broth

Tryptone	12	gm
Yeast extract	24	gm
Glycerol	4	ml

Adjusted to 900ml with distilled H_2O, Sterilized by autoclaving

Allowed to cool to room temperature

Adjusted volume to 1000ml with 100ml of a filter sterilized solution of 0.17M KH_2PO_4 and 0.72M K_2HPO_4

3. Reagents for using in plasmid mini-preparation

3.1 3 M Sodium Acetate pH 7.0

$NaAcet.3H_2O$	40.8	gm

Adjusted pH to 7.0 with NaOH/HCl

Dissolved in 100 ml DW and keep at 4 °C

3.2 Potassium Acetate

Potassium Acetate	29.4	gm
Glacial acetic acid	11.5	ml

Dissolved in 100 ml DW and keep at 4 °C.

3.3 10 M NaOH

NaOH	200	gm

Dissolved in 500 ml DW and keep at 4 °C.

3.4 10% SDS

SDS	5	gm

Dissolved in 50 ml DW and store at room temperature.

3.5 7.5 M NH_4 Acetate

NH_4 Acetate	57.8	gm

Dissolved in 100 ml DW and keep at 4 °C.

3.6 1 M glucose buffer

D-glucose	18.02	gm

Dissolved all ingredients in DW and fill up to 100 ml.

Autoclaved and keep at 4 °C.

3.7 0.5 M EDTA pH 8.0

EDTA	37.22	gm
DW	100	ml

Adjusted pH to 8.0, add DW to 200 ml and keep at 4 °C.

3.8 10X glucomix

1 M glucose buffer	50	ml
0.5 M EDTA pH 8.0	20	ml
1 M Tris pH 8.0	25	ml
DW	5	ml

Autoclaved and keep at 4 °C.

3.9 1X glucomix-lysozyme solution

10X glucomix	300	µl
Lysozyme stock (50mg/ml in DW)	300	µl
DW	2.4	ml

Kept on ice or store at 4 °C for 7 days.

3.10 0.1 M $CaCl_2$

$CaCl_2$ 1.11 gm

Dissolved in 100 ml distilled water.

Sterilized by autoclave and kept at 4 °C.

3.11 85% glycerol

Glycerol 42.5 ml

Added distilled water to 100 ml.

Mixed well, sterilized by autoclave and stored at RT

4. Reagents for SDS-polyacrylamide gel electrophoresis (SDS-PAGE) and Western blotting

4.1 1.5 M Tris-HCl, pH 8.8

Tris-base 18.15 gm

Dissolved in 75 ml deionized distilled water.

Adjusted pH to 8.8 with concentrated HCL.

Adjusted the volume to 100 ml with deionized distilled water and stored at 4 °C.

4.2 0.5 M Tris-HCl, pH 6.8

Tris-base	6.0	gm

Dissolved in 75 ml deionized distilled water.

Adjusted pH to 6.8 with concentrated HCl.

Adjusted the volume to 100 ml with deionized distilled water and stored at 4 °C.

4.3 Running buffer

Tris-base	1.51	gm
Glycine	7.20	gm
Sodium dodesyl sulfate	0.5	gm

Dissolved in 500 ml deionized distilled water and kept at 4 °C.

4.4 Blotting buffer

Tris-base	3.03	gm
Glycine	14.41	gm
SDS	0.5	gm

Added deionized distilled water to 700 ml and mixed well.

Added 200 ml of methanol

Adjusted the volume to 1,000 ml with deionized distilled water and kept at 4 °C.

4.5 Copolymerization of 4% stacking gel (5 ml)

Stock acrylamide 30%	0.83	ml
0.5 M Tris-HCl pH 6.8	0.63	ml
10% SDS	0.05	ml
DW	3.40	ml
10% Ammonium persulfate	0.05	ml
TEMED	0.01	ml

4.6 Copolymerization of 12% stacking gel (10 ml)

Stock acrylamide 30%	4.00	ml
Gel buffer pH 8.8	2.50	ml
10% SDS	0.10	ml
DW	3.30	ml
10% Ammonium persulfate	0.10	ml
TEMED	0.01	ml

5. Reagents for using in ELISA

5.1 0.05 M carbonate buffer, pH 9.6

Na_2CO_3	0.159 gm
$NaHCO_3$	0.293 gm
NaN_3	0.02 gm

Dissolved all ingredients in deionized distilled water and filled up to 90 ml.

Adjusted pH to 9.6.

Adjusted the volume to 100 ml with deionized distilled water and kept at room temperature.

5.2 0.05% Tween20 in TBS (washing buffer)

Tween20	0.5 ml

Dissolved in 1,000 ml PBS.

Mixed well and stored at room temperature.

5.3 Stop reaction solution (1N HCl)

Concentrate HCl	8.3 ml
Distilled water	91.7 ml

Slowly dropped HCl to distilled water, stored at room temperature

6. Reagents for phage precipitation and phage selection

6.1 PEG/NaCl

PEG-8000	100	gm
NaCl	73	gm

Dissolved in ddH20 and adjust volume to 1,000 ml.

Mixed and Filtrated through 0.2 μm Millipore membrane filter.

Stored at 4 ºC.

6.2 0.1M Glycine pH2.5

Glycine	0.375	gm

Dissolved in ddH2O 40 ml and adjusted pH to 2.5 with 1N HCl

Mixed and adjusted volume to 50 ml

Filtrated through 0.2 μm Millipore membrane filter and stored at 4 ºC.

6.3 1M Tris pH8.0

Tris base	6.07	gm

Dissolved in ddH2O 40 ml and adjusted pH to 8.0 with 1N HCl

Mixed and adjusted volume to 50 ml

Filtrated through 0.2 μm Millipore membrane

7. Reagents for Flow cytometry analysis

7.1 4% Paraformaldehyde in PBS

Paraformaldehyde	4	gm
PBS pH 7.2	100	ml

Heat at 56°C until dissolved

Filtrated with 0.2 μm Millipore filter, stored at 4°C.

7.2 1% BSA-PBS-NaN_3

BSA	1	gm
NaN_3	0.09	gm

Dissolved in PBS 100 ml

7.3 0.2% Triton X-100

Triton X-100	0.2	ml

Dissolved in PBS 100 ml

8. Reagents for baculovirus isolation

8.1 20 % sucrose in PBS

Sucrose	20	g

Dissolved in PBS up to 100 ml

Filtered with 0.2 μm Millipore filter, stored at 4°C.

8.2 TNE buffer

1M Tris pH 7.2	1	ml
5 M NaCl	3	ml
0.5 M EDTA	1.14	ml

Filtered with 0.2 μm Millipore filter, stored at 4°C.

8.3 30% sucrose in TNE buffer

Sucrose	30	g

Dissolved in TNE buffer up to 100 ml

Filtered with 0.2 μm Millipore filter, stored at 4°C.

8.4 50% sucrose in D20 water (deuterium water)

Sucrose	50	g

Dissolved in D2O water up to 100 ml

Filtered with 0.2 μm Millipore filter, stored at 4°C.

9. Reagents for hybridoma cell culture

9.1 Incomplete IMDM medium

IMDM powder	1	pack
$NaHCO_3$	3.024	g
Gentamycin (40 μg/ml)	1	ml

Dissolved in ddH_20 and adjust volume to 1,000 ml

Filtered through 0.2 μm Millipore membrane filter.

Mixed and stored at 4 ºC.

9.2 Complete IMDM medium

Incomplete IMDM medium	90	ml
Fetal calf serum	10	ml

Checked sterility before used

9.3 Freezing medium (10%DMSO in 90%FCS)

Fetal calf serum	9	ml
DMSO	1	ml

Freshly preparation before use.

9.4 Turk's solution

Glacial acetic acid	3	ml
1% gential violet	1	ml

Adjusted volume to 100 ml with ddH_2O

9.5 Trypan blue (0.2%)

Trypan blue powder	0.2	gm
PBS pH 7.2	100	ml

Filtrated by Whatman filter paper No. 1 and stored at room temperature.

9. Reagents for insect cell culture

9.1 Incomplete Grace' s insect medium

Grace's insect medium powder	1	pack
$NaHCO_3$	0.35	g

Dissolved in ddH_20 and adjust volume to 750 ml

Adjusted pH to 6.2 and volume to 1,000 ml

Filtered through 0.2 μm Millipore membrane filter.

Mixed and stored at 4 ºC.

9.2 Complete Grace's insect medium

Incomplete Grace's insect medium	83	ml
Fetal calf serum	15	ml
Penicillin-streptomycin	1	ml
L-Glutamine	1	ml
Amphotericin B	0.25	μg

Checked sterility before used

10. Reagents for ELIB-PA

10.1 0.5 M $NaPO_4$

$NaPO_4$	5.9	g

Dissolved in 100 ml of ddH_2O and stored at RT

10.2 0.05% Tween20 in ddH_2O

Tween20	0.5	ml

Dissolved in 1,000 ml of ddH_2O and stored at RT

10.3 0.5% BSA, 0.05% Tween20 in TBS

BSA	0.5	g
Tween20	0.05	ml

Dissolved in 100 ml of TBS and stored at 4 ºC.

10.4 0.05% Tween20 in Tris-Immidazloe

1M Tris-HCl	5	ml
1M Immidazole	0.05	ml
Tween20	0.05	ml

Dissolved in ddH_2O, adjusted to 100 ml, and stored at 4 ºC

10.5 100 mM EDTA

0.5M EDTA	20	ml

Dissolved in ddH_2O, adjusted to 100 ml, and stored at 4 ºC

10.6 10 mM $NiSO_4$

0.1 M $NiSO_4$	10	ml

Adjusted with ddH_2O to 100 ml, and stored at RT

10.7 Tris-NaCl-Urea in series of immidazole

1M Tris-HCL		2	ml
5M NaCl		10	ml
8M Urea		75	ml
1M Immidazole	20mM	2	ml
	40mM	4	ml
	60mM	6	ml
	80mM	8	ml

Adjusted with ddH_2O to 100 ml and stored at 4 ºC

APPENDIX F

PRESENTATIONS AND PUBLICATIONS

List of presentations

1. Enhancement of Adenovital Infection in K562 Cells Using Substance X: a Stratagy for Gene Therary , The First Scientific Meeting in Allied Health Sciences, "Trends of Research in Biomedical Sciences" Faculty of Allied Health Sciences, Thammasat University, 2008 (oral presentation).

2. Enhancement of Adenovital Infection in K562 Cells Using Substance X: a Stratagy for Gene Therary. Higher education commission, 2008 (poster presentation)

3. Displaying of anti-MAp17 scFv antibody on recombinant baculovirus. The 25th Congress on Allergy and Immunology, 2009 (oral presentation).

4. Improving the solubility and binding affinity of scFv against matrix protein of HIV-1 virus (scFvp17) by using FLI-TRAP strategy. Higher education commission, 2010 (oral presentation).

5. Enhancement of Adenovital Infection in K562 Cells Using Substance X: a Stratagy for Gene Therary. RGJ seminar series LXXIV, From Basic Biomedical Research to Sustainable Development. The Royal Golden Jubilee Ph.D. Program and Faculty of Medicine, Chiang Mai University (poster presentation).

List of publications

1. Granio O, Porcherot M, Corjon S, **Kitidee K**, Henning P, Eljaafari A, Cimarell A, Lindholm L, Miossec P, Boulanger P, Hong SS. Improved adenovirus type 5 vector-mediated transduction of resistant cells by piggybacking on coxsackie B-adenovirus receptor-pseudotyped baculovirus. J Virol. 2009; 83(12):6048-66.

Iimpact factor 5.308

2. Lee VS, Tue-ngeun P, Nangola S, **Kitidee K**, Jitonnom J, Nimmanpipug P, Jiranusornkul, Tayapiwatana C. Pairwise decomposition of residue interaction energies of single chain Fv with HIV-1 p17 epitope variants. Mol Immunol. 2010; 47(5):982-990 **Impact factor 3.202**

3. **Kitidee K**, Nangola S, Gonzalez G, Boulanger P, Tayapiwatana C, Hong S-S. Baculovirus display of single chain antibody (scFv) using a novel signal peptide. BMC Biotechnol. 2011; 10(1):80.

Impact factor 2.72

CURRICULUM VITAE

Name	Miss Kuntida Kitidee
Date of birth	April 22nd, 1985
Education	
2000-2002	High school, Sanpatong Witayakom School, Chiang Mai, Thailand
2003-2006	Bachelor of Science (Medical Technology, First class Honor), Faculty of Associated Medical Sciences, Chiang Mai University, Chiang Mai, Thailand
Employment history	
April-September 2007	Research Assistance, Assoc. Prof. Chatchai Tayapiwatana, Faculty of Associated Medical Sciences, Chiang Mai University, Chiang Mai, Thailand

List of publications

1. Granio O, Porcherot M, Corjon S, **Kitidee K**, Henning P, Eljaafari A, Cimarell A, Lindholm L, Miossec P, Boulanger P, Hong SS. Improved adenovirus type 5 vector-mediated transduction of resistant cells by piggybacking on coxsackie B-adenovirus receptor-pseudotyped baculovirus. J Virol. 2009; 83(12):6048-66.

   Iimpact factor 5.308

2. Lee VS, Tue-ngeun P, Nangola S, **Kitidee K**, Jitonnom J, Nimmanpipug P, Jiranusornkul, Tayapiwatana C. Pairwise decomposition of residue interaction energies of single chain Fv with HIV-1 p17 epitope variants. Mol Immunol. 2010; 47(5):982-990

   Impact factor 3.202

3. **Kitidee K**, Nangola S, Gonzalez G, Boulanger P, Tayapiwatana C, Hong S-S. Baculovirus display of single chain antibody (scFv) using a novel signal peptide. BMC Biotechnol. 2011; 10(1):80.

   Impact factor 2.72

Kitidee et al. BMC Biotechnology 2010, 10:80
http://www.biomedcentral.com/1472-6750/10/80

BMC Biotechnology

RESEARCH ARTICLE Open Access

Baculovirus display of single chain antibody (scFv) using a novel signal peptide

Kuntida Kitidee[1,2†], Sawitree Nangola[1,2†], Gaëlle Gonzalez[1], Pierre Boulanger[1], Chatchai Tayapiwatana[2*], Saw-See Hong[1*]

Abstract

Background: Cells permissive to virus can become refractory to viral replication upon intracellular expression of single chain fragment variable (scFv) antibodies directed towards viral structural or regulatory proteins, or virus-coded enzymes. For example, an intrabody derived from MH-SVM33, a monoclonal antibody against a conserved C-terminal epitope of the HIV-1 matrix protein (MAp17), was found to exert an inhibitory effect on HIV-1 replication.

Results: Two versions of MH-SVM33-derived scFv were constructed in recombinant baculoviruses (BVs) and expressed in BV-infected Sf9 cells, N-myristoylation-competent scFvG2/p17 and N-myristoylation-incompetent scFvE2/p17 protein, both carrying a C-terminal HA tag. ScFvG2/p17 expression resulted in an insoluble, membrane-associated protein, whereas scFvE2/p17 was recovered in both soluble and membrane-incorporated forms. When coexpressed with the HIV-1 Pr55Gag precursor, scFvG2/p17 and scFvE2/p17 did not show any detectable negative effect on virus-like particle (VLP) assembly and egress, and both failed to be encapsidated in VLP. However, soluble scFvE2/p17 isolated from Sf9 cell lysates was capable of binding to its specific antigen, in the form of a synthetic p17 peptide or as Gag polyprotein-embedded epitope. Significant amounts of scFvE2/p17 were released in the extracellular medium of BV-infected cells in high-molecular weight, pelletable form. This particulate form corresponded to BV particles displaying scFvE2/p17 molecules, inserted into the BV envelope via the scFv N-terminal region. The BV-displayed scFvE2/p17 molecules were found to be immunologically functional, as they reacted with the C-terminal epitope of MAp17. Fusion of the N-terminal 18 amino acid residues from the scFvE2/p17 sequence (N18E2) to another scFv recognizing CD147 (scFv-M6-1B9) conferred the property of BV-display to the resulting chimeric scFv-N18E2/M6.

Conclusion: Expression of scFvE2/p17 in insect cells using a BV vector resulted in baculoviral progeny displaying scFvE2/p17. The function required for BV envelope incorporation was carried by the N-terminal octadecapeptide of scFvE2/p17, which acted as a signal peptide for BV display. Fusion of this peptide to the N-terminus of scFv molecules of interest could be applied as a general method for BV-display of scFv in a GP64- and VSV-G-independent manner.

* Correspondence: asimi002@hotmail.com; saw-see.hong@univ-lyon1.fr
† Contributed equally
[1]University Lyon 1, INRA UMR-754, Retrovirus & Comparative Pathology, 50, avenue Tony Garnier, 69366 Lyon Cedex 07, France
[2]Division of Clinical Immunology, Faculty of Associated Medical Sciences, Chiang Mai University, and Biomedical Technology Research Center, National Center for Genetic Engineering & Biotechnology, National Sciences and Technology Development Agency at the Faculty of Associated Medical Sciences, Chiang Mai University, Chiang Mai 50200, Thailand
Full list of author information is available at the end of the article

Background

The arsenal of HIV-1 antivirals available today includes a broad variety of drugs directed to viral targets which have a critical role at various steps of the virus life cycle. Inhibitors of virus-cell attachment and fusion, reverse transcription, protease-mediated maturation cleavage of viral protein precursors, and provirus integration into the host-cell genome, can be administered in multiple types of associations to minimize the emergence of resistance in highly active antiretroviral therapies (HAART). Among all the antiretroviral molecules, antibodies occupy a special position as they can inhibit HIV-1 replication by interfering with multiple steps of virus-cell interaction. Extracellular antibodies can neutralize HIV-1 at the early phase of cell attachment or entry of the virus [1]. On the other hand, intracellular antibodies (or intrabodies) can block virus replication by interfering with different processes, such as intracellular trafficking of incoming virions or assembly and egress of the virus progeny. The design of virus-resistant cells via intracellular expression of specific single chain fragment variable (scFv) antibodies directed to the virus has been successfully used to block HIV-1 replication *in vitro* [2-4]. The viral proteins which have been targeted by these intrabodies include structural proteins, such as the envelope glycoprotein gp120 [5] or the matrix protein MAp17 [6], the viral enzyme reverse transcriptase [7], and the auxiliary proteins Tat [8,9] and Vif [10,11].

The baculovirus (BV) *Autographa californica* multiple nucleopolyhedrovirus (AcMNPV) is an insect virus with a large double-stranded DNA genome packaged in a membrane-enveloped, rod-shaped protein capsid [12]. BVs have been extensively used over two decades as expression vectors for the production of recombinant proteins in insect cells [13]. The current interest of BVs resides in their promiscuous nature as gene transfer vectors, capable of transducing a large repertoire of established and primary cells, of both mammalian and nonmammalian origins [14,15]. Recombinant BVs carrying nonviral glycoproteins fused or nonfused to their own envelope glycoprotein GP64 have been advantageously used in the baculovirus-display technology and its multiple biological and therapeutic applications [16,17]. For example, fusion of scFv specific for the carcinoembryonic antigen (CEA) to GP64 conferred to the BV vector displaying scFv-CEA a targeting and binding specificity to CEA-expressing cells [18,19]. However, the fusion to GP64 restricts the display to the poles of the virions as well as the number of copies of fusion proteins, and other strategies using fusion to VSV-G glycoprotein have therefore been proposed [16,17,20,21].

It has been shown that the intracellular expression of a scFv derived from a monoclonal antibody (MH-SVM33) directed to a highly conserved C-terminal epitope of the HIV-1 MAp17 domain [22,23], scFv/p17, resulted in an efficient antiviral effect, as determined using CAp24-based ELISA and reverse transcription assays [6]. The MH-SVM33 epitope was localised near the MAp17-CAp24 junction and has been found to be accessible on recombinant Gag precursor (Pr55Gag), as shown by the high level of immunoreactivity of virus-like particles (VLP) produced in Sf9 cells and analyzed *in situ* by immunoelectron microscopy [24]. However, the exact molecular mechanism of the scFv/p17-mediated inhibitory activity has yet to be determined, since the MAp17 protein is involved in multiple viral functions within the infected cell (reviewed in [25]).

The original goal of our study was to try and elucidate the mechanism of the scFv/p17-mediated inhibitory activity, and its potential use for diagnostic or therapeutic applications. Insect cells infected by AcMNPV expressing Pr55Gag (AcMNPV-Pr55Gag) have been shown to produce vast amounts of VLP mimicking immature virions [26]. AcMNPV-Pr55Gag-infected Sf9 cells represent a convenient model for studying HIV-1 assembly [24,27-32], coencapsidation of Gag and partner proteins [33-35], and Gag processing by viral protease coexpressed in *trans* [36,37]. We constructed two recombinant BVs expressing scFv/p17 in two different formats. The N-myristoylation-competent version scFvG2/p17 carried a sequence which started with the N-terminal dipeptide Met-Gly, while the N-myristoylation-incompetent version scFvE2/p17 started with Met-Glu. Both scFV were incapable of blocking the assembly of VLP, or be copackaged with Pr55Gag into VLP. However, we found that scFvE2/p17 was incorporated into the baculoviral envelope (BV-E2/p17), and retained its anti-MAp17 functionality when displayed at the surface of BV particles. BV-E2/p17 represented therefore a potential biological tool for depletion of soluble MAp17 protein, or/and for competition with HIV-1 MAp17 receptors in *in vitro* or *ex vivo* experiments [25]. Interestingly, we found that another scFv molecule, referred to as scFv-M6-1B9 [38,39] and directed towards CD147 (also known as M6, OK, 5F7, TCSF, Basigin or EMMPRIN), was also displayed at the surface of baculoviral particles when fused to the same N-terminal octadecapeptide sequence from scFvE2/p17, abbreviated N18E2. This suggested that the N-terminal octadecapeptide sequence N18E2 carried the BV envelope addressing function and acted as a signal peptide for BV display. The fusion of this octadecapeptide sequence to the N-terminus of scFv molecules of biological interest could be used as a general strategy for BV-display, and as an alternative to fusion to GP64 or VSV-G.

Methods

Insect cells and baculovirus infection

Spodoptera frugiperda Sf9 cells were maintained as monolayers at 28°C in Grace's insect medium supplemented with 10% fetal bovine serum (FBS, Sigma), penicillin (200 U/ml), and streptomycin (200 μg/ml; Gibco-Invitrogen). They were infected with one, or coinfected with two or more recombinant BVs simultaneously at a multiplicity of infection (MOI) ranging from 2.5 to 20 pfu/cell, as previously described [24,28].

Construction of scFv against HIV-1 MAp17 and CD147

The hybridoma cell line MH-SVM33C9/ATCC HB-8975 was obtained from the American Type Culture Collection (ATCC, Manassas, VA). The monoclonal antibody MH-SVM33 reacts with the conserved epitope ^{121}DTGHSSQVSQNY^{132} at the C-terminus of the matrix protein (MAp17) of HIV-1 [22,23]. Total RNA was extracted from hybridoma cells using the RNeasy Mini kit (Qiagen Inc., Hilden, Germany), and the first strand of cDNA was synthesized using the oligodT-18 primer of the Transcriptor High Fidelity cDNA synthesis kit (Roche, Mannheim, Germany). The variable regions (V) of heavy (V_H) and light chains (V_L) were then amplified from cDNA using specific forward (Fw) and reverse (Rev) primers. Fw-V_HP17 (5'-ATATGCTAGCGGCCCAGGCGGCCCAGATCCAGTTGGTGCAGT-3') and Rev-V_HP17 (5'-CGACCCTCCACCGCGGACCCGCCACCTCCAGACCCTCCGCCACCTGCA GAGACAGTGACCAGAGTCCC-3') were used for the V_H fragment, and Fw-V_LP17 (5'-GGGTCCGGCGGTGGAGGGTCGGATGTTGTGATGACCCAGACTCCA-3') and Rev-V_LP17 (5'-ATATAAGCTTTCATTAAGCGTAGTCCGGAACGTCGTACGGGTACTGGCCGCCCTGGCCTT TGATTTCCAGC-3') for the V_L fragment. The fragment encoding the single-chain antibody to MAp17 (scFv/p17) was constructed by overlapping PCR using Fw-V_HP17 and Rev-V_LP17 primers, both containing a *Sfi* I site (shown underlined). The construction and characterization of HA-tagged scFv M6-1B9 directed against CD147 have been described in a previous study [38,39].

Recombinant BV

Foreign genes were inserted into the genome of AcMNPV, under the control of a chimeric AcMNPV-*Galleria mellonella* MNPV polyhedrin promoter in the case of recombinant HIV-1 Gag polyproteins [24,28,29,31,32], or under the control of the AcMNPV polyhedrin promoter in the case of pBlueBac4.5-derived vectors. AcMNPV-Pr55Gag, which expressed the N-myristoylated full-length Gag polyprotein (Pr55Gag) of HIV-1, has been described in detail in previous studies [30-32,36,40]. The recombinant AcMNPV expressing CAR (BV^{CAR}), the high affinity receptor for Coxsackie B and Adenovirus, has been described and characterized in a previous study [41]. BV^{CAR} virions have been shown to display the CAR glycoprotein at their surface [41]. A DNA fragment coding for H_6MA-CA, a non-N-myristoylated, carboxyterminal-truncated version of HIV-1 Gag polyprotein containing the matrix (MA) and capsid (CA) domains with an oligo-histidine (H_6) tag at its N-terminus, was generating using the following pairs of primers: the first pair consisted of Fw primers 5'-CTAGCATGGGTGCGAGAG-3' and 5'-CATGGGTGCGAGAGCG-3' and the second pair consisted of Rev primers 5'-CTTACTACAAAACTCTTGCTTTATG-3' and 5'-GTACCTTACTAC AAAACTCTTGC-3'. Two PCR reactions were performed using the HIV-1 plasmid pNL4-3 as the template. The PCR products from both reactions were then mixed, denatured, and hybridized to obtain DNA fragments with *Nhe* I and *Kpn* I cohesive ends, competent for ligation to pBlueBac4.5-His intermediate vector linearized with *Nhe* I and *Kpn* I. Plasmid pBlueBac4.5-His was derived from pBlueBac4.5 (Invitrogen, San Diego, CA) by insertion of a sequence coding for the (H_6) tag and a GSGSAS linker upstream to the *Nhe* I site. Sf9 cells were cotransfected with pBlueBac4.5-H_6MA-CA and linearised BV DNA (Bac-N-Blue™ Transfection kit; Invitrogen). Positive Sf9 cells harboring recombinant BVs were isolated using the blue plaque selection method after beta-galactosidase staining. Recombinant BV, abbreviated BV-H_6MA-CA, was isolated using the blue plaque selection method as above. Recombinant H_6MA-CA protein was produced in Sf9 cells infected with BV-H_6MA-CA. Sf9 cells were harvested at 48 h post infection (pi), and H_6MA-CA protein recovered from clarified Sf9 cell lysate by affinity chromatography on Ni^{2+}-NTA-agarose column (Qiagen, Hilden, Germany), as previously described [42]. Protein concentration in H_6MA-CA samples was determined by Bradford protein assay (Pierce; Thermo Fisher Scientific Inc., Rockford, IL, USA). Recombinant H_6MA-CA protein was used as the antigenic substrate for scFvG2/p17 and scFvE2/p17 in ELISA and co-immunoprecipitation experiments.

The DNA fragment encoding scFv/p17, obtained as described above, was cloned into the *Nhe* I and *Hind* III sites of the pBlueBac4.5 plasmid. The 5' and 3' ends of scFv/p17 fragment in the pBlueBac-scFv/p17 vector were then modified by oligonucleotide insertion at both *Nhe* I and *Hind* III sites, to obtain two versions of the scFv/p17 cDNA. One encoded the dipeptide Met-Gly at the N-terminus of scFv/p17, generating the scFvG2/p17 clone, the other the dipeptide Met-Glu, generating the scFvE2/p17 clone. At the 3' end of both clones, we inserted an oligonucleotide encoding the Influenza A virus hemagglutinin epitope YPYDVPDYA (HA tag). Sf9 cells were then cotransfected with the resulting plasmid

harboring the scFv/p17 coding sequence and linearised BV DNA. Recombinant BVs were isolated using the blue plaque selection method, as described above

The DNA fragment for the HA-tagged scFv M6-1B9 was amplified using plasmid pComb3X-scFv-M6-1B9 as the template [39], with the M6-1B9 Fw primer (5'-GAGGAGGAGCTGGCCCAGGCGGCCCAGATCCAG-TTGGTGCAGTCTGGAGAGCTAGTGATGACCCA-GACTCCAGC-3') encoding the N-terminal 18 amino acids of scFvE2/p17 (^{1}MEASLAAQAAQIQLVQSG^{18}), and the M6-1B9 Rev primer (5'-CTCCTCCTC-GGCCGCCCTGGCCACTAGTGACAGATGGGGCTG-3'). The scFv-M6-1B9 was then cloned into the *Sfi* I site of *Sfi* I-restricted pBlueBac-scFvE2. The recombinant BV was isolated as described above, and abbreviated BV-N18E2/M6.

Isolation of BV particles

Concentrated stocks of recombinant BV expressing scFv/p17 molecules, BV-scFvG2/p17 and BV-scFvE2/p17, respectively, were prepared as follows [41]. Infected Sf9 cell culture supernatants were harvested at 50 to 60 h post infection (pi), and clarified by centrifugation at 2,400 rpm and 4°C for 10 min. Aliquots (11-ml) of clarified culture supernatant were subjected to ultracentrifugation at 28,000 rpm for 1 h at 4°C through a 1-ml sucrose cushion (20% sucrose, w:v in PBS) in Beckman SW41 rotor. Each baculoviral pellet was resuspended by gentle shaking in sterile phosphate-buffered saline (PBS) overnight at 4°C (100 μl per centrifuge tube). The titers of BV suspensions ranged usually between 5×10^9 and 1×10^{10} pfu/ml, as determined by plaque titration in Sf9 cells (pfu/ml), which corresponded to 1×10^{12} to 5×10^{12} BV physical particles per ml [12,41]. When needed, e.g. for electron microscopy, BV particles were further purified by isopycnic ultracentrifugation in linear sucrose-D_2O gradient [35,40]. Gradients (10-ml total volume, 30-50%, w:v) were generated from a 50% sucrose solution made in D_2O buffered to pH 7.2 with NaOH, and a 30% sucrose solution made in 10 mM Tris-HCl, pH 7.2, 150 mM NaCl, 5.7 mM Na_2EDTA. The gradients were centrifuged for 18 h at 28,000 rpm in a Beckman SW41 rotor. 0.5 ml-fractions were collected from the top, and proteins analyzed by SDS-PAGE and Western blotting with the required antibodies. BV particles were recovered in fractions with an apparent density ranging from 1.08 to 1.15.

Cell fractionation and scFv purification

BV-infected Sf9 cells were harvested between 48 and 72 h pi. After cell lysis, cellular fractionation was performed using the FractionPREP™ Cell Fractionation System (Medical & Biological Laboratories Co. Ltd., Nagoya, Japan). Four subcellular protein fractions were thus obtained, cytosol, nucleus, membrane/particulate and cytoskeletal fractions. The scFvE2/p17 protein was purified by affinity selection on anti-HA tag antibody Affimatrix gel (Roche Applied Science, IN, USA), following the manufacturer's instructions. Each fraction eluted from the affinity gel, using elution buffer containing HA peptide (Roche Applied Science) as binding competitor to displace the bound proteins, was analyzed by SDS-PAGE, and scFvG2/p17 or scFvE2/p17 detected by Western blotting, using anti-HA tag antibody, as described below.

Gel electrophoresis, membrane transfer and antibodies

Polyacrylamide gel electrophoresis of SDS-denatured protein samples (SDS-PAGE), and immunoblotting analysis have been described in detail in previous studies [34,35,40]. Briefly, proteins were electrophoresed in SDS-denaturing, 10%-polyacrylamide gel and electrically transferred to nitrocellulose membrane (Hybond™-C-extra; Amersham Biosciences). Blots were blocked in 5% skimmed milk in Tris-buffered saline (TBS) containing 0.05% Tween-20 (TBS-T), rinsed in TBS-T, then successively incubated with mouse monoclonal antibody to Influenza A virus hemagglutinin epitope YPYDVPDYA (HA tag antibody; Sigma, St Louis, MO, USA), or primary rabbit anti-Gag antibody, followed by relevant anti-IgG secondary antibodies, at working dilutions ranging from 1:1,000 to 1:10,000. Anti-HIV-1 Gag rabbit polyclonal antibody (laboratory-made; [35]) was raised in rabbit by injection of bacterially-expressed, GST-fused and affinity-purified carboxyterminally truncated Gag protein consisting of the full-length MA domain and the first seventy-eight residues of the CA domain (*Pst* I site; gag_{Lai} sequence). Monoclonal antibody against baculoviral envelope GP64 glycoprotein, clone AcV1 was purchased from Santa Cruz Biotechnology (Santa Cruz Biotechnology, Inc., Santa Cruz, CA, USA). Apparent molecular weights were estimated by comparison with prestained protein markers (Precison Plus Protein™ Standards, Dual Color; BioRad Laboratories, Inc., Bio-Rad France). For protein quantification, blots were scanned and protein bands were quantitated by densitometry, using the VersaDoc image analyzer and the Quantity One program (BioRad).

Indirect ELISA

The functionality of recombinant scFv/p17 was evaluated by their binding activity to the synthetic MAp17 peptide ^{121}DTGHSSQVSQNY^{132} (GenScript; Piscataway, USA) and H_6MA-CA protein prepared as above, in standard indirect ELISA procedure. In brief, aliquots (100 μl) of MA p17 peptide solution at 50 μg/ml, or of H_6MA-CA protein solution at 5 μg/ml in coating buffer (0.1 M $NaHCO_3$, pH 9.6) were incubated overnight at

4°C in 96-well microtiter plates (NUNC, Roskilde, Denmark). The coated wells were blocked with 200 μl of blocking buffer (2% bovine serum albumin in TBS; TBS-BSA) for 1 h at room temperature (RT), then washed five times with washing buffer (0.05% Tween-20 in TBS; TBS-T). Aliquots (100 μl) from clarified cellular lysates of BV-G2/p17- or BV-E2/p17-infected Sf9 cells in blocking buffer was added to each well and incubation proceeded for 1 hr at RT. After five cycles of washing with TBS-T, monoclonal anti-HA tag antibody (Sigma) was added at dilution 1:2,500 in TBS-BSA, and incubated for 1 hr at RT. After extensive washing with TBS-T, the reaction was developed by addition of 100 μl p-nitrophenylphosphate substrate (Sigma), and OD measured at 405 nm using an ELISA plate reader at the optimum time. The antigen-binding activity of scFv-M6-1B9 and chimeric scFvE2/M6-1B9 was assessed in ELISA using immobilized recombinant CD147-biotin carboxyl carrier protein (BCCP) fusion protein as the antigen, produced as previously described [39].

Competition ELISA

Microtiter plates (NUNC) were coated with 50 μl of 10 μg/ml of avidin in coating buffer (0.1 M NaHCO3, pH 6.8) and incubated overnight at 4°C in moist chamber. The coated wells were then blocked with 200 μl of blocking buffer (2% BSA in TBS) for 1 h at RT, then washed four times with washing buffer (0.05% Tween-20 in TBS). 50 μl-aliquots of 50 μg/ml of biotinylated-peptide 17.1 (Bp17.1) in blocking buffer were added to each well and incubated for 1 h at RT. In parallel, scFvE2/p17 purified by anti-HA tag affinity as described above was mixed with p17 peptide at the final peptide concentration of 1 μg/ml, and incubated for 1 h at RT. After washing the wells, the mixture was added to the wells and incubated for 1 h at RT. Bound scFvE2/p17 was monitored by adding 50 μl of HRP-conjugated monoclonal anti-HA tag antibody (Sigma) at dilution 1:1,000 in blocking buffer. The wells were washed four times prior to the addition of 50 μl of 3,3',5,5'-tetramethyl-benzidine (TMB) substrate. Reaction was stopped by addition of 50 μl of 1 N HCl, and optical densities (OD) at 450 nm were measured using an ELISA plate reader. The percentage of inhibition (PI) was given by the following formula: PI = 100-[(B:Bo) × 100], where B and Bo were the OD values for scFvE2/p17 with and without inhibitor, respectively.

Co-immunoprecipitation

Sf9 cells co-infected with BV-E2/p17 (or BV-G2/p17) and BV-H_6MA-CA were harvested by centrifugation at 5,000 rpm for 10 min at 4°C. The cell pellets were washed 3 times with cold TBS, then resuspended in lysis buffer (1% Brij-35 in TBS) and incubated on ice for 45 min. The cell lysates were clarified by centrifugation at 13,000 rpm for 1 h at 4°C, and supernatants added to pre-washed anti-HA tag affinity gel. After incubation overnight at 4°C with gentle shaking, the resin was washed 3 times with washing buffer (20 mM Tris, pH7.5, 0.1 M NaCl, 0.1 mM EDTA, 0.05% Tween20). Immunocaptured proteins were eluted from the affinity gel by heating in SDS-containing buffer (20 mM Tris pH 7,5, 2 mM EDTA, 5% SDS, 20% glycerol, 200 mM DTT, 0.02% bromophenol blue) at 100°C for 5 min. The resin was pelleted by centrifugation and the supernatant analyzed by SDS-PAGE and Western blotting, using anti-His_6 tag and anti-HA tag primary antibodies, both purchased from Sigma.

Immunofluorescence (IF) microscopy

BV-infected Sf9 cell monolayers were harvested at 48 h pi, fixed with 3% paraformaldehyde in phosphate buffered saline (PBS) and permeabilized in 0.2% (v/v) Triton X-100 in PBS. Cells were blocked with 3% BSA in PBS (PBS-BSA), and HA-tagged scFv/p17 detected by reaction with mAb anti-HA (1:10,000 in PBS-BSA) and Alexa Fluor® 488-labeled goat anti-mouse IgG antibody (Molecular Probes, Invitrogen). For double labeling of scFv/p17 and Gag proteins, cell samples were reacted with rabbit anti-Gag antibody (1:1,000 in PBS-BSA) and Alexa Fluor® 546-labeled goat anti-rabbit IgG (Molecular Probes, Invitrogen). Samples were treated with DAPI and mounted on slides. For conventional IF microscopy, images were acquired using an Axiovert 135 inverted microscope (Zeiss) equiped with an AxioCam video camera. For confocal microscopy, samples were analyzed using a Leica TCS SP2 confocal microscope.

Flow cytometry

ScFv-expressing Sf9 cells were resuspended in 200 μl PBS and incubated with monoclonal anti-HA tag antibody for 1 h at room temperature (RT), and at the dilution recommended by the manufacturer (Sigma), then pelleted. The cell pellet was resuspended in 200 μl PBS and reacted with Alexa Fluor® 488-labeled goat anti-mouse IgG antibody (Molecular Probes, Invitrogen). The cell suspension was then diluted with 10 volumes of PBS, and analyzed by flow cytometry using a BD FACSCanto™ II cytometer (Becton Dickinson Biosciences). At least 10,000 events were acquired for each experiment using the DIVA 6 software (Becton Dickinson).

Electron microscopy (EM)

Specimens were processed for EM and observed as previously described [41]. In brief, pelleted virions of BV-E2/p17 and BV-G2/p17 were resuspended in 20 μl-aliquots of 0.14 M NaCl, 0.05 M Tris-HCl buffer, pH

8.2, and adsorbed onto carbon-coated formvar membrane on nickel grids. The grids were incubated with primary antibody (anti-HA tag monoclonal antibody) at a dilution of 1: 50 in TBS for 1 h at room temperature (RT). After rinsing with TBS, the grids were post-incubated with 20-nm colloidal gold-tagged goat anti-mouse IgG antibody (British Biocell International Ltd, Cardiff, UK; diluted to 1: 50 in TBS) for 30 min at RT. After rinsing with TBS, the specimens were negatively stained with 1% uranyl acetate in H_20 for 1 min at RT, rinsed again with TBS, and examined under a JEM 1400 Jeol electron microscope equiped with an Orius-Gatan digitalized camera (Gatan France, 78113 Grandchamp).

Statistics

Results were expressed as mean ± SEM. of *n* observations. Sets of data were compared with an analysis of variance (ANOVA) or a Student's *t* test. Differences were considered statistically significant when $P < 0.05$. Symbols used in figures were (*) for $P < 0.05$, (**) for $P < 0.01$, (***) for $P < 0.001$, and ns for no significant difference, respectively. All statistical tests were performed using GraphPad Prism version 4.0 for Windows (Graphpad Software).

Results

Expression and characterization of scFvG2/p17 and scFvE2/p17 molecules in recombinant BV-infected Sf9 cells

The monoclonal antibody secreted by the MH-SVM33C9 hybridoma cell line reacts with the highly conserved and accessible epitope ^{121}DTGHSSQVSQNY^{132} corresponding to the C-terminus of HIV-1 MAp17 [22-24]. A single chain antibody derived from MH-SVM33 (scFv/p17) and expressed intracellularly showed an inhibitory effect on HIV-1 replication and virus release [6]. We generated two scFv/p17 subclones from the MH-SVM33C9 hybridoma cell line, scFvE2/p17 and scFvG2/p17, of which the full sequence could be communicated upon request. The N-terminal octadecapeptide sequence in scFvE2/p17 read ^{1}MEASLAAQAAQIQLVQSG^{18} , and ^{1}MGLAAQAAQIQLVQSGPE^{18} in scFvG2/p17. Both subclones were also modified at the C-terminus by the addition of a HA-tag, the Influenza A virus hemagglutinin epitope YPYDVPDYA, and when inserted into the baculoviral genome, generated two recombinant BVs, BV-E2/p17 and BV-G2/p17, respectively. The rationale for the N-terminal modification was that the dipeptide Met-Gly at the N-terminus of scFvG2/p17 represented a N-myristoylation signal which would promote the addressing scFvG2/p17 to the same compartment as the N-myristoylated MAp17 protein and Pr55Gag polyprotein. We have shown in previous studies that the Met-Gly signal was functional in insect cells in terms of recognition by N-myristoyl transferase, and that N-myristoylated glycine residue at the N-terminus of Pr55Gag is a prerequisite for plasma membrane addressing of unprocessed Pr55Gag, and budding and egress of membrane-enveloped VLP from Sf9 cells [24,27-36,40].

Sf9 cells infected with BV-G2/p17 or BV-E2/p17 were harvested at 24, 48 and 72 h post infection (pi), lysed in hypotonic buffer, and the kinetics of synthesis of scFvG2/p17 and scFvE2/p17 was analyzed by SDS-PAGE and Western blotting using anti-HA tag antibody. The extracellular culture medium was analyzed in parallel. We found that scFvE2/p17 protein (migrating with an apparent molecular mass of 30 kDa) was detectable as early as 24 h, and was maximal at 72 h pi. In contrast, scFvG2/p17 was detected at later times (48 h pi), and in 4- to 5-fold lower amounts, compared to scFvE2/p17 at 48-72 h pi (Figure 1a). However, both scFvE2/p17 and scFvG2/p17 proteins were stable over a period of 72 h, with no major breakdown products detected in the Western blot patterns.

Cell lysates were then clarified by centrifugation, and scFvG2/p17 and scFvE2/p17 were probed in soluble fraction (S) and insoluble pellet (P), respectively. We found that 15-20% of the whole recombinant scFvE2/p17 protein synthesized was recovered as soluble material, as determined by scanning and densitometric analysis of the protein bands on blots, with a maximum at 48 h pi (Figure 1b; leftmost half of the panel). The proportion of soluble scFvG2/p17 was lower (Figure 1b; rightmost half), with only 8-10% of scFvG2/p17 protein recovered in the soluble fraction. The difference in the intracellular levels of the two recombinant proteins could not be explained by a higher level of scFvG2/p17 secretion, compared to scFvE2/p17, as no scFvG2/p17 protein was detected in the culture medium at any time pi. Only scFvE2/p17 protein was detectable in the extracellular medium, as described below.

Cellular distribution of scFvG2/p17 and scFvE2/p17 in recombinant BV-infected Sf9 cells

We next performed cell fractionation to determine in which subcellular compartments the majority of scFvE2/p17 and scFvG2/p17 proteins were localized. Of note, the distinction between cytosol (Cy), membranes and organelles (Mb), nucleus (Nu) and cytoskeleton (Sk) was only operational, and did not preclude probable cross contaminations between different fractions. With this restriction in mind, scFvE2/p17 was found to be associated with the cytosolic fraction and nuclear pellet in similar amounts (ca. 20-25% each), but larger quantities (50-60%) were recovered in the insoluble fraction of cytoskeletal proteins (Figure 1c; leftmost half of the panel). Only small amounts of scFvE2/p17 were detected in the membrane fraction (Figure 1c, Mb lane). The

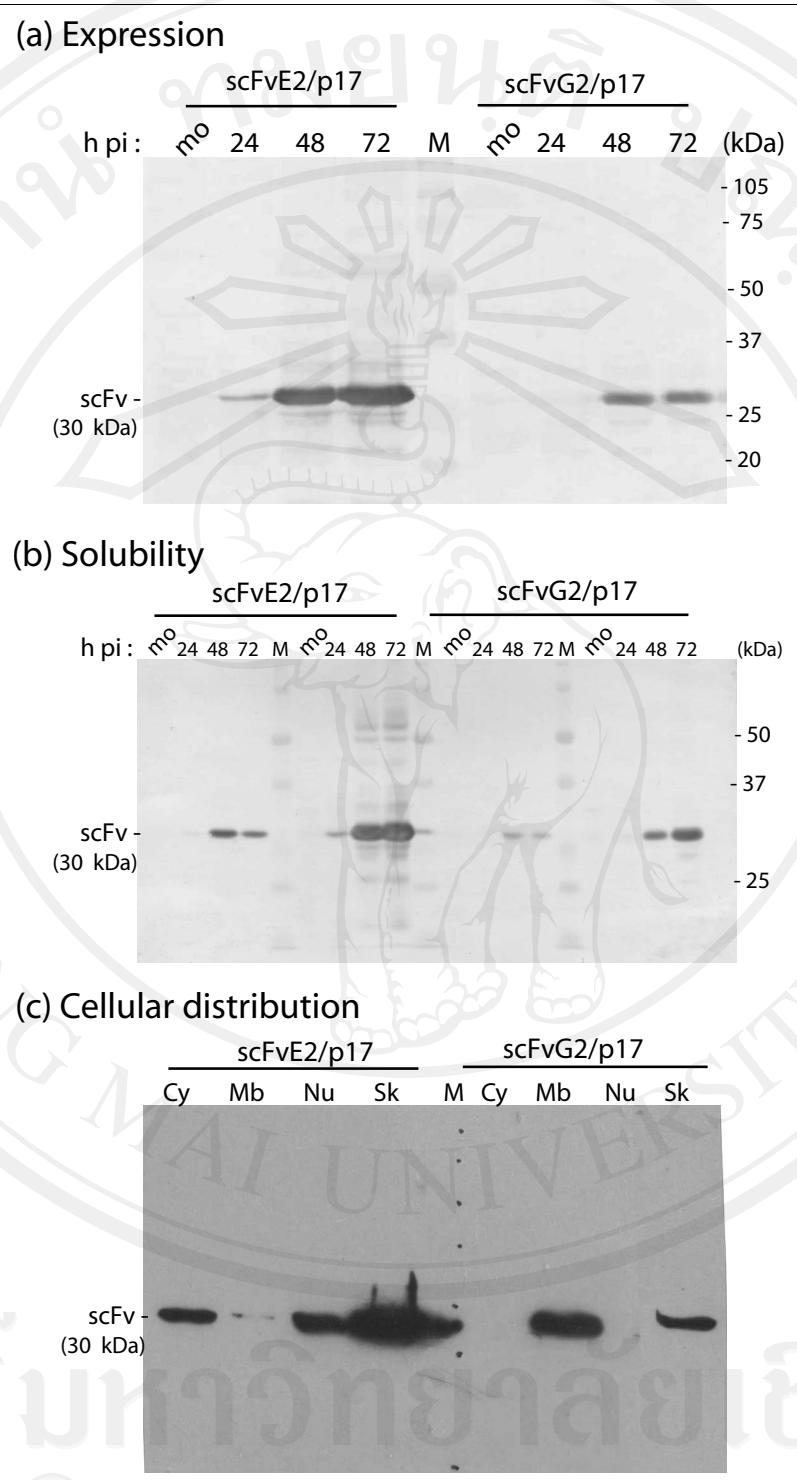

Figure 1 Expression, solubility and cellular localization of scFvE2/p17 and scFvG2/p17 in Sf9 cells. **(a)**, ***Level of expression***. Sf9 cells were mock-infected (lanes mo), or infected with BV-E2/p17 or BV-G2/p17, and harvested at 24, 48 and 72 h pi, as indicated on top of the panel. Whole cell lysates were analyzed by SDS-PAGE and Western blotting using anti-HA tag antibody. **(b),** ***Solubility***. Lysates of mock-infected cells (mo) or BV-E2/p17- or BV-G2/p17-infected cells harvested at 24, 48 and 72 h pi, as indicated on top of the panel were clarified by centrifugation, and soluble fraction (S) and pelletable material (P) analyzed as above. M, molecular mass markers, with their apparent molecular masses indicated in kilodaltons (kDa) on the right side of the blots. **(c),** ***Cell fractionation***. Sf9 cells infected with BV-E2/p17 or BV-G2/p17 as indicated on top of the panel were harvested at 48 h pi and processed for cell fractionation into cytosolic compartment (Cy), membranes (Mb), nuclear compartment (Nu) and cytoskeletal-associated proteins (Sk). Subcellular fractions were analyzed by SDS-PAGE and Western blotting using anti-HA tag antibody.

pattern of subcellular localization was different for the scFvG2/p17 protein, which was undetectable in the cytosolic and nuclear fractions, but distributed unequally between membrane and cytoskeletal fractions, two-thirds and one-third of the total, respectively (Figure 1c, rightmost half of the panel). Thus, the N-terminal G^2 mutation conferred two new properties to scFvG2/p17, compared to its scFvG2/p17 counterpart, (i) a lower level of expression, and (ii) a relocation to and strong association with the membranal fraction. The membrane association of scFvG2/p17 determined by cell fractionation was *a priori* consistent with the membrane targeting expected for a N-myristoylated protein.

Cellular localization of scFvG2/p17 and scFvE2/p17 was then studied *in situ*. BV-infected Sf9 cells were harvested at 48 h pi and examined in immunofluorescence (IF) microscopy or analyzed by flow cytometry using anti-HA tag antibody, with or without membrane permeabilization with detergent. Fluorescent signal of scFvE2/p17 was detected in both nonpermeabilized (Figure 2A, i) and Triton X100-permeabilized cells (Figure 2A, ii), whereas scFvG2/p17 fluorescence was only detectable in permeabilized cells (not shown). Flow cytometry of HA tag-positive cells confirmed the accessibility of scFvE2/p17 at the surface of nonpermeabilized cells, and the absence of significant amounts of scFvG2/p17 molecules at the cell surface (Figure 2B). Considering

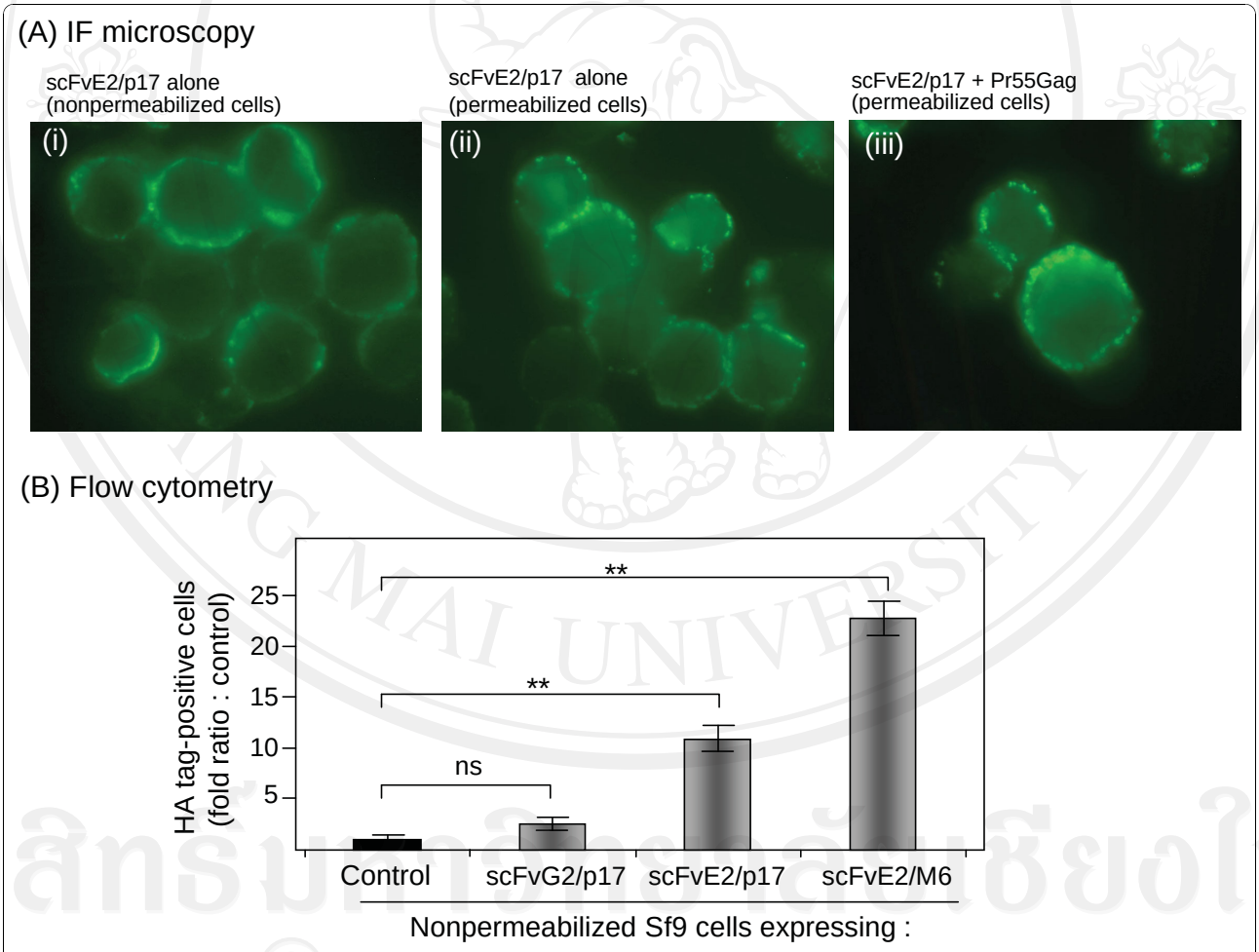

Figure 2 *In situ* analysis of scFvE2/p17 and scFvG2/p17 proteins in Sf9 cells. **(A), *Immunofluorescence (IF) microscopy***. Sf9 cells expressing scFvE2/p17 alone (**i, ii**), or coexpressing scFvE2/p17 and Pr55Gag (**iii**), were harvested at 48 h pi and nonpermeabilized **(i)**, or permeabilized with Triton X-100 **(ii, iii)**. Cells were reacted with anti-HA tag monoclonal antibody followed by Alexa Fluor® 488-labeled complementary antibody. **(B), *Flow cytometry***. Nonpermeabilized Sf9 cells expressing scFvE2/p17, scFvG2/p17 or the scFv-N18E2/M6 chimera were harvested at 48 h pi, reacted with antibodies as in (A), and analyzed by flow cytometry. Results shown were the proportion of HA tag-positive cells, expressed as the fold ratio over the values of control cells, attributed the value of 1. Control consisted of BV^{CAR}-infected cells, i.e. cells expressing irrelevant membrane glycoprotein. BV^{CAR} was a recombinant BV expressing the human CAR glycoprotein, and BV^{CAR}-infected cells released CAR-displaying virions in the extracellular medium [41]. Average of three separate experiments, m ± SEM; (**), $P < 0.01$; ns, not significant.

the poor recovery of scFvE2/p17 in the membranal fraction upon cell fractionation (refer to Figure 1c), the results of IF microcopy and flow cytometry suggested that the majority of scFvE2/p17 molecules were addressed to the plasma membrane and highly accessible at the cell surface, but proned to dissociate from the membrane upon cell disruption and fractionation, and to relocate into the soluble fraction. In contrast, we observed a major intracellular retention of most of the scFvG2/p17 molecules. Together with the data of cell fractionation (Figure 1c), this suggested that scFvG2/p17 protein was in majority sequestered in the intracellular membrane network.

When Sf9 cells were coinfected with two recombinant BVs to coexpress scFvE2/p17 and N-myristoylated Pr55Gag, we detected no significant change in the IF pattern of scFvE2/p17, compared to single infected cells expressing scFvE2/p17 alone (Figure 2A, compare panels ii and iii). This suggested that there was no major cellular redistribution of the scFvE2/p17 molecules in the presence of the Gag precursor. Similarly, no cellular redistribution of scFvG2/p17 was observed when coexpressed with Pr55Gag (not shown).

Immunological characterization of extracellular scFvE2/p17 molecules: functionality and specificity

(i) Antigen recognition by scFvE2/p17 in vitro

Since a significant proportion of scFvE2/p17 molecules occurred as soluble intrabody in the cytosolic fraction, we tested lysates of BV-E2/p17-infected Sf9 cells for the antigen binding activity of scFvE2/p17 in ELISA. Two types of immobilized antigens were used: a synthetic peptide p17.1, which reproduced the epitope sequence from HIV-1_{LAI} MAp17 (^{121}DTGHSSQVSQNY^{132}), and corresponded to the immunogen used to generate MH-SVM33; a recombinant H_6MA-CA protein of 39 kDa, which carried the same epitope as p17.9 (Table 1), but was embedded in the Gag polyprotein. The binding data from ELISA clearly showed that recombinant scFvE2/p17 reacted with its specific epitope in both configurations (Figure 3a, b), and in a dose-dependent manner (Figure 3c). Competition ELISA indicated that scFvE2/p17 bound to its epitope with a higher affinity when it was used as free p17.1 peptide, compared to the H_6MA-CA polyprotein used at equivalent epitope molarities (Figure 4a), suggesting that scFvE2/p17 preferentially bound to cleaved matrix protein MAp17, compared to non processed Gag precursor.

Table 1 Affinity of scFvE2/p17 for different variants of the conserved C-terminal epitope of HIV-1 MAp17[(a)]

Competitor	Epitope	Binding competition vs p17.1 (%)	Origin or HIV-1 isolate
Unrelated antigen (negative control)	CD147 (M6)	5.2 ± 2.9	-
17.1 (positive control)	DTGHSSQVSQNY	89.5 ± 1.6	LAI [(b)]
17.3	DTGHSSQ**I**SQNY	74.7 ± 10.2	1M-1005 [(c)]
17.7	DTGHSSQ**A**SQNY	44.0 ± 18.0	g22s2 [(d)]
17.8	DTGHS**K**QVSQNY	81.5 ± 9.5	4 [(e)]
17.9	DTG**NN**SQVSQNY	68.8 ± 2.2	pNL4.3 [(f)]
Inverted p17.1	YNQSVQSSHGTD	3.8 ± 1.5	-

[(a)] Competition for scFvE2/p17 binding between the dodecapeptide p17.1 (corresponding to residues 121-132 in the MAp17 from HIV-1_{LAI} used as immunogen) and other epitope variants was determined by ELISA, as examplified in Figure 4c. Data presented are m ± SEM (n = 3). Residues differing from the LAI prototype sequence are in bold.

[(b)] [63].

[(c)] [64].

[(d)] [43].

[(e)] [65].

[(f)] [66].

(ii) HIV-1 strain-specificity of antigen recognition by scFvE2/p17 and scFvG2/p17

Although the MAp17 epitope recognized by the monoclonal antibody MH-SVM33 is highly conserved among HIV-1 strains, there are some subtle differences in amino acid sequence. To assess the stringency of scFvE2/p17 towards HIV-1 MAp17 variants, we tested five different MAp17 peptides versus the original peptide epitope p17.1 in competition ELISA (Table 1). All MAp17 peptide variants competed with p17.1 to significant levels, considering that control homologous competition (bound p17.1 vs free p17.1) showed a 90% binding inhibition (Figure 4a, and Table 1). The lowest competition was observed for peptide p17.7, which corresponded to the MAp17 epitope of isolate g22s2, a molecular clone of HIV-1 isolated from HAART treated AIDS patients [43]. The difference between p17.7 and p17.1 corresponded to an Ala-Val mutation at position 128 in the MA domain. Valine carries a bulkier and more sterically hindered side chain, compared to alanine, and many examples have been reported in the literature of highly deleterious effects provoked by Ala-to-Val substitutions, in terms of protein conformation and function [44,45]. Competition ELISA was also performed using p17.1 versus a synthetic peptide of identical composition but of inverted sequence, YNQSVQSSHGTD. No competition was observed (Table 1), implying that N-to-C orientation of the peptide sequence and the C-terminal position of tyrosine residue-132 were crucial for the recognition of the epitope by scFvE2/p17.

The affinity and binding specificity of scFvG2/p17 to the different MAp17 peptides was also tested using competition ELISA, as above. Since only a minor fraction of recombinant scFvG2/p17 protein was recovered in the soluble cytosolic fraction, clarified lysates of cells

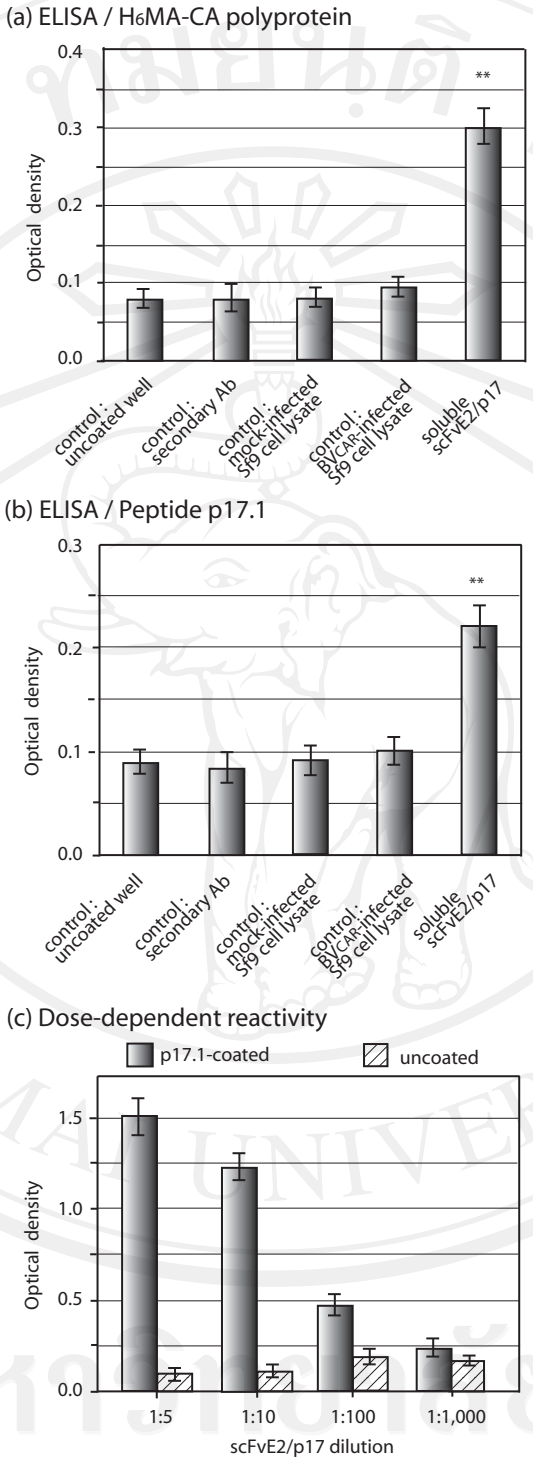

Figure 3 Functionality of soluble scFvE2/p17: antigen recognition. Sf9 cells were mock-infected or infected with BV^{CAR} (expressing irrelevant recombinant protein), or BV-E2/p17, and harvested at 48 h pi. Sf9 cell lysates were clarified by centrifugation, and reacted in ELISA with immobilized antigen. **(a)**, H_6MA-CA protein; **(b, c)**, synthetic peptide p17.1 (^{121}DTGHSSQVSQNY^{132} epitope). Negative controls were, from left to right: uncoated well, antigen-coated well without addition of scFvE2/p17-containing lysate, mock-infected cell lysate, and BV^{CAR}-infected cell lysate, respectively. **(c)**, Dose-dependent immunoreactivity of scFvE2/p17 towards p17.1 peptide. Soluble scFvE2/p17 from Sf9 cell lysates was affinity-purified on anti-HA tag antibody-coupled agarose beads. Average of three separate experiments, m ± SEM; (**), $P < 0.01$; ns, not significant.

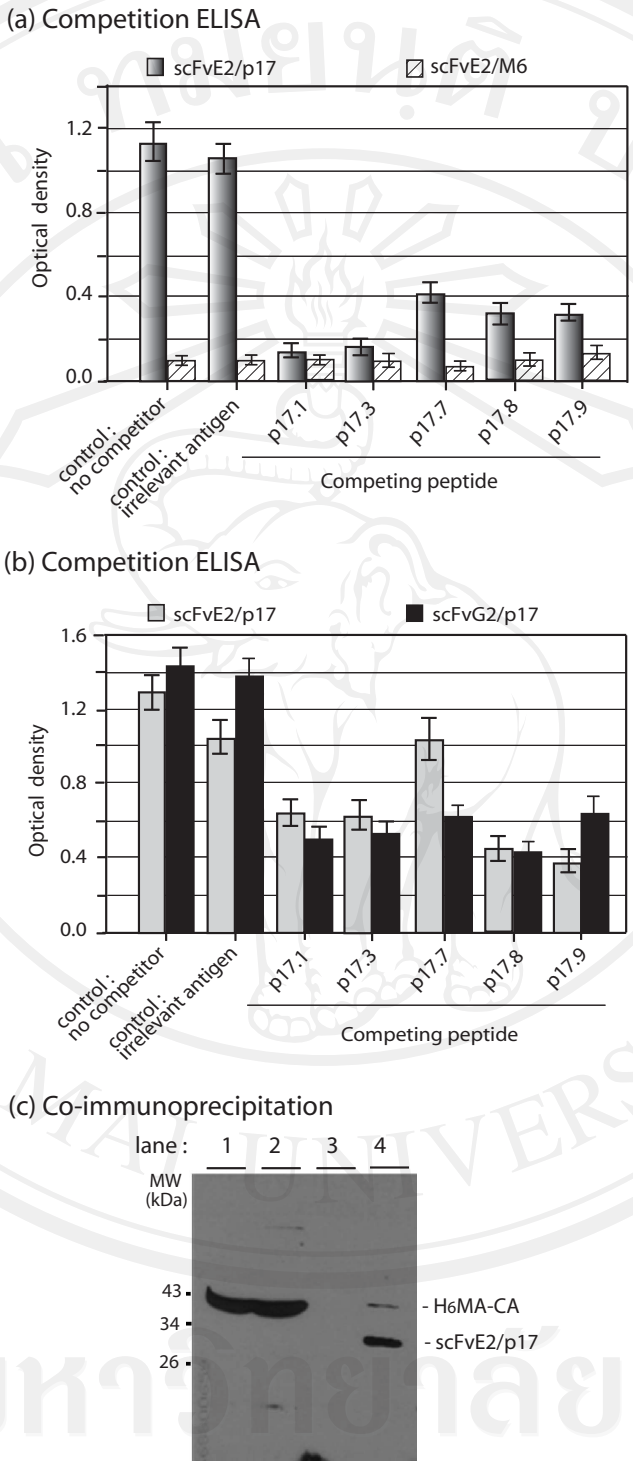

Figure 4 Immunological characterization of scFvE2/p17: epitope specificity and affinity. **(a)**, Soluble scFvE2/p17 from Sf9 cell lysates was analyzed in competition ELISA using solid support-adsorbed p17.1 versus soluble p17.1 (homologous, positive control), or versus MAp17 epitope variants p17.3, p17.7 and p17.9. Negative controls consisted of ELISA in the absence of competing peptide (no competitor), or ELISA in the presence of irrelevant antigen (CD147), or irrelevant scFv (scFv-M6-1B9). Average of three separate experiments, m ± SEM. **(b)**, Isolation of H_6MA-CA-scFvE2/p17 complexes. Lysates of cells coexpressing H_6MA-CA and HA-tagged scFvE2/p17 were separated on affinity matrix consisting of anti-HA tag antibody-coupled agarose beads, and fractions analyzed by SDS-PAGE and Western blotting, using anti- His_6 tag and anti-HA tag antibodies. Lane 1, whole cell lysate; lane 2, flow-through fraction; lane 3, column wash; lane 4, fraction eluted with SDS-PAGE loading buffer.

expressing scFvG2/p17 were concentrated by adsorption onto anti-HA tag-agarose gel, and specific elution of scFvG2/p17 protein was carried out using HA peptide-containing buffer. No significant difference was observed between scFvG2/p17 and scFvE2/p17 in terms of reactivity with MAp17 epitope variants (Figure 4b). The lack of difference in the antigen-binding function of soluble scFvG2/p17 and scFvE2/p17 indicated that the apparent poorer solubility of scFvG2/p17 compared to scFvE2/p17 was likely due to its addressing to membranal and cytoskeletal compartments, and not to major changes in its overall conformational structure and/or complementary-determining regions. This underlined the importance of the N-terminal sequence, which harboured the only difference between scFvG2/p17 and scFvE2/p17.

Functionality of scFvE2/p17 and scFvG2/p17 as intrabodies

(i) Antigen binding

Although our recombinant scFvE2/p17 was active *in vitro* in ELISA, we sought to determine whether intracellular scFvE2/p17 molecules could bind *in situ* to their MAp17 epitope embedded in Gag polyprotein. Sf9 cells were co-infected with two recombinant BVs, one expressing scFvE2/p17 (or scFvG2/p17), the other expressing the non-N-myristoylated Gag polyprotein substrate H_6MA-CA. Possible antigen-intrabody complexes present in cell lysates were isolated by affinity chromatography on anti-HA tag-agarose gel. The pattern of SDS-PAGE and Western blot analysis showed that most of the Gag polyprotein H_6MA-CA was recovered in the flow-through fraction, and that only a minor fraction bound to the column as H_6MA-CA-scFvE2/p17 complex (Figure 4b, lane 4). This suggested that scFvE2/p17 intrabody and the non-N-myristoylated H_6MA-CA protein segregated in separate cellular compartments and that only a small proportion of the scFvE2/p17 molecules could bind to H_6MA-CA. This might also suggest that scFvE2/p17 intrabody had a relatively low affinity for its Gag-embedded p17 epitope, compared to fully processed protein MAp17 with accessible p17 epitope at its C-terminus, or free C-terminal p17 peptide. These different hypotheses are not mutually exclusively. No detectable antigen-scFv complex was found with scFvG2/p17 (not shown), which confirmed that the majority of scFvG2/p17 accumulated in an insoluble form, and/or in a cellular compartment inaccessible to cytoplasmic Gag polyprotein.

(ii) Effect of scFvE2/p17 on VLP production

As shown earlier by IF microscopy, Pr55Gag had no significant influence on the cellular distribution of scFvE2/p17 protein (refer to Figure 2A, iii). To further study the mechanism of HIV-1 antiviral effect of MH-SVM33-derived scFv/p17 [6], we investigated the possibility that scFvE2/p17, via its binding to MAp17, could modify the intracellular trafficking and assembly pathway of Pr55Gag molecules. Sf9 were co-infected with two recombinant BVs, one expressing the N-myristoylated Pr55Gag precursor, the other scFvE2/p17. Pr55Gag synthesis was analyzed in whole cell lysates, and VLP production assayed in parallel in the culture medium, as described in previous studies [34,35,40]. No negative effect on Pr55Gag protein synthesis and on VLP assembly was detected in the presence of scFvE2/p17 (data not shown). Possible coencapsidation of Pr55Gag and scFvE2/p17 molecules into VLP during the assembly process was also investigated. Extracellular VLP were isolated from the culture medium, and their protein composition analyzed by SDS-PAGE and Western blotting using anti-Gag and anti-HA tag antibodies: no scFvE2/p17 was detected in the VLP fraction (not shown). This was in contrast to the BV particle fraction, as shown below.

Biophysical status of extracellular scFvE2/p17 protein: soluble versus particulate

As mentioned above, a significant amount of scFvE2/p17 protein was recovered in the extracellular medium of BV-E2/p17-infected Sf9 cells. These extracellular scFvE2/p17 molecules might occur as soluble protein, or as particle-associated material, e.g. released within membrane microvesicles or exosomes, or associated with cell debris. In order to determine the status of extracellular scFvE2/p17 protein, samples from culture mediun were subjected to isopycnic ultracentrifugation analysis in sucrose-D_2O density gradients [35,40]. Gradient fractions were analyzed by SDS-PAGE and Western blotting, using anti-baculoviral envelope glycoprotein GP64 and anti-HA tag antibodies. We found that the fractions positive for the C-terminal HA tag of scFvE2/p17 coincided with the anti-GP64-reacting fractions, and corresponded to particulate material sedimenting with the apparent density of BV particles of the viral progeny, d = 1.15-1.08 (Figure 5). This suggested that scFvE2/p17 was associated with the BV particles, either coencapsidated with the baculoviral proteins or inserted into the viral envelope. In the latter case, scFvE2/p17 molecules could be exposed at the surface of the BV particles with their active site accessible for epitope binding.

Immuno-EM analysis of baculoviral progeny of BV-E2/p17

In order to confirm the reality of this surface exposure, samples of extracellular medium of BV-G2/p17- and BV-E2/p17-infected Sf9 cells were analyzed by isopycnic ultracentrifugation in sucrose-D_2O gradients, and fractions sedimenting at 1.15-1.08 were deposited on grids, immunogold labeled with anti-HA tag antibody, and observed under the electron microscope. BV-G2/p17

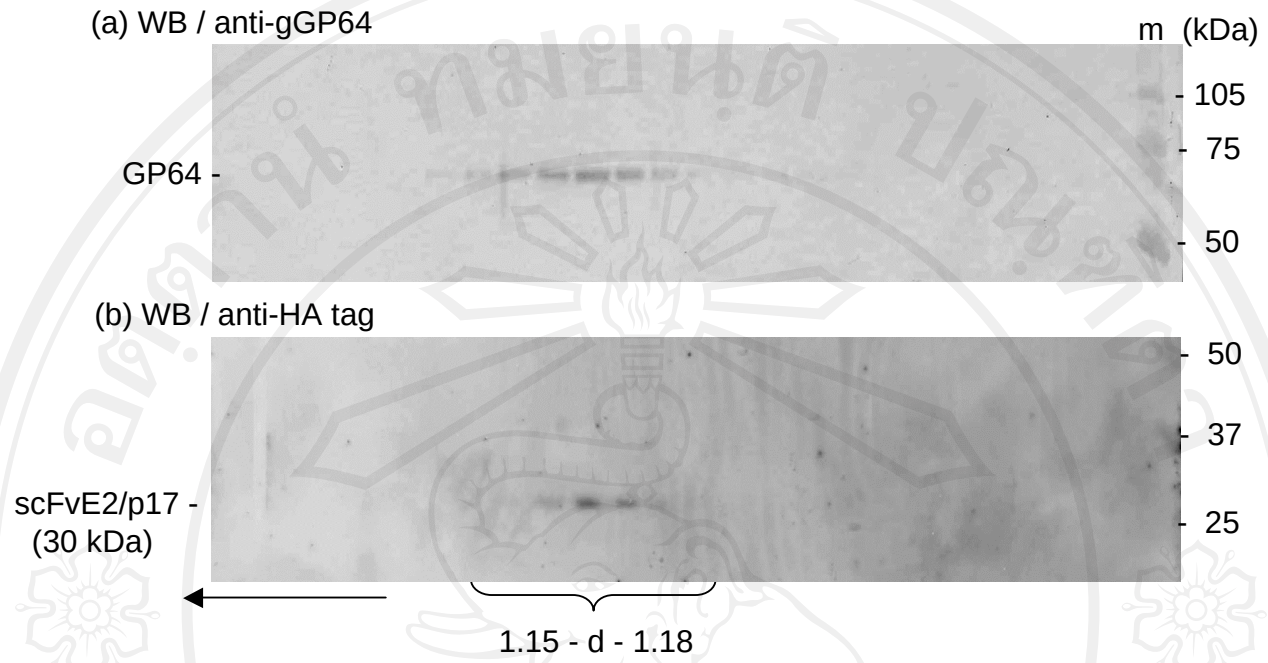

Figure 5 BV display of scFvE2/p17 (BV-E2/p17). Samples of culture medium of Sf9 cells infected with BV-E2/p17 were harvested at 72 h pi and analyzed by isopycnic ultracentrifugation in sucrose-D_20 gradients, as described under Materials and Methods. Gradient fractions were analyzed by SDS-PAGE and Western blotting, using **(a)** monoclonal antibody to the baculoviral GP64 envelope glycoprotein for detection of baculovirus progeny, and **(b)** anti-HA tag monoclonal antibody for detection of scFvE2/p17.

virions were never seen associated with gold grains, and most immunogold labeling was found at distance from BV particles, and corresponded to nonspecific, background labeling (not shown). The absence of anti-HA labeling of BV-G2/p17 virions in immuno-EM was consistent with the absence of detectable scFvG2/p17 protein in the extracellular medium, as mentioned above. Under the same experimental conditions however, anti-HA tag immunogold labeling was found to be associated with virions of BV-E2/p17 (Figure 6). The immuno-EM analysis therefore confirmed that scFvE2/p17 molecules were truely incorporated into the baculoviral envelope. Such incorporation of foreign proteins into the baculoviral envelope has already been described with human membrane glycoprotein CAR [41].

Immunological functionality and topology of scFvE2/p17 displayed on the baculoviral envelope

The observation that BV-displayed scFvE2/p17 was accessible to anti-HA tag antibodies in immuno-EM analysis strongly suggested that the C-terminal HA tag was oriented outwards. This orientation was already suggested by IF microscopy of intact cells expressing scFvE2/p17 (refer to Figure 2A, i). The next experiments were designed to assess the topological orientation of the scFvE2/p17 molecule in the baculoviral envelope, and, more importantly, to determine the degree of accessibility of its antigen-binding regions. BV-E2/p17 virions were immobilized on ELISA plate and probed with anti-HA tag antibody. The positive reaction indicated that the carboxyterminal region of scFvE2/p17 was exposed at the surface of the virions (Figure 7a), and that the insertion of scFvE2/p17 in the baculoviral envelope mimicked the orientation of class II membrane glycoproteins, with the aminoterminal region anchored in the baculoviral envelope, as depicted in Figure 7b.

The antigen binding activity of BV-displayed scFvE2/p17 was then determined by ELISA, using immobilized H_6MA-CA protein or synthetic peptide p17.1. In this assay, BV-E2/p17 virions displaying scFvE2/p17 were used as the equivalent of primary antibodies, and bound virions were detected using monoclonal antibody directed towards the baculoviral glycoprotein GP64. Both H_6MA-CA protein and p17.1 peptide were recognized by BV-E2/p17 virions (Figure 7c and 7d), which indicated that the BV-displayed scFvE2/p17 molecules retained their antigen-binding capacity.

BV-display of HA-tagged anti-CD147 scFv-M6-1B9

ScFv expressed in recombinant BV-infected insect cells are not naturally or spontaneously addressed to the baculoviral envelope, and different methods have been developed to obtain baculoviral envelope insertion of various scFv molecules, including fusion to GP64 or to

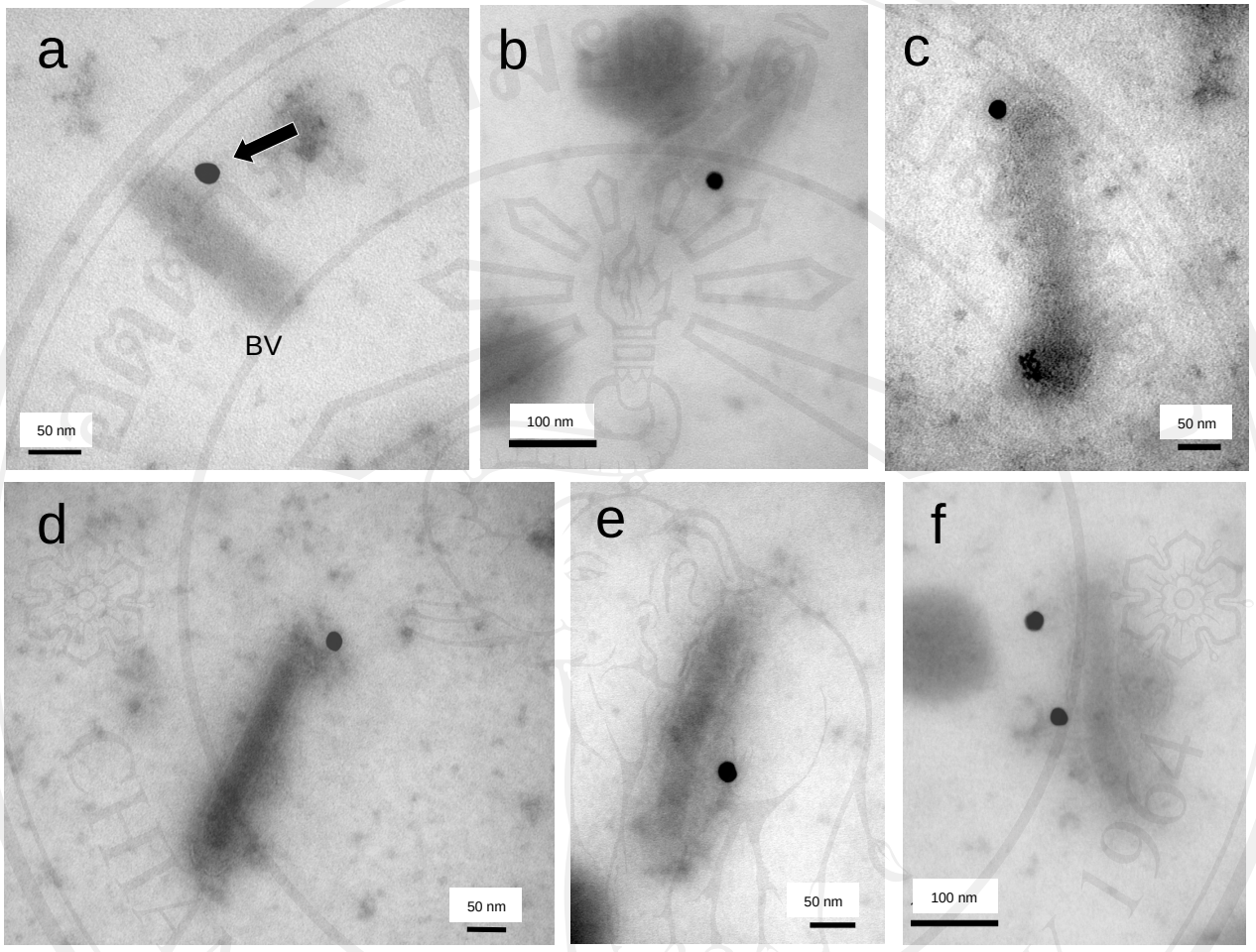

Figure 6 Immuno-electron microscopy of BV particles carrying scFvE2/p17 (BV-E2/p17). Samples of baculovirus progeny recovered from the culture medium of Sf9 cells infected with BV-E2/p17 and harvested at 72 h pi were deposited on grids and negatively stained with uranyl acetate. Specimens were reacted with anti-HA tag monoclonal antibody, followed by anti-mouse IgG antibody coupled to 20-nm colloidal gold grains. Different fields are presented in panels (a) to (f). Arrow in **(a)** points to a gold grain associated with a BV particle (BV). In **(f)**, two gold grains are seen associated with one BV particle.

VSV-G stem [16-21]. Although scFvE2/p17 did not contain any consensus signal peptide for membrane addressing, we postulated that in Sf9 cells, the N-terminal octadecapeptide sequence ^{1}MEASLAAQAAQIQLVQSG^{18} (abbreviated N18E2), was responsible for the intracellular trafficking and targeting of scFvE2/p17 to the site of BV budding, where it became inserted into the baculoviral envelope. To test this hypothesis, N18E2 was fused to the N-terminus of a non-related scFv, the HA-tagged scFv-M6-1B9, which recognizes the membrane glycoprotein CD147 [38,39]. When expressed in HeLa or 293 cells, scFv-M6-1B9 occurred as an active anti-CD147 intrabody, provoking the intracellular retention of CD147 and the blockage of its surface expression [38,39]. Our resulting chimeric scFv construct, abbreviated scFv-N18E2/M6, was expressed in Sf9 cells using a recombinant BV vector (BV-N18E2/M6). ScFv-N18E2/M6 molecules were detected in significant levels at the surface of nonpermeabilized cells harvested at 48 h pi, as for scFvE2/p17 (refer to Figure 2B). The baculoviral progeny from BV-N18E2/M6-infected cells was then isolated by ultracentrifugation and analyzed by ELISA (not shown) and immuno-EM (Figure 8) using anti-HA tag antibody. Both methods showed the accessibility of the HA tag at the surface of BV particles. In the electron micrograph shown in Figure 8d, two baculovirus particles were seen as a V-shape dimer pointing to one gold grain. This might represent the cross-linking of two particles via the two Fab domains of a single antibody molecule, although it could not be excluded that one antibody would bind to one particle, while the other would be in close proximity.

We also tested the antigen-binding capability of BV-displayed chimeric scFv-N18E2/M6, using the recombinant

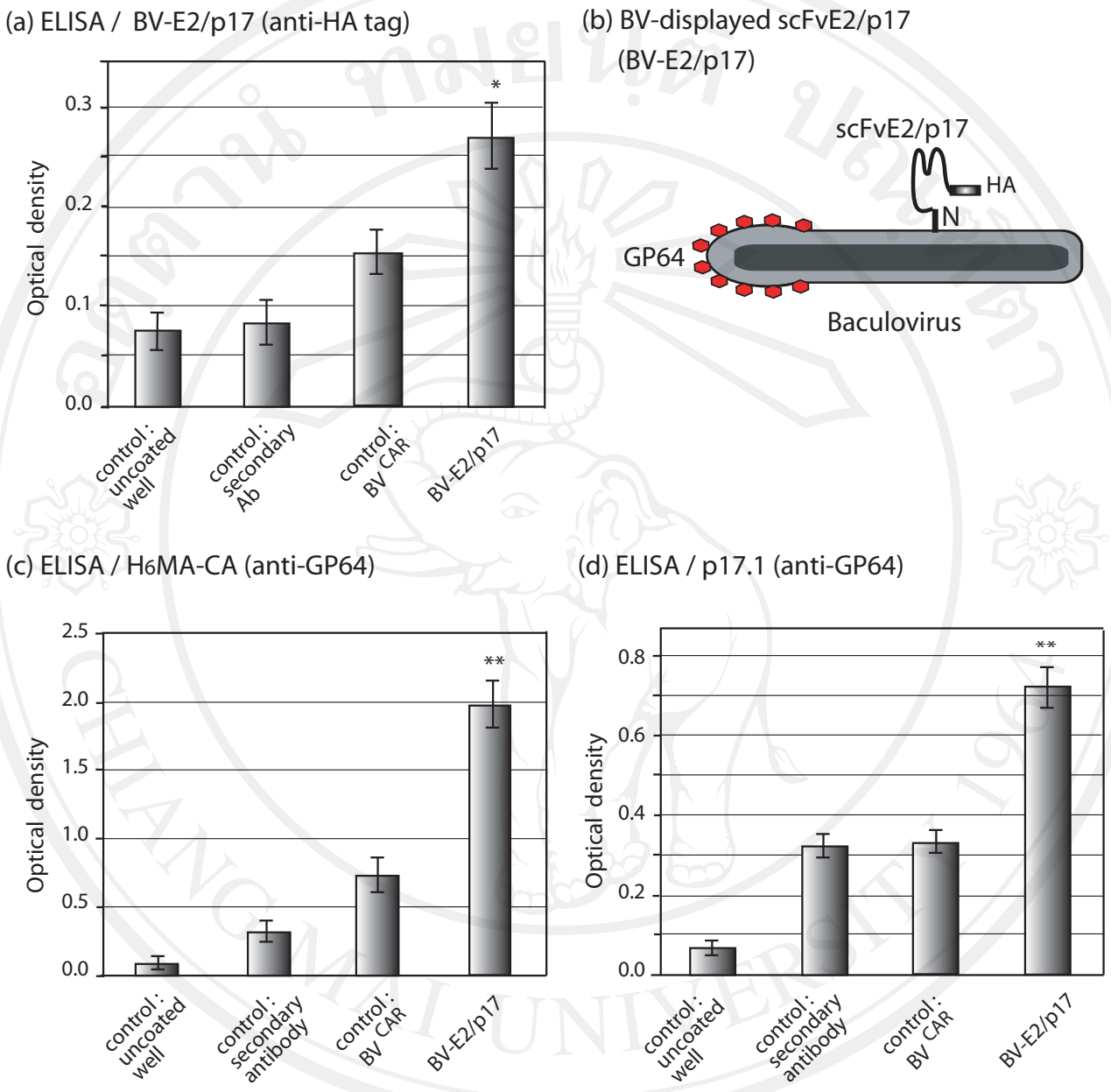

Figure 7 Topology and functionality of BV-displayed scFvE2/p17 molecules. Baculoviral progeny recovered from the culture medium of Sf9 cells infected with BV-E2/p17 was isolated by ultracentrifugation. **(a)**, BV-E2/p17 virions were immobilized on ELISA plate and reacted with anti-HA tag monoclonal antibody and peroxidase-labeled complementary antibody. Controls were from left to right, respectively: uncoated well, well coated with antigen with no BV addition, and well coated with antigen with addition of irrelevant baculovirus particles (CAR-displaying BV^{CAR}; [41]). **(b)**, Schematic model of scFvE2/p17 molecule displayed at the surface of a BV particle. GP64, baculoviral envelope major glycoprotein. BV-E2/p17 virions were reacted in ELISA with immobilized antigen, **(c)** H_6MA-CA-embedded p17 epitope, or **(d)** synthetic peptide p17.1. Average of three separate experiments, m ± SEM; (*), $P < 0.05$); (**), $P < 0.01$).

CD147-BCCP fusion protein as immobilized antigen in ELISA, as previously described [39]. The data showed that the chimeric scFv-N18E2/M6 molecules present at the surface of BV particles conserved their antigen-binding function and their specificity towards CD147 (Figure 9). These results suggested that the fusion of the N18E2 peptide to scFv-M6-1B9 was able to confer to the chimeric scFv-N18E2/M6 protein the capacity to be addressed to the BV budding sites at the plasma membrane and to be incorporated into the baculoviral envelope. They also suggested that N18E2 could function as a universal N-terminal signal peptide for BV-display of functional scFv of biological interest. A scheme of the general strategy of stepwise construction of BV particles displaying scFv

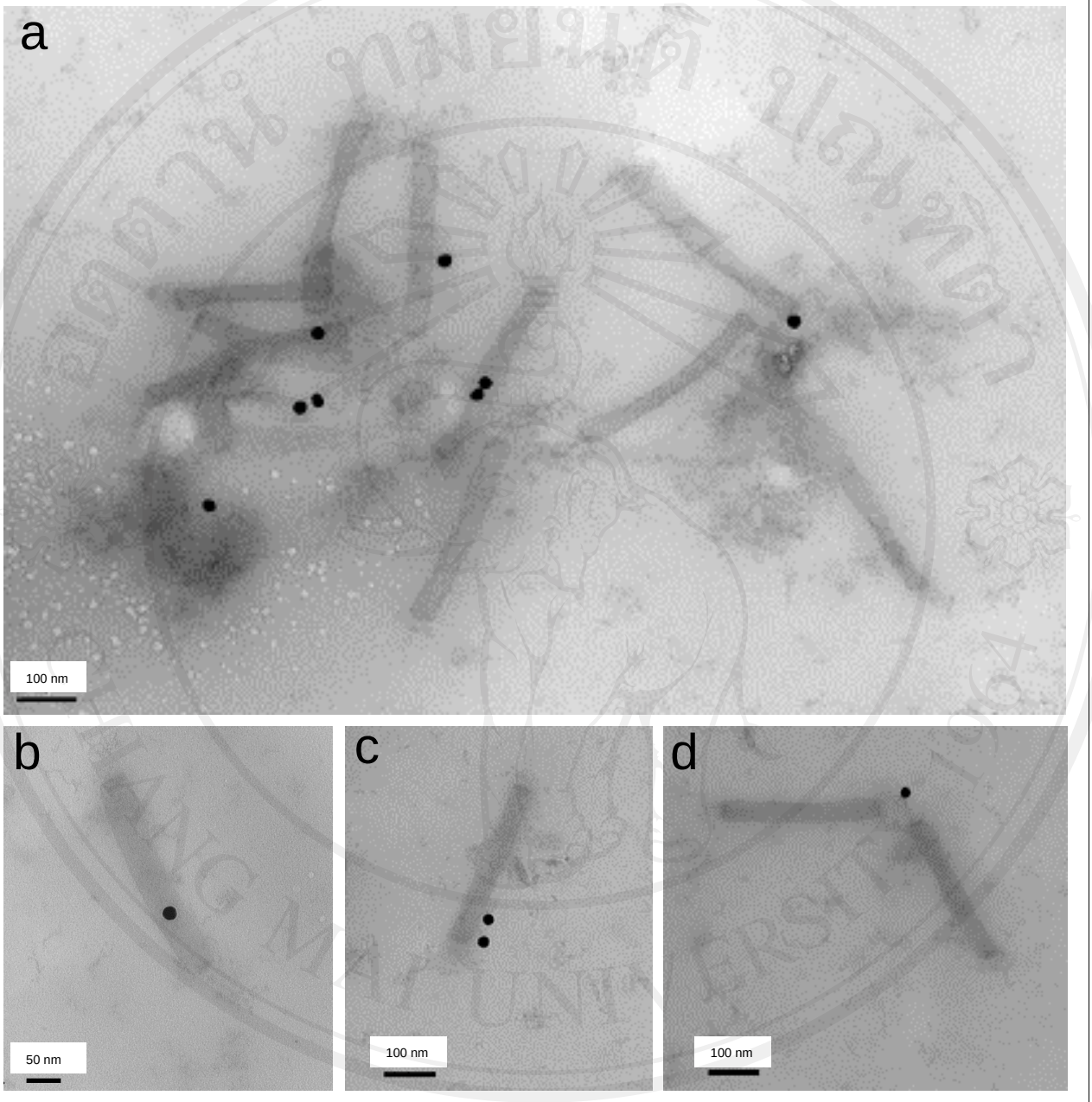

Figure 8 Immuno-electron microscopy of BV particles carrying chimeric scFv-N18E2/M6 (BV-N18E2/M6). Samples of baculoviral progeny recovered at 72 h pi from the culture medium of Sf9 cells infected with BV-N18E2/M6 were deposited on grids and negatively stained with uranyl acetate. Specimens were reacted with anti-HA tag monoclonal antibody, followed by anti-mouse IgG antibody coupled to 20-nm colloidal gold grains. Different fields are presented in panels (a) to (d). **(a)**, General view of a cluster of immunogold-labeled BV-N18E2/M6 particles. **(b-d)**, Enlargement of immunogold-labeled BV-N18E2/M6 particles.

molecules of interest equiped with our signal octadecapeptide N18E2 is presented in Figure 10.

Discussion

Despite several recent studies, little information is available at the molecular level on the molecular factors and mechanisms involved in the secretory pathway of insect cells in general, and the lepidopterian Sf9 cells in particular [46]. Secreted recombinant proteins are usually obtained by fusion of the protein of interest to the N-terminal leader peptide of the honeybee pro-mellitin (MBM-SP) [47,48]. However, this strategy does not always guarantee the secretion of the recombinant protein. For example, scSCR20, a MBM-SP-leaded scFv

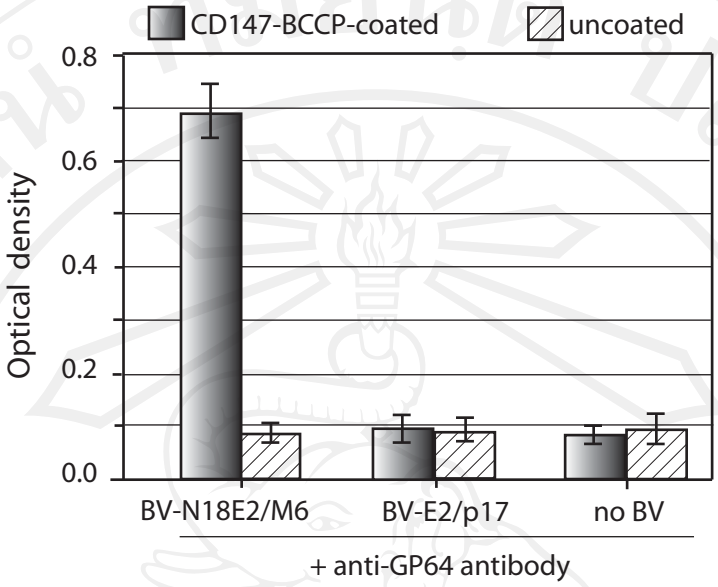

Figure 9 Functional analysis of BV-displayed chimeric scFv-N18E2/M6. The antigen-binding capacity and specificity of chimeric scFvE2/M6 displayed on the BV particle envelope was assessed by indirect ELISA, as described in a previous study [38,39]. Aliquots of BV-N18E2/M6 and control BV-E2/p17 particles recovered from BV-infected Sf9 cells were added to CD147-BCCP-linked avidin-coated wells, and incubated for 1 h at RT. After washing steps, bound viral particles were detected by addition of anti-baculoviral envelope glycoprotein GP64 in TBS-BSA. Average of three separate experiments, m ± SEM. (**), $P < 0.01$.

derived from an anti-African cassava mosaic virus monoclonal antibody [49] was not secreted in the culture medium of BV-infected insect cell lines from *Spodoptera frugiperda*, *Trichoplusia ni*, and *Mamestra brassicae*. However, scSCR20 molecules were released at high levels in the culture medum of *Drosophila* cell lines stably expressing MBM-SP-fused scSCR20 [50]. Likewise, certain types of scFv expressed in insect cells using recombinant BV have been recovered in the extracellular medium although they lack an insect cell leader peptide [51]. The most probable explanation was that specific features of recombinant scFv, such as their own N-terminal amino acid sequence or/and other downstream domain(s), can influence their behaviour in BV-infected cells.

BV-display has been used for almost a decade for immunisation purposes, gene delivery, or development of eukaryotic libraries [14,17,52,53]. Conventional BV-display involves baculoviral envelope glycoprotein GP64 manipulations [17,18,52], or the use of the VSV-G stem [16,17,20,21]. This differs from the incorporation of foreign proteins or glycoproteins into the baculoviral envelope without fusion to GP64, such as the envelope incorporation and display of functional human beta-2 adrenergic receptor (ß2AR) described in an earlier study [54]. In a more recent work, we demonstrated the incorporation of the human CAR glycoprotein into the baculoviral envelope. CAR is the high affinity receptor for adenovirus serotype 5 (Ad5) and is a resident glycoprotein of the human cell plasma membrane. The baculoviral envelope-incorporated CAR was fully functional at the surface of BV^{CAR} virions, and enabled the formation of BV^{CAR}-Ad5 complexes, mediated by the interaction between the adenoviral fiber and CAR. We have used this strategy of BV^{CAR}-Ad5 duo formation to transduce Ad5-refactory cells [41].

It was relatively easy to conceive that human ß2AR and CAR molecules, even though expressed in heterologous system, could be displayed on the baculoviral envelope since both are resident membrane glycoproteins. It was rather unexpected for scFvE2/p17, which was an artificial molecule extrinsic to the BV-insect cell system. Moreover, in the case of scFvE2/p17, the scFv molecule was not constructed for membrane targeting, in contrast to scFvG2/p17 which carried the specific Met-Gly dipeptide signal for N-myristoylation by N-myristoyl-transferases. Comparison of the amino acid sequences of scFvE2/p17 and scFvG2/p17, which both lacked any consensus leader peptide, showed that they only differed by three residues at their N-terminus, M(EAS)L for scFvE2/p17, versus M(G)L for scFvG2/p17. The results of these minor sequence changes were

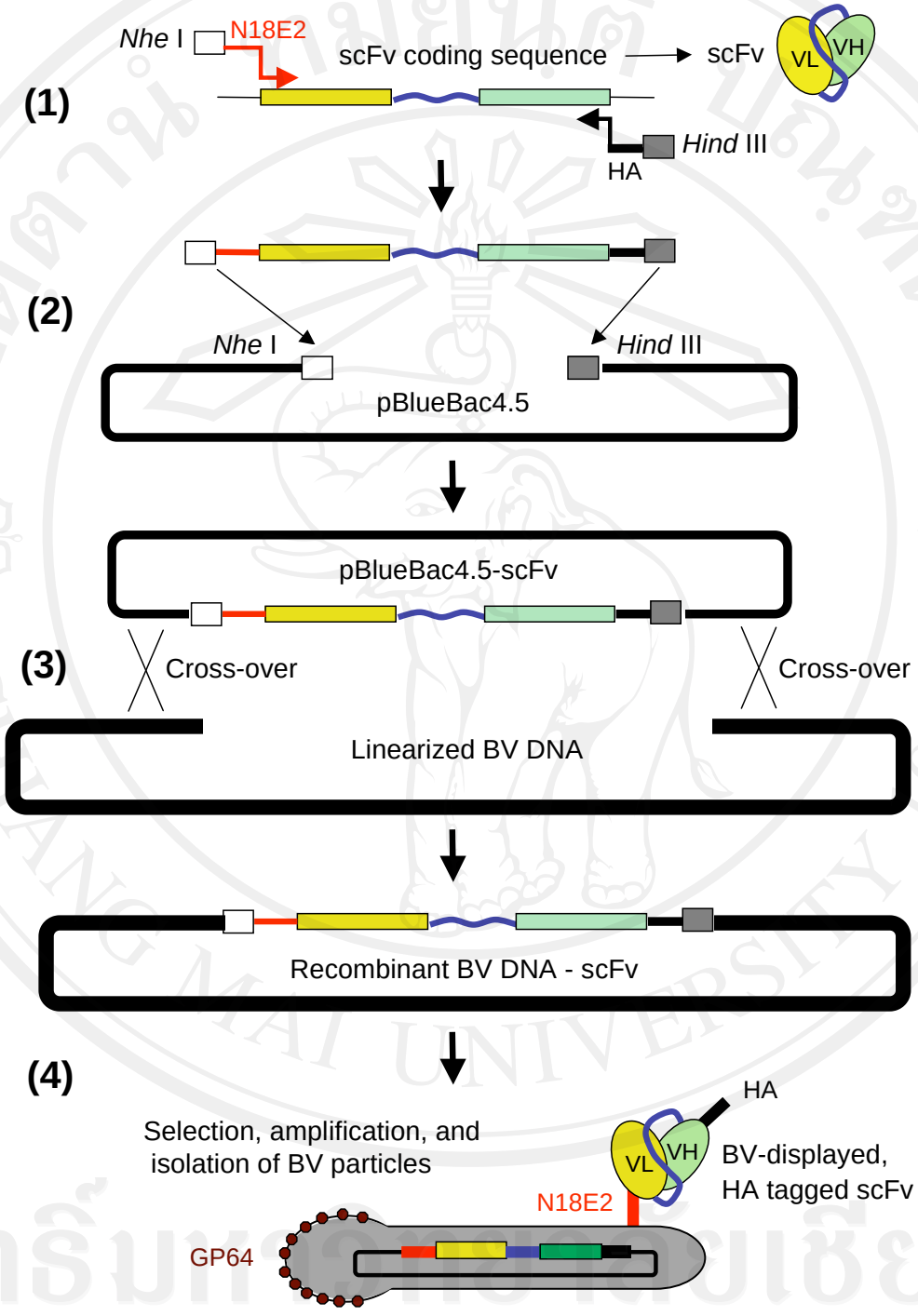

Figure 10 Generation of recombinant BV vector designed for display of scFv using the N18E2 signal peptide. Shown is the stepwise construction and isolation of BV-N18E2/scFv, a recombinant BV designed to expose at its surface scFv molecules of interest equiped with the signal octadecapeptide N18E2. ***Step (1)*** : PCR amplification of the scFv coding sequence, using a Fw 5'-primer containing a *Nhe* I site and the N18E2 coding sequence, and Rev 3'-primer encoding a HA tag and a *Hind* III site. ***Step (2)*** : insertion of N18E2-scFv-HA-encoding DNA fragment into the baculoviral intermediate plasmid pBlueBac4.5, digested with *Nhe* I and *Hind* III. ***Step (3)*** : cotransfection of insect cells with pBlueBac4.5-N18E2-scFv-HA and linearized baculoviral DNA, and homologous recombination. ***Step (4)*** : Isolation of plaques positive for recombinant baculoviral clone harboring N18E2-scFv-HA (e.g. blue plaque selection); amplification and isolation of recombinant BV expressing N18E2-scFv-HA, and displaying N18E2-scFv-HA on the baculoviral envelope.

drastic in terms of scFv solubility, cell compartmentalization and extracellular release. Recombinant scFvG2/p17 protein expressed in Sf9 cells was inexploitable since it was insoluble and trapped in the membrane pellet.

Recombinant scFvE2/p17 however was recovered simultaneously under two different forms: (i) as soluble scFv molecules from lysates of BV-infected Sf9 cells, and (ii) as BV-displayed scFv in the culture medium of the BV-infected Sf9 cell cultures. Both forms could be used as biological tools for different purposes. Soluble scFvE2/p17 could serve in conventional diagnostic assays for HIV-1 Gag detection, through specific recognition of the conserved MAp17 epitope. MAp17 functions as a structural component of HIV-1 virions, but also as a viral cytokine which binds to a cellular receptor, p17R [55,56], when released by HIV-infected cells. In the case of BV-displayed scFvE2/p17, the potential applications would be different. For example, if one considers the virokine properties of soluble MAp17 and the importance of inflammatory response at the mucosal sites of HIV-1 entry [55,56], one could envisage to use pelletable, BV-displayed scFvE2/p17 in experimental models of infected mucosae to deplete soluble MAp17 from the extracellular medium, or/and to compete with MAp17 for binding to p17R.

To assess the role of the N-terminal domain of scFvE2/p17 in the process of membrane addressing and scFv display on the baculoviral envelope, we fused the N-terminal octadecapeptide ^{1}MEASLAAQAA-QIQLVQSG^{18} (abbreviated N18E2) to another bioactive scFv molecule, scFv-M6-1B9. The ligand of scFv-M6-1B9 is M6, also called CD147 [38,39], a transmembrane glycoprotein highly expressed in various types of malignant cells [57] and tumors, e.g. nasopharyngeal carcinoma [58]. CD147 acts as an inducer of extracellular matrix metalloproteinases (EMMPRIN is another acronym for CD147) to promote tumor growth, invasion, metastasis and neoangiogenesis, and is a prognostic marker for invasiveness in prostate cancer [59] and thyroid carcinoma [60]. CD147 is also involved in atherosclerosis plaque instability [61] and in the regulatory inhibition of starvation-induced autophagy in human hepatoma cells [62].

We expressed the chimeric scFv-N18E2/M6 molecule in recombinant BV-infected Sf9 cells, and found that the BV progeny displayed scFv-N18E2/M6 on the baculoviral envelope. This suggested that the N-terminal octadecapeptide N18E2 carried the function required for BV-display of scFv molecules, and could be considered as a BV envelope addressing/anchoring signal peptide. This was further supported by the comparison of the structural domains of scFv downstream of the N18E2 peptide: scFv-N18E2/M6 and scFvE2/p17 differed by the successive order of their variable regions, VL-linker-VH from the N- to C-terminus in scFv-M6-1B9, versus VH-linker-VL in scFvE2/p17. This implied that the nature of the variable region downstream of N18E2 had little influence, if any, on the membrane addressing of chimeric, N18E2-fused scFv.

Although the molecular mechanism of cell trafficking of our chimeric scFv-N18E2/M6 molecule still remained to be elucidated in molecular terms, our present data provided a novel concept and platform for engineering scFv molecules competent for BV-display.

Conclusion

In the present study, we identified a N-terminal octadecameric peptide sequence, N18E2, which mediated the plasma membrane addressing and anchoring of scFv into the baculoviral envelope, and acted as a BV-envelope display signal. N18E2 could therefore be used in a general technology for BV-display of bioactive molecules such as scFv. In previous studies, we provided evidence that scFv-M6-1B9 was biologically active as an intrabody, and could be used to diminish the expression of CD147 at the surface of human cells [38,39]. The data presented here showed that scFv-M6-1B9 was also functional when displayed on the BV vector envelope. One might therefore envisage to use scFv-N18E2/M6-displaying BV particles as CD147-targeted vectors in future protocols of cancer biotherapy, to transfer therapeutic genes (e.g. suicide genes or proapoptotic genes) to CD147-overexpressing malignant cells. Since the baculoviral envelope glycoprotein GP64 is a low specificity attachment protein which allows BV to enter a wide variety of cells originating from mammalian or non-mammalian species [14,41], it will be necessary to block the GP64 binding activity of such vectors, and/or place the desired therapeutic gene under the control of a tumor-specific promoter, in order to avoid any bystander effect on cells of the surrounding tissues.

Acknowledgements

This work was supported by the French Agency for AIDS Research (ANRS, DendrAde contract 2007-2008), the Centre National de la Recherche Scientifique (FRE-3011), the French Cystic Fibrosis Foundation (Vaincre La Mucoviscidose, Contracts VLM TG-07-02 & TG-08-01), the University Lyon-1, and the Hospices Civils de Lyon (HCL) on the French side. It was supported by the Commission on Higher Education of Thailand, and the Franco-Thai Cooperation in Higher Education on the Thai side. KK was supported by the AMS-IRD URI-174 PHPT Franco-Thai Cooperation Program for High Education and Research, and a CHE-PhD-THA scholarship from the Commission on Higher Education, Ministry of Education, Thailand. SSH is an INSERM scientist and the recipient of a Contrat d'Interface HCL-INSERM. We are grateful to Elisabeth Errazuriz, Chantal Thevenon and Jonathan Girard (Centre Commun d'Imagerie de Laennec), for their valuable assistance in our electron microscopy and flow cytometry analyses, to Tanatporn Chunkeson for her expert technical help, and to Cathy Berthet for her efficient secretarial aid.

Author details
[1]University Lyon 1, INRA UMR-754, Retrovirus & Comparative Pathology, 50, avenue Tony Garnier, 69366 Lyon Cedex 07, France. [2]Division of Clinical Immunology, Faculty of Associated Medical Sciences, Chiang Mai University, and Biomedical Technology Research Center, National Center for Genetic Engineering & Biotechnology, National Sciences and Technology Development Agency at the Faculty of Associated Medical Sciences, Chiang Mai University, Chiang Mai 50200, Thailand.

Authors' contributions
KK and SN carried out the genetic construction of recombinant baculoviral clones, the biological and functional characterization of the recombinant proteins, and participated in the discussions. GG carried out the flow cytometry and immunoelectron microscopy analyses. PB participated in the immunoelectron microscopy analyses and wrote the manuscript. SSH participated in the genetic constructs. CT, SSH and PB conceived the study, participated in its coordination and designed the experimental strategies. All authors read and approved the final manuscript.

Received: 24 June 2010 Accepted: 19 November 2010
Published: 19 November 2010

References

1. Pantophlet R, Burton DR: **GP120: target for neutralizing HIV-1 antibodies.** *Annu Rev Immunol* 2006, **24**:739-769.
2. Marasco WA: **Intrabodies as antiviral agents.** *Curr Top Microbiol Immunol* 2001, **260**:247-270.
3. Marasco WA, Sui J: **The growth and potential of human antiviral monoclonal antibody therapeutics.** *Nat Biotechnol* 2007, **25**:1421-1434.
4. Paillard F: **Intrabodies to human immunodeficiency virus type 1.** *Hum Gene Ther* 1999, **10**:1425-1427.
5. Marasco WA, Haseltine WA, Chen SY: **Design, intracellular expression, and activity of a human anti-human immunodeficiency virus type 1 gp120 single-chain antibody.** *Proc Natl Acad Sci USA* 1993, **90**:7889-7893.
6. Tewari D, Goldstein SL, Notkins AL, Zhou P: **cDNA encoding a single-chain antibody to HIV p17 with cytoplasmic or nuclear retention signals inhibits HIV-1 replication.** *J Immunol* 1998, **161**:2642-2647.
7. Maciejewski JP, Weichold FF, Young NS, Cara A, Zella D, Reitz MSJ, Gallo RC: **Intracellular expression of antibody fragments directed against HIV reverse transcriptase prevents HIV infection in vitro.** *Nat Med* 1995, **1**:667-673.
8. Bai J, Sui J, Zhu RY, Tallarico AS, Gennari F, Zhang D, Marasco WA: **Inhibition of Tat-mediated transactivation and HIV-1 replication by human anti-hCyclinT1 intrabodies.** *J Biol Chem* 2003, **278**:1433-1442.
9. Marasco WA, LaVecchio J, Winkler A: **Human anti-HIV-1 tat sFv intrabodies for gene therapy of advanced HIV-1-infection and AIDS.** *J Immunol Methods* 1999, **231**:223-238.
10. Goncalves J, Silva F, Freitas-Vieira A, Santa-Marta M, Malhó R, Yang X, Gabuzda D, Barbas C: **Functional neutralization of HIV-1 Vif protein by intracellular immunization inhibits reverse transcription and viral replication.** *J Biol Chem* 2002, **277**:32036-32045.
11. Aires da Silva F, Santa-Marta M, Freitas-Vieira A, Mascarenhas P, Barahona I, Moniz-Pereira J, Gabuzda D, J. G: **Camelized rabbit-derived VH single-domain intrabodies against Vif strongly neutralize HIV-1 infectivity.** *J Mol Biol* 2004, **340**:525-542.
12. Slack J, Arif BM: **The baculoviruses occlusion-derived virus: virion structure and function.** *Adv Virus Res* 2007, **69**:99-165.
13. Possee RD: **Baculoviruses as expression vectors.** *Curr Opin Biotech* 1997, **8**:569-572.
14. Hu YC: **Baculoviral vectors for gene delivery: a review.** *Curr Gene Ther* 2008, **8**:(1):54-65.
15. Kost TA, Condreay JP, Jarvis DL: **Baculovirus as versatile vectors for protein expression in insect and mammalian cells.** *Nat Biotechnol* 2005, **23**:567-575.
16. Mäkelä AR, Oker-Blom C: **The baculovirus display technology–an evolving instrument for molecular screening and drug delivery.** *Comb Chem High Throughput Screen* 2008, **11**:86-98.
17. Mäkelä AR, Oker-Blom C: **Baculovirus display: a multifunctional technology for gene delivery and eukaryotic library development.** *Adv Virus Res* 2006, **68**:91-112.
18. Mottershead DG, Alfthan K, Ojala K, Takkinen K, Oker-Blom C: **Baculoviral display of functional scFv and synthetic IgG-binding domains.** *Biochem Biophys Res Commun* 2000, **275**:84-90.
19. Ojala K, Mottershead DG, Suokko A, Oker-Blom C: **Specific binding of baculoviruses displaying gp64 fusion proteins to mammalian cells.** *Biochem Biophys Res Commun* 2001, **284**:777-784.
20. Chapple SD, Jones IM: **Non-polar distribution of green fluorescent protein on the surface of Autographa californica nucleopolyhedrovirus using a heterologous membrane anchor.** *J Biotechnol* 2002, **95**:269-275.
21. Ojala K, Koski J, Ernst W, Grabherr R, Jones I, O-B C: **Improved display of synthetic IgG-binding domains on the baculovirus surface.** *Technol Cancer Res Treat* 2004, **3**:77-84.
22. Robert-Hebmann V, Emiliani S, Jean F, Resnicoff M, Traincard F, Devaux C: **Clonal analysis of murine B cell response to the human immunodeficiency virus type 1 (HIV-1)-gag p17 and p25 antigens.** *Mol Immunol* 1992, **29**:729-738.
23. Robert-Hebmann V, Emiliani S, Resnicoff M, Jean F, Devaux C: **Subtyping of human immunodeficiency virus isolates with a panel of monoclonal antibodies: identification of conserved and divergent epitopes on p17 and p25 core proteins.** *Mol Immunol* 1992, **29**:1175-1183.
24. Carrière C, Gay B, Chazal N, Morin N, Boulanger P: **Sequence requirement for encapsidation of deletion mutants and chimeras of human immunodeficiency virus type 1 Gag precursor into retrovirus-like particles.** *J Virol* 1995, **69**:2366-2377.
25. Fiorentini S, Marini E, Caracciolo S, Caruso A: **Functions of the HIV-1 matrix protein p17.** *New Microbiol* 2006, **29**:1-10.
26. Wilk T, Gross I, Gowen BE, Rutten T, de Haas F, Welker R, Kräusslich H-G, Boulanger P, Fuller SD: **Organization of immature human immunodeficiency virus type 1.** *J Virol* 2001, **75**:759-771.
27. Boulanger P, Jones I: **Morphogenesis and maturation of Retroviruses. Use of heterologous expression systems to study retroviral morphogenesis.** In *Curr Topics Microbiol Immunol. Volume 214.* Edited by: Kräusslich H-G. Berlin, Heidelberg, New York: Springer-Verlag; 1996:237-260.
28. Chazal N, Carrière C, Gay B, Boulanger P: **Phenotypic characterization of insertion mutants of the human immunodeficiency virus type 1 Gag precursor expressed in recombinant baculovirus-infected cells.** *J Virol* 1994, **68**:111-122.
29. Chazal N, Gay B, Carrière C, Tournier J, Boulanger P: **Human immunodeficiency virus type 1 MAp17 deletion mutants expressed in baculovirus-infected cells: *cis* and *trans* effects on the Gag precursor assembly pathway.** *J Virol* 1995, **69**:365-375.
30. Hong SS, Boulanger P: **Self-assembly-defective dominant mutants of HIV-1 Gag phenotypically expressed in baculovirus-infected cells.** *J Virol* 1993, **67**:2787-2798.
31. Royer M, Cerutti M, Gay B, Hong SS, Devauchelle G, Boulanger P: **Functional domains of HIV-1 *gag*-polyprotein expressed in baculovirus-infected cells.** *Virology* 1991, **184**:417-422.
32. Royer M, Hong SS, Gay B, Cerutti M, Boulanger P: **Expression and extracellular release of human immunodeficiency virus type 1 Gag precursors by recombinant baculovirus-infected cells.** *J Virol* 1992, **66**:3230-3235.
33. Bouyac M, Courcoul M, Bertoia G, Baudat Y, Gabuzda D, Blanc D, Chazal N, Boulanger P, Vigne R, Spire B: **Human immunodeficiency virus type 1 Vif protein binds to the Pr55GAG precursor.** *J Virol* 1997, **71**:9358-9365.
34. DaFonseca S, Coric P, Gay B, Hong SS, Bouaziz S, Boulanger P: **The inhibition of assembly of HIV-1 virus-like particles by 3-O-(3',3'-dimethylsuccinyl) betulinic acid (DSB) is counteracted by Vif and requires its Zinc-binding domain.** *Virol J* 2008, **5**:162.
35. Huvent I, Hong SS, Fournier C, Gay B, Tournier J, Carriere C, Courcoul M, Vigne R, Spire B, Boulanger P: **Interaction and co-encapsidation of HIV-1 Vif and Gag recombinant proteins.** *J Gen Virol* 1998, **79**:1069-1081.
36. Bardy M, Gay B, Pébernard S, Chazal N, Courcoul M, Vigne R, Decroly E, Boulanger P: **Interaction of human immunodeficiency virus type 1 Vif with Gag and Gag-Pol precursors: co-encapsidation and interference with viral protease-mediated Gag processing.** *J Gen Virol* 2001, **82**:2719-2733.
37. Royer M, Bardy M, Gay B, Tournier J, Boulanger P: **Proteolytic activity in vivo and encapsidation of recombinant HIV-1 proteinase expressed in baculovirus-infected cells.** *J Gen Virol* 1997, **78**:131-142.
38. Intasai N, Tragoolpua K, Pingmuang P, Khunkaewla P, Moonsom S, Kasinrerk W, Lieber A, Tayapiwatana C: **Potent inhibition of OKT3-induced**

T cell proliferation and suppression of CD147 cell surface expression in HeLa cells by scFv-M6-1B9. *Immunobiology* 2009, **214**:410-421.
39. Tragoolpua K, Intasai N, Kasinrerk W, Mai S, Yuan Y, Tayapiwatana C: **Generation of functional scFv intrabody to abate the expression of CD147 surface molecule of 293A cells.** *BMC Biotechnol* 2008, **8**:5.
40. DaFonseca S, Blommaert A, Coric P, Hong SS, Bouaziz S, Boulanger P: **The 3-O-(3',3'-dimethylsuccinyl) derivative of betulinic acid (DSB) inhibits the assembly of virus-like particles in HIV-1 Gag precursor-expressing cells.** *Antiviral Ther* 2007, **12**:1185-1203.
41. Granio O, Porcherot M, Corjon S, Kitidee K, Henning P, Eljaafari A, Cimarelli A, Lindholm L, Miossec P, Boulanger P, *et al*: **Improved adenovirus type 5 vector-mediated transduction of resistant cells by piggybacking on CAR-pseudotyped baculovirus.** *J Virol* 2009, **83**:6048-6066.
42. Fournier C, Cortay J-C, Carbonnelle C, Ehresmann C, Marquet R, Boulanger P: **The HIV-1 Nef protein enhances the affinity of reverse transcriptase for RNA in vitro.** *Virus Genes* 2002, **25**:255-269.
43. Saurya S, Lichtenstein Z, Karpas A: **Characterization of gag gene of plasma HIV type 1 in combination therapy-treated AIDS patients with high viral load and stable CD4+ T cell counts.** *AIDS Res Hum Retroviruses* 2003, **19**:73-76.
44. Boudin M-L, Rigolet M, Lemay P, Galibert F, Boulanger P: **Biochemical and genetical characterization of a fiber-defective temperature-sensitive mutant of type 2 adenovirus.** *EMBO J* 1983, **2**:1921-1927.
45. Caillet-Boudin M-L, Lemay P, Boulanger P: **Functional and structural effects of an Ala-to-Val mutation in the adenovirus type 2 fibre.** *J Mol Biol* 1991, **217**:477-486.
46. LeDuc PR, Whiteley EM, Bao G, Betenbaugh MJ: **Investigating the secretory pathway of the baculovirus-insect cell system using a secretory green fluorescent protein.** *Biotechnol Prog* 2000, **16**:716-723.
47. Demangel C, Zhouc J, Chood ABH, Shoebridge G, Hallidaye GM, Britton WJ: **Single chain antibody fragments for the selective targeting of antigens to dendritic cells.** *Mol Immunol* 2005, **42**:979-985.
48. Peipp M, Saul D, Barbin K, Bruenke J, Zunino SJ, Niederweis M, Fey GH: **Efficient eukaryotic expression of fluorescent scFv fusion proteins directed against CD antigens for FACS applications.** *J Immunol Methods* 2004, **285**:265-280.
49. Thomas JE, Massalski PR, Harrison BD: **Production of monoclonal antibodies to African cassava mosaic virus and differences in their reactivities with other whitefly-transmitted geminiviruses.** *J gen Virol* 1986, **67**:2739-2748.
50. Reavy B, Ziegler A, Diplexcito J, Macintosh SM, Torrance L, Mayo M: **Expression of functional recombinant antibody molecules in insect cell expression systems.** *Protein Expr Purif* 2000, **18**:221-228.
51. Laroche Y, Demaeyer M, Stassen J-M, Gansemans Y, Demarsin E, Matthyssens G, Collen D, Holvoet P: **Characterization of a recombinant single-chain molecule comprising the variable domains of a monoclonal antibody specific for human fibrin fragment D-dimer.** *J Biol Chem* 1991, **266**:16343-16349.
52. Grabherr R, Ernst W, Oker-Blom C, Jones I: **Developments in the use of baculoviruses for the surface display of complex eukaryotic proteins.** *Trends Biotechnol* 2001, **19**:231-236.
53. Hu YC: **Baculovirus vectors for gene therapy.** *Adv Virus Res* 2006, **68**:287-320.
54. Loisel TP, Ansanay H, St-Onge S, Gay B, Boulanger P, Strosberg AD, Marullo S, Bouvier M: **Recovery of homogeneous and functional beta 2-adrenergic receptors from extracellular baculovirus particles.** *Nat Biotechnol* 1997, **15**:1300-1304.
55. Belyakov IM, Berzofsky JA: **Immunobiology of mucosal HIV infection and the basis for development of a new generation of mucosal AIDS vaccine.** *Immunity* 2004, **20**:247-253.
56. De Francesco MA, Baronio M, Fiorentini S, Signorini C, Bonfanti C, Poiesi C, Popovic M, Grassi M, Garrafa E, Bozzo L, *et al*: **HIV-1 matrix protein p17 increases the production of proinflammatory cytokines and counteracts IL-4 activity by binding to a cellular receptor.** *Proc Natl Acad Sci USA* 2002, **99**:9972-9977.
57. Matsudaira H, Asakura T, Aoki K, Searashi Y, Matsuura T, Nakajima H, Tajiri H, Ohkawa K: **Target chemotherapy of anti-CD147 antibody-labeled liposome encapsulated GSH-DXR conjugate on CD147 highly expressed carcinoma cells.** *Int J Oncol* 2010, **36**:77-83.
58. Du Z-M, Hu C-F, Shao Q, Huang M-Y, Kou C-W, Zhu X-F, Zeng Y-X, Shao J-Y: **Upregulation of caveolin-1 and CD147 expression in nasopharyngeal carcinoma enhanced tumor cell migration and correlated with poor prognosis of the patients.** *Int J Cancer* 2009, **125**:1832-1841.
59. Han ZD, Bi XC, Qin WJ, He HC, Dai QS, Zou J, Ye YK, Liang YX, Zeng GH, Chen ZN, *et al*: **CD147 expression indicates unfavourable prognosis in prostate cancer.** *Pathol Oncol Res* 2009, **15**:369-374.
60. Tan H, Ye K, Wang Z, Tang H: **CD147 expression as a significant prognostic factor in differentiated thyroid carcinoma.** *Transl Res* 2008, **152**:143-149.
61. Yoon YW, Kwon HM, Hwang KC, Choi EY, Hong BK, Kim D, Kim HS, Cho SH, Song KS, Sangiorgi G: **Upstream regulation of matrix metalloproteinase by EMMPRIN; extracellular matrix metalloproteinase inducer in advanced atherosclerotic plaque.** *Atherosclerosis* 2005, **180**:37-44.
62. Gou X, Ru Q, Zhang H, Chen Y, Li L, Yang H, Xing J, Chen Z: **HAb18G/CD147 inhibits starvation-induced autophagy in human hepatoma cell SMMC7721 with an involvement of Beclin 1 down-regulation.** *Cancer Sci* 2009, **100**:837-843.
63. Peden K, Emerman M, Montagnier L: **Changes in growth properties on passage in tissue culture of viruses derived from infectious molecular clones of HIV-1LAI, HIV-1MAL, and HIV-1ELI.** *Virology* 1991, **185**:661-672.
64. Sanchez-Merino V, Nie S, Luzuriaga K: **HIV-1-specific CD8+ T cell responses and viral evolution in women and infants.** *J Immunol* 2005, **175**:6976-6986.
65. Nagai H, Wada K, Morishita T, Utsumi M, Nishiyama Y, Kaneda T: **New estimation method for highly sensitive quantitation of human immunodeficiency virus type 1 DNA and its application.** *J Virol Methods* 2005, **124**:157-165.
66. Adachi A, Gendelman HE, Koenig S, Folks T, Willey R, Rabson A, Martin MA: **Production of acquired immunodeficiency syndrome-associated retrovirus in human and nonhuman cells transfected with an infectious molecular clone.** *J Virol* 1986, **59**:284-291.

doi:10.1186/1472-6750-10-80
Cite this article as: Kitidee *et al.*: Baculovirus display of single chain antibody (scFv) using a novel signal peptide. *BMC Biotechnology* 2010 **10**:80.

JOURNAL OF VIROLOGY, June 2009, p. 6048–6066 Vol. 83, No. 12
0022-538X/09/$08.00+0 doi:10.1128/JVI.00012-09

Improved Adenovirus Type 5 Vector-Mediated Transduction of Resistant Cells by Piggybacking on Coxsackie B-Adenovirus Receptor-Pseudotyped Baculovirus▽

Ophélia Granio,[1]† Marine Porcherot,[1]† Stéphanie Corjon,[1] Kuntida Kitidee,[1,2] Petra Henning,[3] Assia Eljaafari,[4] Andrea Cimarelli,[5] Leif Lindholm,[6] Pierre Miossec,[4] Pierre Boulanger,[1,7] and Saw-See Hong[1]*

Université Lyon I, Laboratoire de Virologie et Pathologie Humaine, CNRS FRE 3011, Faculté de Médecine Claude Bernard and IFR Laennec, 7, rue Guillaume Paradin, 69372 Lyon, France[1]; Division of Clinical Immunology, Faculty of Associated Medical Sciences, Chiang Mai University, Chiang Mai, 50200 Thailand[2]; Institute for Biomedicine, Department of Microbiology and Immunology, University of Göteborg, P.O. Box 435, SE 40530 Göteborg, Sweden[3]; Department of Immunology and Rheumatology, Hôpital Edouard Herriot, 69437 Lyon, France[4]; LaboRetro, Department of Human Virology, Ecole Normale Supérieure de Lyon, INSERM U 758, Université Lyon I, IFR128 BioSciences Lyon-Gerland, Lyon-Biopole, 46, Allée d'Italie, 69364 Lyon, France[5]; Got-A-Gene AB, Östra Kyviksvägen 18, SE 42930 Kullavik, Sweden[6]; and Laboratoire de Virologie Médicale, Centre de Biologie Est, Hospices Civils de Lyon, 59, Boulevard Pinel, 69677 Bron, France[7]

Received 5 January 2009/Accepted 27 March 2009

Taking advantage of the wide tropism of baculoviruses (BVs), we constructed a recombinant BV (BV^{CAR}) pseudotyped with human coxsackie B-adenovirus receptor (CAR), the high-affinity attachment receptor for adenovirus type 5 (Ad5), and used the strategy of piggybacking Ad5-green fluorescent protein (Ad5GFP) vector on BV^{CAR} to transduce various cells refractory to Ad5 infection. We found that transduction of all cells tested, including human primary cells and cancer cell lines, was significantly improved using the BV^{CAR}-Ad5GFP biviral complex compared to that obtained with Ad5GFP or BV^{CAR}GFP alone. We determined the optimal conditions for the formation of the complex and found that a high level of BV^{CAR}-Ad5GFP-mediated transduction occurred at relatively low adenovirus vector doses, compared with transduction by Ad5GFP alone. The increase in transduction was dependent on the direct coupling of BV^{CAR} to Ad5GFP via CAR-fiber knob interaction, and the cell attachment of the BV^{CAR}-Ad5GFP complex was mediated by the baculoviral envelope glycoprotein gp64. Analysis of the virus-cell binding reaction indicated that the presence of BV^{CAR} in the complex provided kinetic benefits to Ad5GFP compared to the effects with Ad5GFP alone. The endocytic pathway of BV^{CAR}-Ad5GFP did not require Ad5 penton base RGD-integrin interaction. Biodistribution of BV^{CAR}-Ad5Luc complex in vivo was studied by intravenous administration to nude BALB/c mice and compared to Ad5Luc injected alone. No significant difference in viscerotropism was found between the two inocula, and the liver remained the preferred localization. In vitro, coagulation factor X drastically increased the Ad5GFP-mediated transduction of CAR-negative cells but had no effect on the efficiency of transduction by the BV^{CAR}-Ad5GFP complex. Various situations in vitro or ex vivo in which our BV^{CAR}-Ad5 duo could be advantageously used as gene transfer biviral vector are discussed.

Adenoviruses (Ads) are extensively used today as gene transfer vectors for in vitro, ex vivo, and in vivo gene transfer protocols (reviewed in reference 65). Cell entry of human Ad type 5 (Ad5), the serotype most widely used as a gene vector, occurs most efficiently by the receptor-mediated endocytosis pathway (reviewed in references 64 and 65), via the coxsackievirus B-adenovirus receptor (CAR) (3, 77) and αvβ3/αvβ5 integrins (84, 85), although alternative receptors have been described (11, 12, 14, 27). Cell surface expression of CAR differs with different cell types, and this represents one of the major determinants of the efficiency of Ad5-mediated transduction (43). The ubiquitous nature of CAR is responsible for transduction of nontarget tissues by Ad vectors. Paradoxically, many target cells such as dermal fibroblasts, synoviocytes, mesenchymal stem cells (MSCs), peripheral blood mononuclear cells (PBMCs), and dendritic cells (DCs), express no or very low levels of CAR at their surface and are relatively resistant to Ad transduction (14, 15, 19). Much work has been done with different strategies to promote the entry of Ad5 into CAR-defective cells. These strategies include (i) the genetic modification of Ad capsid proteins to carry cell ligands (2, 15, 20, 28, 49, 50), (ii) pseudotyping Ad5 vectors with fibers from other serotypes (13, 57, 74, 86), (iii) using bispecific adapters or peptides (25, 40), (iv) chemical modification of Ad (9, 42), and (v) tethering on nanoparticles (7). The limitations to these strategies are that modifications of the Ad capsid are susceptible to negatively affecting the virus growth or viability, due to an alteration of virion assembly,

* Corresponding author. Mailing address: Laboratoire de Virologie et Pathologie Humaine, CNRS FRE 3011, Faculté de Médecine and IFR Laennec, 7, rue Guillaume Paradin, 69372 Lyon, France. Phone: (33) 4 7877 8621. Fax: (33) 4 7877 8751. E-mail: sawsee.hong@sante.univ-lyon1.fr.
† These authors contributed equally to this work.
▽ Published ahead of print on 8 April 2009.

stability, the viral uncoating process, and/or intracellular trafficking (13, 51).

Other viruses which are gaining popularity as gene transfer vectors are the baculoviruses (BVs). *Autographa californica* multiple nucleopolyhedrosis virus (AcMNPV) is an insect virus with a large double-stranded DNA genome packaged in a membrane-enveloped, rod-shaped protein capsid (70). Since the 1980s, the BV-insect cell expression system has been highly exploited for the production of recombinant proteins. In the mid-1990s, it was shown that recombinant BVs carrying reporter genes under cytomegalovirus (CMV) or retroviral Rous sarcoma virus promoter efficiently expressed reporter genes in mammalian cells (6, 22, 38, 41, 44, 69), as well as in avian cells (72) and fish cells (45). Since then, BVs have been reported to transduce numerous cells originating from species as various as humans, bovines, and fish (8, 32, 41, 73). As gene transfer vectors, BVs have been found to be rapidly inactivated by human serum complement (23), but exposing decay-accelerating factor (DAF) at the surface of BV by fusion with the baculoviral envelope glycoprotein can overcome this inactivation (33). BVs also have a good biosafety profile due to their incapacity to replicate in mammalian cells (31).

Taking advantage of the ability of BVs to transduce a large repertoire of cells of invertebrate and vertebrate origins, including human primary cells, we investigated whether a recombinant AcMNPV could act as a carrier or macroadapter for Ad5 vectors to enter Ad5-refractory cells. To this aim, we pseudotyped AcMNPV virions with the high-affinity receptor for Ad5, the human CAR glycoprotein (BV^{CAR}), to enable the formation of complexes between vector particles of BV^{CAR} and Ad5-green fluorescent protein (Ad5GFP) mediated by Ad5 fiber and CAR interaction. We found that transduction of cell lines which were poorly permissive to Ad5, including human cancer cells and primary cells, was significantly improved using this strategy of piggybacking Ad5 vector on BV^{CAR}. More importantly, the increase in BV^{CAR}-Ad5-mediated transduction was obtained with a low range of Ad5 inputs, i.e., at multiplicities of infection (MOI) of less than 50 Ad5 vector particles per cell. We also found that the cell transduction enhancement observed with BV^{CAR}-Ad5 required the direct coupling of Ad5 to BV^{CAR} via fiber-CAR binding and that the cell attachment of the complex was mediated by the baculoviral envelope glycoprotein gp64. Kinetic analysis of virus-cell binding showed that the presence of BV^{CAR} in the complex was beneficial to Ad5 vector, not only in terms of tropism but also in terms of number of cell-bound virions and rate of cell attachment. In addition, the endocytic pathway of BV^{CAR}-Ad5 did not require Ad5 penton base RGD-integrin interaction. When administered in vivo to nude BALB/c mice, BV^{CAR}-Ad5 complex showed the same biodistribution as that of control Ad5 vector injected alone. In vitro, transduction of CAR-negative cells by BV^{CAR}-Ad5 was insensitive to coagulation factor X (FX), in contrast to Ad5 vector alone.

Our novel strategy of gene delivery using the BV^{CAR}-Ad5 duo could be advantageously applied to various situations in vitro or ex vivo, e.g., for transducing Ad5-refractory cells when Ad5 capsid modifications cannot be envisaged, when oncolytic Ads need to be delivered to tumors via nonpermissive cell carriers belonging to the immune system, or when the simultaneous delivery of two transgenes by two separate vectors might be beneficial in terms of timing and/or level of cellular expression of the transgene products.

MATERIALS AND METHODS

Cells. (i) Cell lines. *Spodoptera frugiperda* (Sf9) cells were maintained as monolayers at 28°C in Grace's insect medium supplemented with 10% fetal bovine serum (FBS) and antibiotics (Invitrogen). Chinese hamster ovarian cells (CHO), human embryonic kidney cells (HEK-293), human rhabdomyosarcoma cells (RD), human ovarian carcinoma cells (SKOV3), and human breast carcinoma cells (SKBR3) were purchased from the American Type Culture Collection (ATCC, Manassas, VA) and grown in Iscove's medium supplemented with 10% FBS and 50 mg/ml gentamicin (Invitrogen). CAR-expressing CHO cells (CHO-CAR) were obtained from J. Bergelson (3).

(ii) Primary cells. Human synoviocytes were obtained from synovial tissue from rheumatoid arthritis patients undergoing joint surgery. Human dermal fibroblasts were obtained from the skin of a patient undergoing joint surgery for osteoarthritis. Both synoviocytes and dermal fibroblasts were isolated by enzyme digestion and cultured in Dulbecco modified Eagle medium supplemented with 10% FBS and antibiotics (76) and were used between passages 4 and 9. Human MSC cultures were established using the French National protocol of the SFGM-TC Society. Briefly, bone marrow aspirates were obtained from the posterior iliac crest of healthy donors after their consent was given, and bone marrow mononuclear cells were isolated by Ficoll density gradient centrifugation (Lymphoprep; Abcys, Veyrier-du-Lac, France). Mononuclear cells (2.5×10^5/ml) were seeded in α-minimal essential medium (Gibco BRL, Paisley, United Kingdom) supplemented with 10% FBS, 2 mM L-glutamine, and 100 U/ml penicillin-streptomycin. Cells were allowed to adhere for 48 h followed by the removal of nonadherent cells. Medium and nonadherent cells were removed every 3 days thereafter. When culture was confluent, adherent cells were detached using trypsin and reseeded into a new flask, for expansion. At the third passage, MSCs were identified by immunophenotypic criteria based on the expression of CD73, CD90, and CD105 and the absence of expression of CD45, CD34, CD14, CD19, and HLA-DR before use (46). Monocyte-derived human DCs were obtained as follows. Immature DCs were differentiated from primary monocytes obtained from PBMCs of healthy donors upon incubation for 4 to 6 days with 100 ng/ml of interleukin 4 and granulocyte-macrophage colony-stimulating factor, as previously described (16). Both interleukin 4 and granulocyte-macrophage colony-stimulating factor were from R&D. Cells were maintained in complete RPMI 1640 medium supplemented with 10% fetal calf serum (BioWest). All experiments using human primary cells were performed in accordance with ethical guidelines and regulations and received approval from the Institutional Review board of the Laennec School of Medicine.

Human Ads and BVs. Replication-deficient Ad5 vectors (E1 deleted) expressing GFP (Ad5GFP) under the CMV promoter were propagated in HEK-293 cells. The penton base mutant Ad5EGD-GFP, encoding GFP and carrying an RGD-to-EGD alteration at position 340 in the penton base coding sequence, has been described elsewhere (13, 83). The fiber mutant Ad5GFP-R7ΔKnob, carrying a short shafted fiber with seven repeats (R7) and complete deletion of the knob (ΔKnob), has been described in detail in previous studies (20, 28, 50, 51). Ad5Luc, expressing the luciferase gene in the deleted E3 region of the Ad5 genome under the control of the simian virus 40 promoter, was obtained from Frank Graham (University of Ontario, Hamilton, Ontario, Canada) and described in previous studies (27, 56). Ad stocks were purified by CsCl gradient ultracentrifugation by conventional methods (13). The recombinant AcMNPV expressing CAR (BV^{CAR}) was constructed by cloning the human full-length CAR gene DNA into the NheI and KpnI cloning sites of pBlueBac (Invitrogen) downstream to the polyhedrin promoter, as described in previous studies (36, 37). The CAR gene DNA was isolated by digestion of the pcDNA-hCAR1 plasmid (obtained from Kerstin Sollerbrant, Karolinska Institutet, Stockholm, Sweden [71]) with NheI and KpnI. The recombinant BV expressing GFP under the CMV promoter (BV-GFP) was kindly provided by Norman Maitland (University of York at Heslington, York, United Kingdom). BV^{CAR} and BV-GFP were propagated by infection of Sf9 cells at a MOI of 1 to 2. Concentrated stocks of recombinant BV were prepared as follows. Infected cell supernatants were harvested at 48 to 60 h postinfection (p.i.), clarified by centrifugation at 2,400 rpm and 4°C for 10 min, and subjected to ultracentrifugation at 28,000 rpm for 1 h at 4°C through a 20% sucrose cushion. The viral pellet was resuspended by gentle shaking in sterile phosphate-buffered saline (PBS) overnight at 4°C, and further purified by isopycnic ultracentrifugation in a linear sucrose-D_2O gradient (10, 34). Gradients (10-ml total volume, 30 to 50% [wt/vol]) were generated from a 50% sucrose solution made in D_2O buffered to pH 7.2 with NaOH and a 30% sucrose solution made in 10 mM Tris-HCl, pH 7.2, 150 mM NaCl, 5.7 mM

Na_2-EDTA. The gradients were centrifuged for 18 h at 28,000 rpm in a Beckman SW41 rotor. Fractions (0.5 ml) were collected from the top, and proteins were analyzed by sodium dodecyl sulfate-polyacrylamide gel electrophoresis (SDS-PAGE) and Western blotting with the required antibodies. Baculovirions pseudotyped with CAR were produced by single infection of Sf9 cells with BV^{CAR} and isolated from infected cell culture supernatant as described above. Infectious titers of BV vector stocks were determined using the plaque assay on Sf9 cells.

Generation of BV^{CAR}- Ad5 complex. The infectivity index, defined as the ratio of infectious virions (determined by the plaque assay method and expressed as PFU per ml) to the total number of physical virus particles per ml (vp/ml), ranged from 1:100 to 1:500 for BVs (80), a value which was about 5- to 20-fold lower than that of Ad5, which was routinely about 1:20 to 1:30. The titer in physical vp of BV and Ad5 vectors was determined by absorbance measurement at 260 nm (A_{260}) of 1-ml samples of SDS-denatured virions (0.1% SDS for 1 min at 56°C) in a 1-cm-path-length cuvette, using the respective formulas A_{260} of $1.0 = 1.1 \times 10^{12}$ vp/ml for Ad5 (genomic DNA = 36 kbp) and A_{260} of $1.0 = 0.3 \times 10^{12}$ vp/ml for BV (genomic DNA = 134 kbp). Infectious titers of concentrated stocks of BV^{CAR} were usually 5×10^9 to 1×10^{10} PFU/ml, and the corresponding physical particle titers ranged between 1×10^{12} and 5×10^{12} vp/ml. Ad5GFP particle titers ranged from 1×10^{12} to 2×10^{12} vp/ml, with infectious titers between 2×10^{10} and 5×10^{10} PFU/ml. To generate BV^{CAR}-Ad5GFP complexes with different virus ratios, we considered only the respective titers in vp/ml. In standard experiments, samples of BV^{CAR} and Ad5GFP virions in 50 mM Tris-HCl (pH 8.0) buffer were mixed and adjusted to a total volume of 20 to 30 μl with the same buffer and then incubated for 1 h at 37°C.

Antibodies and proteins. Monoclonal anti-CAR antibody (clone E1.1 [19]) was obtained from Silvio Hemmi (University of Zürich, Zürich, Switzerland). The monoclonal anti-gp64 antibody clone AcV1 (Santa Cruz Biotechnology, Inc.) was used at a working dilution of 1:50 for immunoelectron microscopy. Mouse monoclonal antibody 7A7 directed against the fiber knob domain has been characterized in a previous study (27). Group-specific antihexon monoclonal antibody 4C3 was provided by W. C. Russell (University of St. Andrews, St. Andrews, Scotland) (29, 55, 66). Rabbit anti-Ad5 virion, anti-penton base, and antifiber were all laboratory made (13, 36, 37, 60). Human coagulation FX was purchased from Haematologic Technologies, Inc. (Essex Junction, VT) and used at the normal adult plasma concentration of 8 μg/ml. Adenoviral capsid proteins, hexon, fiber, and penton (base-plus-fiber) proteins were recovered from the pool of excess soluble Ad5 proteins present in Ad5-infected cell lysates used for vector stock preparations. Capsid proteins were purified to homogeneity according to a three-step procedure including ammonium sulfate precipitation and two chromatographic steps using high-performance liquid chromatography (BioLogic DuoFlow; Bio-Rad), as described in detail in previous studies (5, 58).

Cell transduction assays. Cells for transduction assays were prepared in 24-well plates containing 1×10^5 cells per well. Complexes of BV^{CAR} and Ad5GFP virions (BV^{CAR}-Ad5GFP) were prepared by preincubating appropriate volumes of each virus in a total volume of 300 μl of Dulbecco modified Eagle medium for 1 h at 37°C. The complexes were then added to the cells and incubated for an additional hour at 37°C, after which 200 μl prewarmed medium was added to each well. Cellular expression of GFP was observed at 36 h posttransduction, using an inverted microscope (Axiovert-135; Zeiss, Switzerland). Fluorescence images were taken using an AxioCam digital camera (Zeiss), analyzed using an Axio Vision program, and quantitated by flow cytometry analysis. For quantification, cells were fixed with 2% paraformaldehyde in PBS overnight and rinsed once with PBS and the proportion of GFP-positive cells was determined by fluorescence-activated cell sorting analysis (Dako Galaxy).

Real-time quantitative PCR. DNA was extracted from murine tissues using the QIAamp DNA blood minikit (Qiagen, Courtaboeuf, France). Ad5 genomes were assayed using the following fiber gene primers for real-time PCR (9): GCTACAGTTTCAGTTTTGGCTG (sense) and GTTGTGGCCAGACCAG TCCC (reverse). BV genomes were assayed using the following gp64 gene primers (1): ATGAGCAGACACGCAGCTTTT (sense) and GCTGAATGTG GGCAAAGAGG (reverse). The murine beta-actin gene was used as an internal control, with the following primers: GCTGTGTTCTTGCACTCCTTG (sense) and CGCACGATTTCCCTCTCAGC (reverse). Real-time PCR was performed using a LightCycler 480 (Roche Diagnostics, Meylan, France), and results were expressed as the number of viral genome copies per cell.

Electron microscopy. Virions of BV^{CAR} and BV^{CAR}-Ad5GFP complexes were diluted in 20 μl 0.14 M NaCl, 0.05 M Tris-HCl buffer, pH 8.2 (Tris-buffered saline [TBS]), and adsorbed onto carbon-coated Formvar membranes on grids. The grids were incubated with primary antibody (monoclonal anti-CAR or anti-gp64 antibody) at a dilution of 1:50 in TBS for 1 h at room temperature (RT). After being rinsed with TBS, the grids were postincubated with 20-nm colloidal gold-tagged goat anti-mouse immunoglobulin G (IgG) antibody (British Biocell International Ltd., Cardiff, United Kingdom; diluted to 1:50 in TBS) for 30 min at RT. After being rinsed with TBS, the specimens were negatively stained with 1% uranyl acetate in H_2O for 1 min at RT, rinsed again with TBS, and examined under a JEM 1400 JEOL electron microscope (EM) equipped with an Orius-Gatan digitalized camera (Gatan, Grandchamp, France).

Animal model. All procedures were performed on 5-week-old female BALB/c *nu/nu* mice (Charles River Laboratories, St. Germain sur l'Arbresle, France). Studies involving animals, including housing and care, method of euthanasia, and experimental protocols, were conducted in accordance with a code of practice established by the Experimentation Review Board from the Laennec School of Medicine. These studies were routinely inspected by the Attending Veterinarian to ensure continued compliance with the proposed protocols (63). Mice received intravenously in the tail vein 2×10^{10} vp of Ad5Luc per mouse (control animals) or BV^{CAR}-Ad5Luc complex formed in the ratio of 15 BV^{CAR} to 1 Ad5Luc (2×10^{10} vp of Ad5Luc and 3×10^{11} vp of BV^{CAR} per mouse). At 48 and 96 h after injection, the mice were anesthetized and injected subcutaneously with endotoxin-free luciferin (Luciferin-EF; Promega, Madison, WI) in PBS at 125 mg/kg of body weight, and 10 min later the whole-body bioluminescence was visualized using the NightOWL II LB 983 imaging system (Berthold Technologies GmbH, Bad Wildbad, Germany). After noninvasive whole-body imaging, the animals were sacrificed and the level of luciferase expression was assayed in different organs, using a Lumat LB 9507 luminometer (Berthold), as previously described (25, 27). Results were expressed as relative light units per mg of protein in the respective cell lysates.

RESULTS

Pseudotyping BV with human CAR glycoprotein: qualitative aspects. We constructed a recombinant BV expressing the full-length human CAR glycoprotein (BV^{CAR}) under the control of the polyhedrin promoter and determined whether progeny viruses produced from BV^{CAR}-infected cells carried the CAR glycoprotein on their envelope. Baculovirions released in the culture medium were concentrated by ultracentrifugation on a sucrose cushion and further purified by ultracentrifugation on a linear sucrose density gradient. The fractions at density 1.10 to 1.15 which contained the BV particles were pooled and analyzed by SDS-PAGE and Western blotting using anti-gp64 and anti-CAR antibodies. A discrete band of anti-CAR-reacting protein species migrating at 45 kDa (an apparent molecular mass consistent with that of CAR glycoprotein) was found to be associated with BV^{CAR} virions (Fig. 1a). This band was absent from the control, parental BV vector (AcMNPV-β-Gal expressing bacterial β-galactosidase). Baculovirions were then analyzed by immunoelectron microscopy, after deposition on EM grids. EM grids were reacted with anti-CAR monoclonal antibody, followed by a secondary antibody coupled to 20-nm colloidal gold particles, and examined under the EM. Under our experimental conditions, most anti-CAR gold grains were found to be associated with virus particles of CAR-pseudotyped BV^{CAR}, and exceptionally so in the background (Fig. 1b and c). Most baculovirions carried a single gold grain (Fig. 1d and e) and occasionally two, three, or more gold grains (Fig. 1f and g). With control parental BV virions incubated in parallel with anti-CAR and immunogold-labeled secondary antibody, we observed only background labeling (not shown).

As CAR-CAR interactions contribute to the intercellular tight junctions (24, 82), we expected to find BV^{CAR}-BV^{CAR} complexes under the EM. This was the case, and pairwise associations of BV^{CAR} virions lying side by side were observed (Fig. 2A, subpanels a to d), although at a low frequency (≤5% of total BV^{CAR} virions examined). Interestingly, after anti-

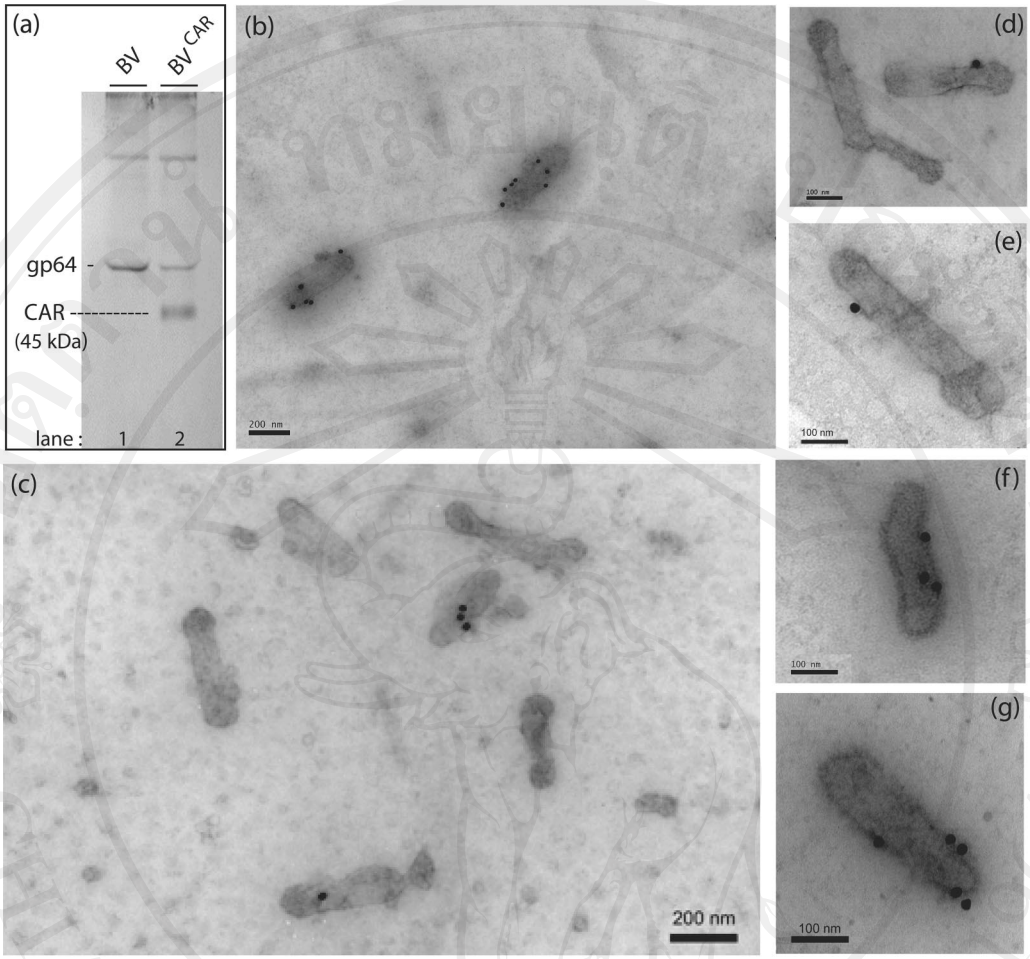

FIG. 1. Pseudotyping BV with human CAR glycoproteins. (a) Western blot analysis of control, parental (BV), and CAR-pseudotyped baculovirions (BV^{CAR}). BV (lane 1) and BV^{CAR} (lane 2) purified by ultracentrifugation were analyzed by SDS-PAGE and immunoblotting, using anti-gp64 and anti-CAR monoclonal antibodies and anti-mouse IgG conjugate. (b to g) Immuno-EM analysis. Virion samples deposited on grids were negatively stained with uranyl acetate and then reacted with monoclonal antibody against CAR, followed by anti-mouse antibody tagged with 20-nm colloidal gold. (b and c) General views of immunogold-stained BV^{CAR} preparations. Note the immunogold labeling associated with BV^{CAR} virions and the low level of background labeling. (d to g) Enlargement of anti-CAR gold-labeled BV^{CAR} virions. The number of grains associated per virion ranged from 0 (c and d) to 7 (b), with the highest frequency at 1, as shown in panels d and e.

CAR immunogold labeling of the BV^{CAR} samples adsorbed on grids, gold grains were often seen at the zone of contact between the two virions (Fig. 2A, subpanels a to d), suggesting that the BV^{CAR}-BV^{CAR} complexes occurred via true CAR-CAR interactions.

Efficiency of CAR pseudotyping of BV: quantitative aspects. The efficiency of pseudotyping of baculovirions by the foreign CAR glycoprotein was evaluated in comparison to the viral envelope glycoprotein gp64, a structural component of the virion called peplomer (70). Samples of BV^{CAR} virions were reacted on grids with a monoclonal antibody against gp64, followed by 20-nm colloidal gold-labeled anti-mouse IgG antibody, and examined under the EM. We found that most gold labeling localized near the head of the baculovirion (Fig. 2B), as expected from the gp64 topology (70).

The numbers of anti-gp64 and anti-CAR gold grains per virus particle were then counted in a population of 70 to 100 individual baculovirions. In our anti-gp64 labeling experiments, ca. 15% of baculovirions carried no grain, implying that this percentage represented the experimental threshold of detection for the baculoviral envelope glycoprotein gp64. For anti-CAR labeling, the number of unlabeled baculovirions was not significantly different and ranged from 16 to 23% (Fig. 3a). In both types of labeling, the most abundant population consisted of baculovirions carrying a single gold grain. Baculovirions with two, three, or more grains were found in both types of labeling, although at a significantly lower frequency (Fig. 3a; also Fig. 1 and 2). Taken together, these results indicated (i) that recombinant BV expressing CAR produced viral progeny pseudotyped by CAR glycoproteins and (ii) that the immunogold labeling (and hence the accessibility) of foreign CAR molecules on the BV^{CAR} envelope was almost as efficient as that of the structural gp64 glycoproteins.

Topology of CAR molecules at the surface of BV^{CAR} virions. To analyze the topology of gp64 and CAR molecules on the baculoviral envelope, we arbitrarily divided the baculovirions into 100 map units (mu) and measured the distance between the center of a 20-nm gold grain and the tip of the virus head.

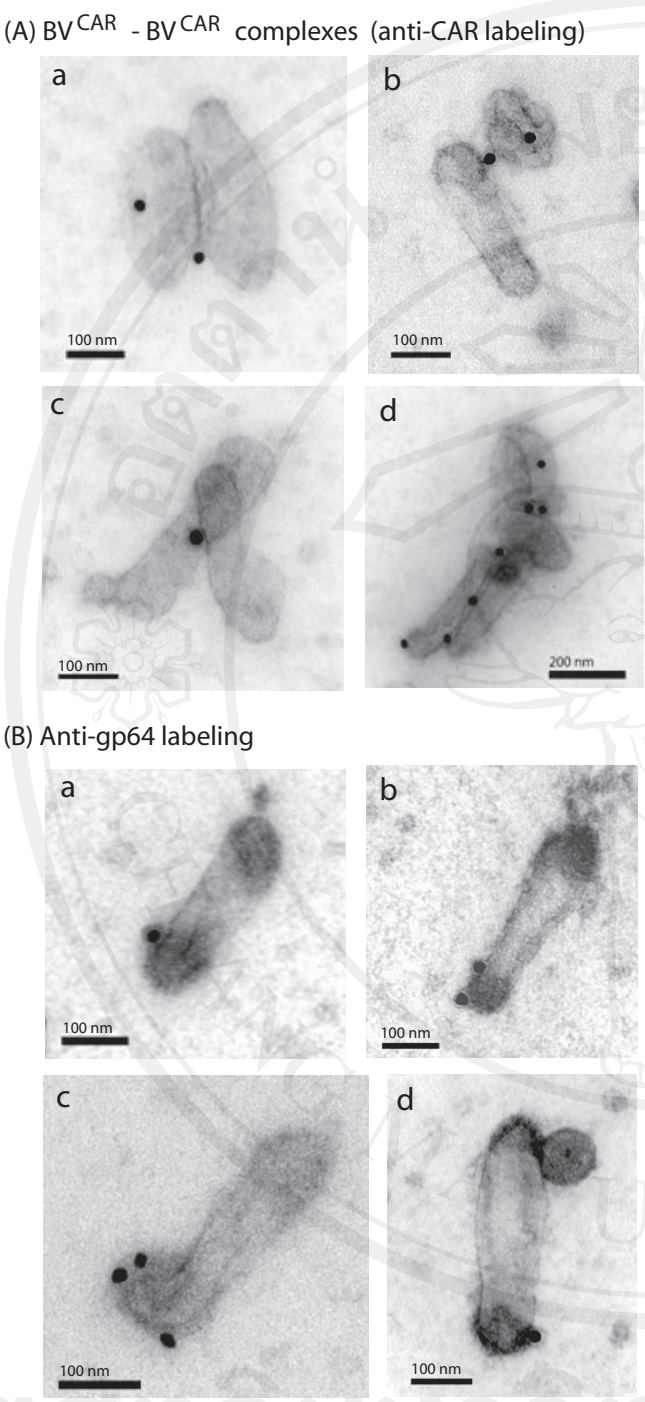

FIG. 2. EM and immuno-EM of BV^{CAR}. (A) Occurrence of BV^{CAR}-BV^{CAR} complexes. Samples of CAR-pseudotyped baculovirions (BV^{CAR}) were deposited on grids, negatively stained with uranyl acetate, and then reacted with monoclonal antibody against CAR, followed by anti-mouse antibody tagged with 20-nm colloidal gold, as in Fig. 1. Shown are spontaneously occurring pairwise (a to c) or multiple (d) associations of BV^{CAR} virions. (B) Anti-gp64 immunogold labeling of CAR-pseudotyped baculovirions. (a to c) BV^{CAR} virions deposited on grids were negatively stained with uranyl acetate and then reacted with monoclonal antibody against peplomer gp64, followed by anti-mouse antibody tagged with 20-nm colloidal gold grains. (d) Same reaction as in panels a to c performed on BV^{CAR}-Ad5GFP complexes deposited on grids. Note that gp64 and Ad5GFP virions are positioned at opposite poles of the baculovirion.

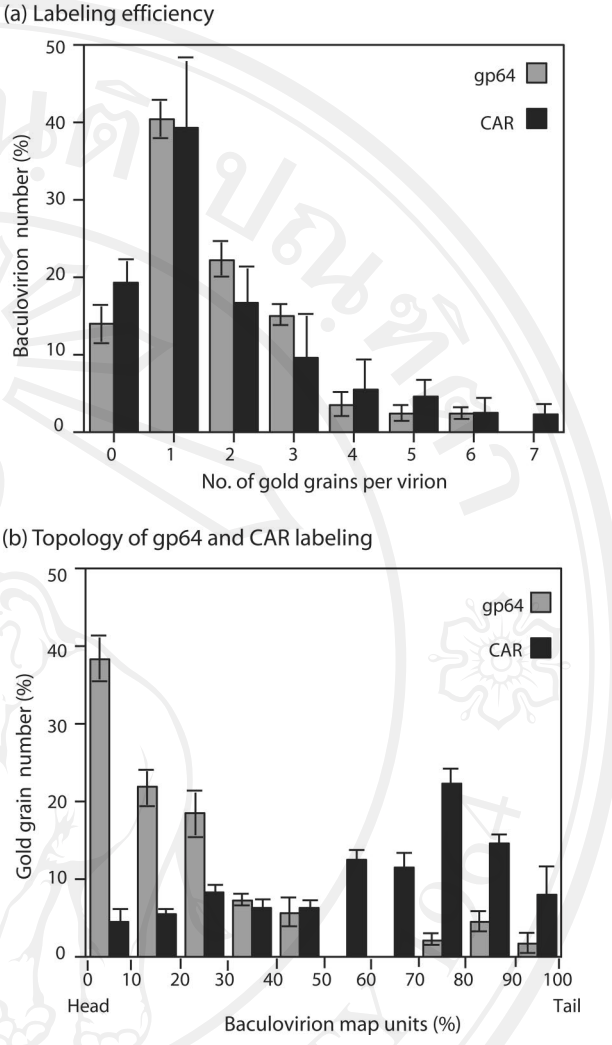

FIG. 3. Immunogold labeling of BV^{CAR}. (a) Comparison of the labeling efficiency of BV^{CAR} samples using anti-gp64 or anti-CAR monoclonal antibodies. The number of anti-gp64 and anti-CAR gold grains was counted per BV^{CAR} particle, in a population of 70 to 100 virions. (b) Topology of gp64 and CAR molecules on the baculoviral envelope, as determined by immunogold labeling. The position of gold grains on BV^{CAR} virions was determined by measuring the distance of the center of the gold grain to the tip of the virion head. Results were expressed as map units, defined as the percentage of the BV total length, which was assigned the 100% value. Shown are the means of three separate experiments ± SEMs.

In order to compensate for possible distortion and shrinking during the EM process, the results were expressed as the percentage of the full length of the virus (ca. 250 nm), with the virus head being taken as the origin (0%) and the end of the stem being assigned the 100% value. From our knowledge of BV structure (70), we could predict that most of the anti-gp64 gold grains would localize at or near the head of the baculovirions and not along their stem structure. Our EM observations were consistent with this prediction: nearly 40% of all anti-gp64 gold grains counted were found within 0 to 10 mu and 25% were found between 10 and 20 mu (Fig. 3b). Thus, almost two-thirds of the anti-gp64 gold grains localized within 0 to 50 nm. Considering that the approximate size of an IgG molecule

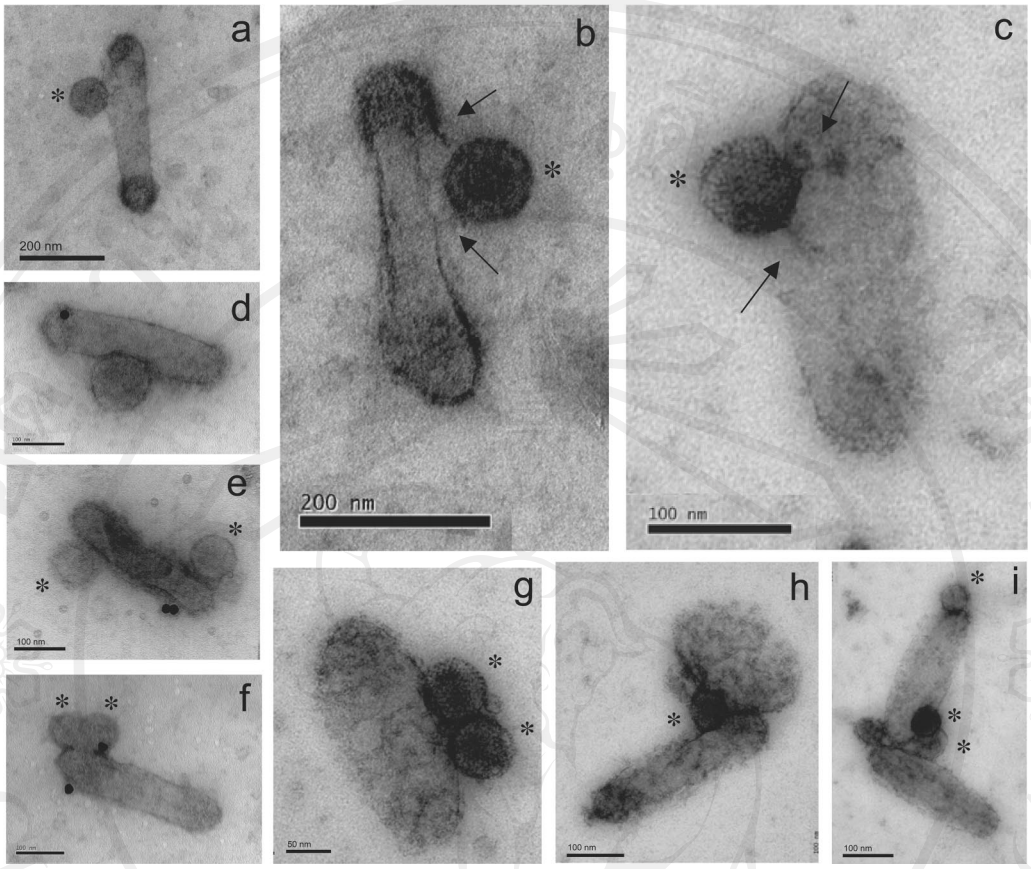

FIG. 4. EM and immuno-EM of BV^{CAR}-Ad5GFP complexes. BV^{CAR}-Ad5GFP complexes deposited on grids were negatively stained with uranyl acetate and examined under the EM (a to c and g to i) or further incubated with anti-CAR monoclonal antibody and 20-nm colloidal gold-tagged anti-mouse antibody (d to f), in order to test the anti-CAR reactivity of the BV^{CAR}-Ad5GFP complex. Ad5GFP virions are marked with asterisks. Panels a to d show BV^{CAR} virions associated with a single particle of Ad5GFP, whereas panels e to g show BV^{CAR} virions associated with two Ad5GFP particles. Panels b and c are enlargements of BV^{CAR}-Ad5GFP complexes showing filamentous structures connecting adenovirions to the baculoviral envelope (arrows). Note that CAR molecules were not all occupied by Ad5GFP virions, since anti-CAR antibodies still reacted with the complexes (d to f). Panels h and i show Ad5GFP virions bridging two BV^{CAR} virions.

is about 15 nm under the EM, the BV-associated primary and secondary antibodies accounted for 30 nm in length and the colloidal gold accounted for an extra 20 nm. The immuno-EM pattern of gp64 labeling was therefore compatible with the localization of the gp64 at the baculoviral pole. In contrast to gp64, the anti-CAR labeling showed a polydisperse pattern: anti-CAR gold grains were found all along the stem of the BV^{CAR} virions, with some preferential sites between 70 and 90 mu (Fig. 3b; also Fig. 1d to g). This suggested that the CAR molecules were excluded from the polar region of the baculoviral envelope in which the gp64 peplomers were inserted. This was confirmed by EM analyses of BV^{CAR}-Ad5GFP complexes, as shown (Fig. 4).

Functionality of human CAR attachment molecules on the baculoviral envelope: occurrence of BV^{CAR}-Ad5GFP complexes. We next determined whether CAR glycoproteins present at the surface of the baculovirion were functional as attachment molecules for Ad5. BV^{CAR} virions were mixed with the same number of Ad5GFP vector particles, incubated for 1 h at 37°C, and examined under the EM after negative staining. Different types of BV^{CAR}-Ad5GFP association were observed, but the most frequently seen consisted of binary complexes, or virus duos, composed of one baculovirion bound to one adenovirion (Fig. 4a to d). Ternary complexes, or virus trios, formed of one BV^{CAR} carrying two Ad5GFP were more rarely observed (Fig. 4e to g). Modifications of the particle ratio between BV^{CAR} and Ad5GFP in the incubation mixture did not change significantly this EM pattern (not shown).

In the majority of the BV^{CAR}-Ad5GFP binary complexes, the Ad particles were found to bind to the stem of BV^{CAR}, an observation consistent with the localization of CAR molecules on the BV^{CAR} envelope, as determined by our anti-CAR immunogold labeling (Fig. 3b). Since an adenovirion carries 12 fiber projections and is therefore multivalent in terms of attachment, we expected that Ad5GFP could bridge two or more BV^{CAR} particles. Such higher-order complexes were observed under the EM, although on rare occasions: they mainly consisted of ternary complexes formed of one Ad5GFP bound to two BV^{CAR} particles (Fig. 4h and i).

Examination of BV^{CAR}-Ad5GFP complexes under the EM at high resolution revealed that some adenovirions were linked to their BV carriers via filamentous structures which resembled the adenoviral fiber. In some cases, two filaments could be distinguished (Fig. 4b and c, arrows). This suggested that the

binding of Ad5GFP to CAR molecules could occur via more than one valence.

This observation raised the question of the degree of occupancy and/or accessibility of CAR molecules inserted in the baculoviral envelope. To address this issue, BV^{CAR}-Ad5GFP complexes were reacted on grids with anti-CAR antibody followed by secondary 20-nm gold-tagged antibody, as described above. Many individual BV^{CAR} particles which were associated with one or two Ad5GFP particles were still labeled by anti-CAR and carried one (Fig. 4d) or several (Fig. 4e and f) gold grains. This indicated that when BV^{CAR}-Ad5GFP complexes were formed in a binding reaction involving equal numbers of the two viruses, several CAR molecules present at the BV^{CAR} surface were still unoccupied and available for anti-CAR antibody binding or CAR-CAR interaction. This was also suggested by the anti-CAR labeling of BV^{CAR}-BV^{CAR} complexes shown in Fig. 2A. Taken together, these results indicated that CAR functioned as a bona fide Ad5 attachment molecule at the surface of the baculovirions.

Transduction of CAR-negative CHO cells by BV^{CAR}-Ad5GFP complex. (i) Transduction efficiency. The functionality of our BV^{CAR}-Ad5GFP complex and the capacity of BV^{CAR} to mediate Ad5 gene delivery by overcoming the lack of CAR at the cell surface were first assessed on CHO cells, which are CAR negative and poorly permissive to Ad5 (3). The transduction level obtained with a BV^{CAR}-Ad5GFP complex generated with a ratio of Ad5GFP to BV^{CAR} vp (physical particles) of 1 to 10 in the mix was greatly enhanced, compared to Ad5GFP alone at a similar MOI of Ad5GFP vector (Fig. 5A, subpanels a and c). As quantified by flow cytometry, 65 to 70% of CHO cells were transduced by the BV^{CAR}-Ad5GFP complex at an MOI range of 100 to 500 in terms of Ad5GFP vp/cell, compared to 10 to 15% in control samples transduced by Ad5GFP alone at the same MOI (Fig. 5B, subpanel a).

(ii) Contribution of BV^{CAR} to the augmentation of Ad5-mediated transduction efficiency. The role of BV^{CAR} in the transduction enhancement by the complex was evaluated using BV^{CAR}GFP alone. BV^{CAR}GFP was a recombinant AcMNPV expressing the GFP gene under the control of the CMV promoter (the same promoter as that in Ad5GFP) and was pseudotyped with CAR by coinfection of Sf9 cells with BV^{CAR}. The level of CHO cell transduction obtained with BV^{CAR}GFP (Fig. 5A, subpanel b) was lower than that with the BV^{CAR}-Ad5GFP complex but higher than that with Ad5GFP at the same MOI (Fig. 5A, subpanels c and a, respectively). This suggested that both viruses contributed to the enhancing effect on transduction by the virus duo but that BV^{CAR} contributed to a higher level than did Ad5GFP.

(iii) Specificity of transduction by BV^{CAR}-Ad5GFP complex. CHO-CAR is a CHO-derived cell line which constitutively expresses CAR and is fully susceptible to Ad5 infection (3). CHO-CAR cells were infected with BV^{CAR}-Ad5GFP, at a constant MOI of BV^{CAR} and various MOIs of Ad5GFP, or with Ad5GFP alone at the same MOI as that in the complex. At a low MOI (less than 50 vp/cell, corresponding to 2 to 5 PFU/cell), CHO-CAR cells were transduced with a slightly higher efficiency by BV^{CAR}-Ad5GFP than by Ad5GFP alone (1.5- to 2-fold; Fig. 5B, subpanel b), but this effect was no longer observed at a higher MOI (100 to 500 vp/cell; Fig. 5B, subpanel b). The absence of enhanced transduction of Ad5-permissive cells by the BV^{CAR}-Ad5GFP complex suggested that this effect was specific in nature.

(iv) Role of CAR glycoproteins in BV^{CAR}-mediated cell transduction. The AcMNPV envelope glycoprotein gp64 represents the major cell attachment component of this virus (59). Gp64 binds to insect cell plasma membrane receptors (70), as well as to a large repertoire of mammalian cell surface glycoproteins (31, 32, 41). In order to determine the respective roles of baculoviral gp64 and extrinsic CAR glycoprotein in the efficiency of cell transduction, CHO and CHO-CAR cells were incubated with the CAR-pseudotyped vector BV^{CAR}GFP at different MOIs. CHO-CAR cells were found to be significantly more permissive to BV^{CAR}GFP than were CHO cells (two- to threefold; Fig. 5C). This suggested that BV^{CAR}GFP could use different pathways to attach to and enter CHO cells, e.g., one involving gp64 and its cellular ligand(s) and the other mediated by interaction between BV-displayed CAR molecules and cell plasma membrane-exposed CAR. This was reminiscent of the CAR-CAR interaction suggested by the EM observation of dimers of CAR-pseudotyped baculovirions (Fig. 2A).

Transduction of CAR-negative human cells by BV^{CAR}-Ad5GFP complex. (i) Nontumor cell line. Human glandular tracheal cells (MM39) fail to express CAR and are poorly permissive to Ad5 (14, 15, 17). As was observed with CHO cells, a net augmentation of the transduction efficiency was obtained when MM39 cells were incubated with BV^{CAR}-Ad5GFP, compared to control MM39 samples transduced with a single vector at the same MOI, Ad5GFP or BV^{CAR}GFP (Fig. 6A).

(ii) Cancer cell lines. Gene transduction mediated by BV^{CAR}-Ad5GFP complexes was also evaluated on rhabdomyosarcoma cells (RD), ovarian carcinoma cells (SKOV3), and breast carcinoma cells (SKBR3), three human cancer cell lines which were poorly transduced by Ad5 (20). The efficacy of BV^{CAR}-Ad5GFP transduction was significantly higher than that of transduction with Ad5GFP alone for the three types of cancer cells (Fig. 6B). For RD cells, the percentage of transduced cells improved by almost 1 order of magnitude, from 5% with Ad5GFP to 45% with BV^{CAR}-Ad5GFP, and for SKOV3 cells, the augmentation was seven- to eightfold higher, from 2.5% (with Ad5GFP) to 21% (with BV^{CAR}-Ad5GFP). However, in the case of SKBR3 cells, which were slightly permissive to Ad5, the increase in transduction was only two- to threefold, from 12% (Ad5GFP) to 35% (BV^{CAR}-Ad5GFP). As for CHO and MM39 cells, the levels of transduction of RD and SKBR3 cells by the control vector BV^{CAR}GFP alone was intermediate between those of Ad5GFP and BV^{CAR}-Ad5GFP. Interestingly, the level of SKOV3 transduction was almost equivalent using BV^{CAR}-Ad5GFP and using BV^{CAR}GFP (Fig. 6B), confirming that the contribution of BV^{CAR} to the transduction enhancement by the BV^{CAR}-Ad5GFP complex was greater than that of Ad5GFP.

Transduction of human primary cells by BV^{CAR}- Ad5GFP complex. Several types of human primary cells have been reported to be refractory to or poorly transduced by Ad5 vectors, e.g., dermal fibroblasts and synoviocytes (76). These cells were transduced with aliquots of virus inoculum containing increasing MOIs of Ad5GFP mixed with a constant BV^{CAR} input (500 vp/cell) and analyzed by fluorescence microscopy and flow cytometry. For dermal fibroblasts, a progressive increase in transduction was observed with increasing MOIs of Ad5GFP, and the maximum transduction efficiency (82% GFP-positive

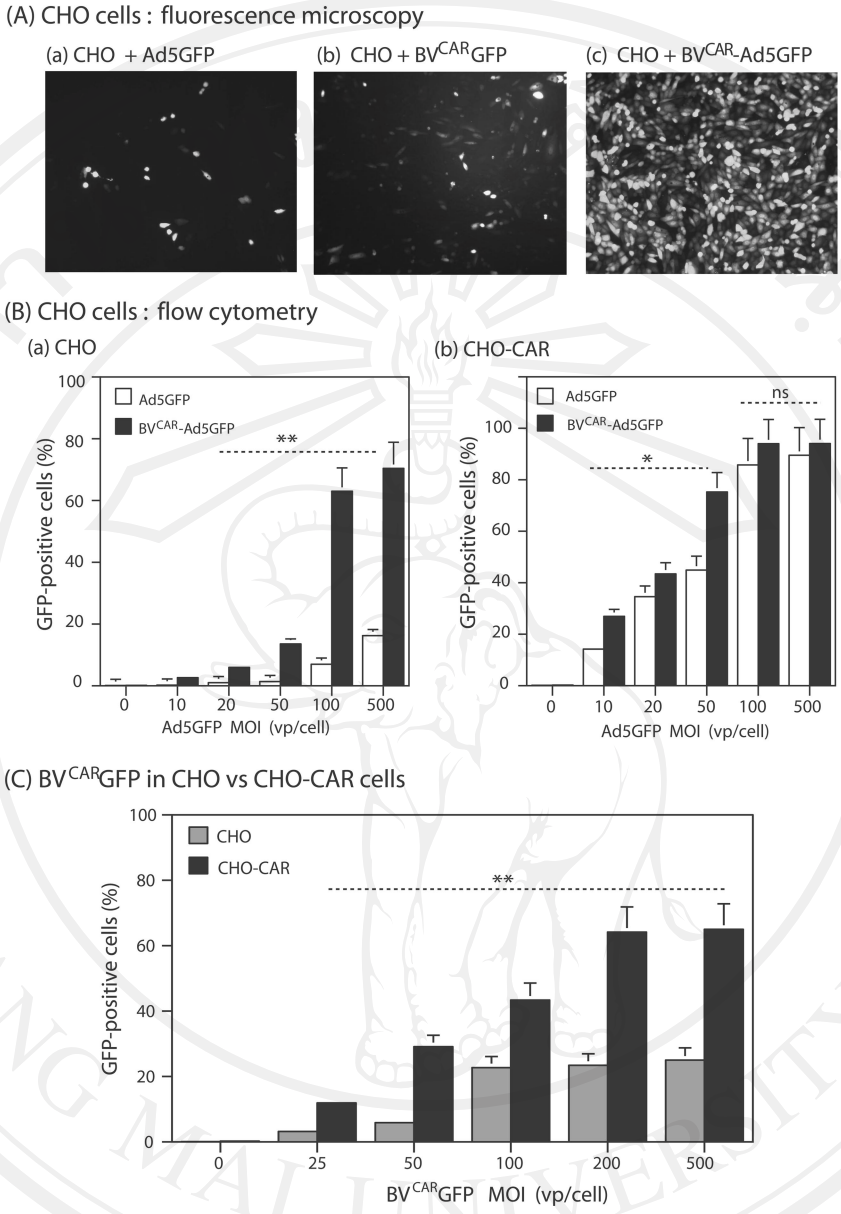

FIG. 5. Transduction of CAR-negative (CHO) or CAR-positive (CHO-CAR) cells by BV^{CAR}-Ad5GFP complex. (A) Fluorescent microscopy. CHO cells were transduced by Ad5GFP alone (MOI of 100 vp/cell) (a), BV^{CAR}GFP alone (1,000 vp/cell) (b), or BV^{CAR}-Ad5GFP complex (Ad5GFP MOI of 100 vp/cell; Ad5GFP/BV^{CAR} vp ratio of 1:10) (c). (B) Flow cytometry. Bar graph representation of the efficiency of transduction of CHO (a) or CHO-CAR (b) by Ad5GFP alone (open bars) or BV^{CAR}-Ad5GFP complex (solid bars). Complexes were generated by mixing a constant amount of BV^{CAR} (corresponding to 500 vp/cell) with increasing amounts of Ad5GFP, as indicated on the *x* axis. (C) Transduction efficiency of CHO cells by control vector BV^{CAR}GFP. Flow cytometry analysis of CHO cells (gray bars) or CHO-CAR cells (black bars) transduced by BV^{CAR}GFP alone at increasing MOIs, as indicated on the *x* axis. Results, expressed as the percentages of GFP-positive cells, represent the means of three separate experiments ± SEMs. *, $P < 0.05$; **, $P < 0.01$; ns, no significant difference.

cells) was reached at an Ad5GFP MOI of 20 vp/cell (Fig. 7a). Transduction of synoviocytes using BV^{CAR}-Ad5GFP complex was analyzed using the same range of viral complex inputs. Synoviocytes were moderately permissive to Ad5, and only 20% of cells were transduced at an Ad5GFP MOI of 20 vp/cell. However, a transduction of 80% of cells was obtained using the BV^{CAR}-Ad5GFP complex at the Ad5GFP dose of 20 vp/cell (Fig. 7b).

The efficiency of the BV^{CAR}-Ad5GFP complexes was also tested on human MSCs. MSCs were transduced to about 25 to 28% with BV^{CAR}-Ad5GFP, versus 2% with Ad5GFP alone at an MOI of 20, i.e., a 10-fold increase (Fig. 7c). In the case of immature monocyte-derived DCs, there was a moderate increase in transduction with BV^{CAR}-Ad5GFP (twofold), and the number of GFP-positive DCs plateaued at around 12 to 15% at the relatively high Ad5GFP MOI of 500 vp/cell (Fig. 7d). For PBMCs, the transduction levels were low, but the increase was significant, from 0.1% with Ad5GFP alone to 2%

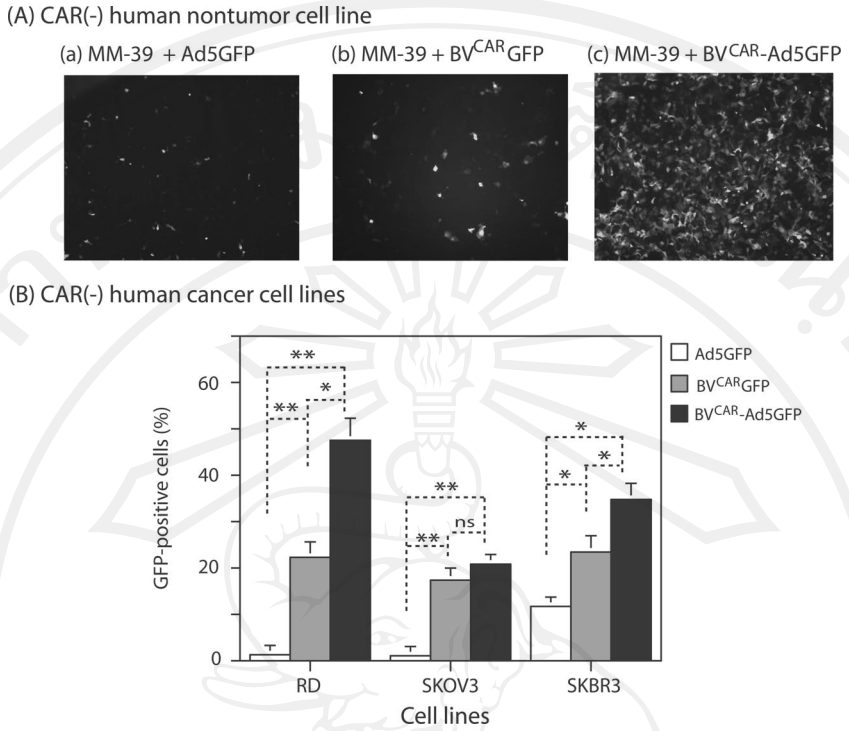

FIG. 6. Transduction of CAR-negative human cell lines by BV^{CAR}-Ad5GFP complex. (A) Nontumor cells. Fluorescent microscopy of MM39 cells transduced by Ad5GFP alone (MOI of 20 vp/cell) (a), BV^{CAR}GFP alone (500 vp/cell) (b), or BV^{CAR}-Ad5GFP complex (Ad5GFP MOI of 20 vp/cell; Ad5GFP/BV^{CAR} vp ratio of 1:25) (c). (B) Tumor cells. Flow cytometry analysis of human cancer cell lines RD, SKOV3, and SKBR3 transduced by Ad5GFP alone (20 vp/cell), BV^{CAR}GFP alone (500 vp/cell), or BV^{CAR}-Ad5GFP complex (Ad5GFP MOI of 20 vp/cell; Ad5GFP/BV^{CAR} vp ratio of 1:25). Results, expressed as the percentages of GFP-positive cells, represent the means of three separate experiments ± SEMs. *, $P < 0.05$; **, $P < 0.01$; ns, no significant difference.

with BV^{CAR}-Ad5GFP at an Ad5GFP MOI of 1,000 vp/cell (Fig. 7e). As for CHO, RD, and SKBR3 cells, the levels of transduction of the primary cells treated with control vector BV^{CAR}GFP was intermediate between those of Ad5GFP and BV^{CAR}-Ad5GFP (Fig. 7).

Requirements for BV^{CAR}- Ad5GFP complex formation and cell transduction enhancement. (i) Transduction efficiency versus ratio of BV^{CAR} to Ad5GFP particles. In order to determine the optimal conditions for cell transduction by the biviral complex, we prepared a range of BV^{CAR}-Ad5GFP mixtures differing in their ratios of BV^{CAR} to Ad5GFP vp and assayed their gene transfer efficiency on two types of primary cells, dermal fibroblasts and synoviocytes. In one set of transduction experiments, the number of BV^{CAR} vector particles was kept constant (500 vp/cell) and Ad5GFP MOI varied from 0.1 to 20 vp/cell. For both cell types, the level of transduction increased in an Ad5GFP dose-dependent manner and 80 to 85% of cells were found to be GFP positive at 20 vp/cell (Fig. 8a). In another set of experiments, Ad5GFP MOI was kept constant (20 vp/cell) whereas BV^{CAR} particles varied from 0 to 1,000 vp/cell (Fig. 8b). A plateau of maximum cell transduction (80 to 85% GFP-positive cells) was obtained for both cell types at a ratio of 20 Ad5GFP to 500 BV^{CAR} particles (Fig. 8b). Increasing the number of BV^{CAR} particles over this value did not augment the transduction efficiency (Fig. 8b).

A wider range of Ad5GFP to BV^{CAR} vp ratios was then tested, and the transduction efficiency was represented as a function of the vp ratio values (Fig. 8c). The bar graph representation followed the Gaussian mode, with the highest transduction efficiency obtained at a ratio of 100 BV^{CAR} to three Ad5GFP particles. We interpreted this value in terms of cell transduction as the result of several parameters influencing the cell transduction. These included (i) the occurrence of a certain number of CAR-negative BVs in the population of virus carrier, as shown above; (ii) the dissociation constant of the equilibrium reaction between free and BV^{CAR}-bound Ad5GFP in the mixture, which has not been experimentally determined for Ad5 virion and pseudotyped BV^{CAR}; and (iii) the cellular response to this viral duo. Unless otherwise stated, we generated BV^{CAR}-Ad5GFP complexes using vp ratios ranging from 20 BV^{CAR}:1 Ad to 30 BV^{CAR}:1 Ad.

(ii) Knob dependence of the Ad5GFP-BV^{CAR} liaison. In order to verify that the Ad5 virions present within the BV^{CAR}-Ad5GFP complexes bound to BV^{CAR} via their fiber knob domain, we transduced dermal fibroblasts with a mixture of BV^{CAR} (at a constant MOI of 500 vp/cell) and Ad5GFP-R7ΔKnob (at increasing MOIs). Ad5GFP-R7ΔKnob carried knob-deleted (ΔKnob) short-shafted fibers of seven repeats (R7) and lacked its CAR-binding domains (20, 28, 50, 51). No detectable enhancement of Ad5GFP-R7ΔKnob-mediated transduction was observed in the presence of BV^{CAR}, compared to Ad5GFP-R7ΔKnob alone, implying that the integrity of the knob domain was indispensable for the positive effect of BV^{CAR} on Ad5 transduction (Fig. 9a).

(iii) Requirement for CAR on the envelope of BV^{CAR}. The enhancement of Ad5GFP-mediated cell transduction in the

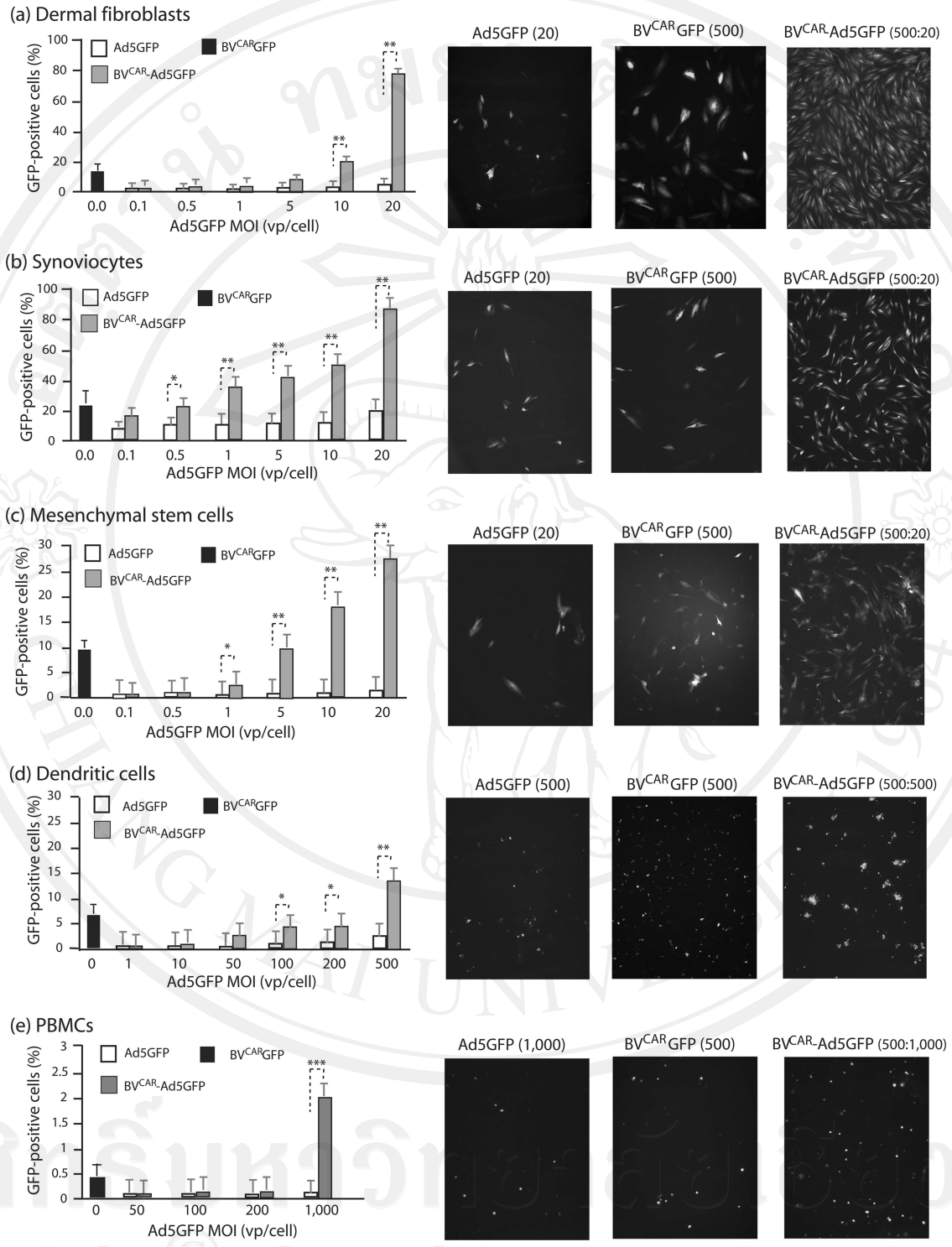

FIG. 7. Transduction of CAR-negative human primary cells by BV^{CAR}-Ad5GFP complex. Graphs on left show flow cytometry results. Bar graph representation of the efficiency of gene transfer mediated by Ad5GFP alone versus BV^{CAR}-Ad5GFP complex in different human primary cells, as indicated above each panel. Cells were transduced by Ad5GFP alone at increasing MOIs or by BV^{CAR}-Ad5GFP complexes at a constant MOI of BV^{CAR} (500 vp/cell) and increasing MOIs of Ad5GFP, as indicated on the *x* axis. Results, expressed as the percentages of GFP-positive cells, represent the means of three separate experiments ± SEMs. The black bars on the far left of the graphs represent the values obtained with the control baculoviral vector BV^{CAR}GFP alone, at an MOI of 500 vp/cell. The right panels show fluorescent microscopy results. Shown are cell samples transduced at the maximal infectivity of each separate vector or biviral complex, as indicated above each panel. Cells were transduced by Ad5GFP alone (left), BV^{CAR}GFP alone (middle), or BV^{CAR}-Ad5GFP complex (right). *, $P < 0.05$; **, $P < 0.01$; ***, $P < 0.005$.

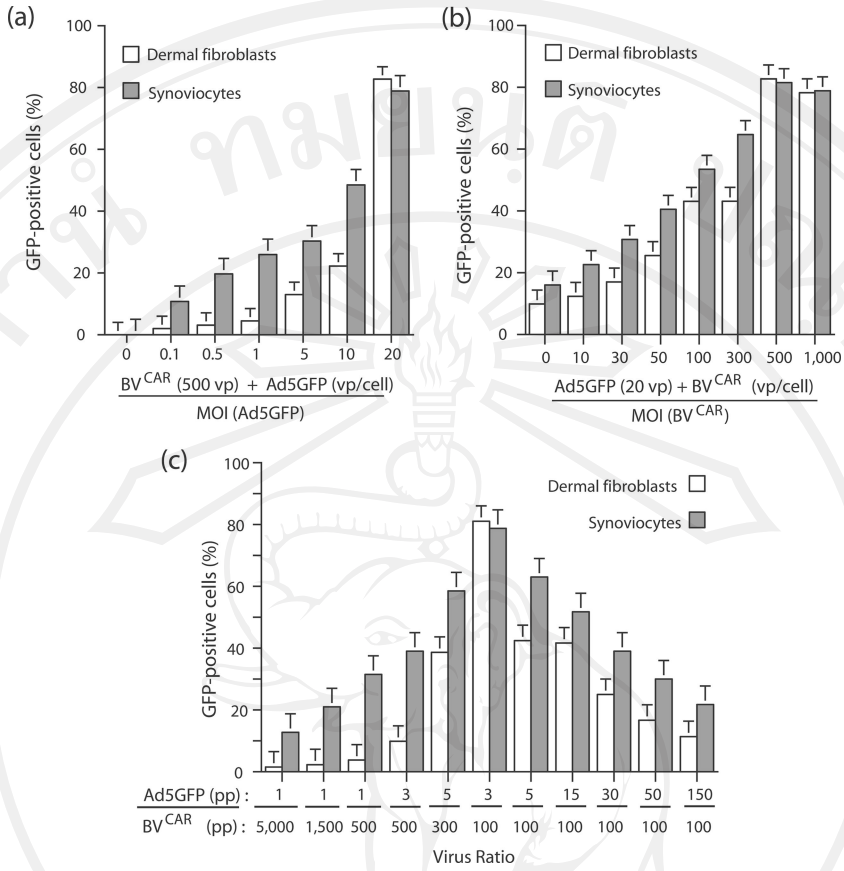

FIG. 8. Influence of BV^{CAR}-to-Ad5GFP ratios on BV^{CAR}-Ad5GFP-mediated transduction of human primary cells. (a) Dermal fibroblasts and synoviocytes were transduced by BV^{CAR}-Ad5GFP complex generated using a constant MOI of BV^{CAR} (500 vp/cell) and various MOIs of Ad5GFP, as indicated on the *x* axis. (b) Cells were transduced by BV^{CAR}-Ad5GFP complex generated using a constant MOI of Ad5GFP (20 vp/cell) and various MOIs of BV^{CAR}, as indicated on the *x* axis. (c) Cell transduction efficiency by BV^{CAR}-Ad5GFP complex was evaluated using a wide range of BV^{CAR}-to-Ad5GFP ratios. The transduction efficiency was expressed as the percentage of GFP-positive cells, assayed by flow cytometry (means of three separate experiments ± SEMs).

presence of BV^{CAR} might be due to a certain degree of nonspecific cellular engulfment of Ad5 vector in the presence of baculovirions and not to the formation of BV^{CAR}-Ad5GFP complex via specific CAR-fiber knob interaction. To address this issue, we mixed Ad5GFP at a constant MOI (10 vp/cell) with nonpseudotyped, parental vector BV at various doses (0, 250, and 500 vp/cell) and analyzed the transduction level of synoviocytes and dermal fibroblasts using the mixture of unbound viruses, in comparison with the transduction mediated by BV^{CAR}-Ad5GFP complexes generated with the same virus ratios. No significant effect on the level of cell transduction was observed with the mixtures of unbound viruses, compared to the corresponding BV^{CAR}-Ad5GFP complexes (Fig. 9b). This indicated that the enhancing effect on cell transduction by the complex depended on the presence of CAR molecules at the surface of the baculovirions and on CAR-mediated interaction with Ad5GFP.

(iv) Blockage of BV^{CAR}-Ad5GFP-mediated cell transduction by anti-CAR antibody. To further demonstrate the role of CAR glycoprotein in bridging Ad5GFP to BV^{CAR} in the dual virus mixture, we analyzed the effect of an anti-CAR monoclonal antibody on dermal fibroblast transduction. Anti-CAR antibody was added at different dilutions during (Fig. 9c) or after (Fig. 9d) the step of virus mixing, when CAR-fiber bonds had already formed. When anti-CAR antibody was added simultaneously to the viral mixture, inhibition of gene transfer was observed in a dose-response manner, and the basal level of transduction was reached in the presence of undiluted antibody sample (Fig. 9c). In contrast, when anti-CAR antibody was added after the mixing, no effect in Ad5 gene transfer was detected (Fig. 9d). These results confirmed the role of CAR in the generation of BV^{CAR}-Ad5GFP complex and its requirement for the cell transduction enhancement.

Mechanism of cellular uptake of BV^{CAR}-Ad5GFP complex. (i) Kinetics of cell binding and uptake of BV^{CAR}-Ad5GFP. There are several parameters, in addition to baculoviral tropism, that might lead to the superior transduction of CAR-negative cells by the dual vector BV^{CAR}-Ad5GFP. In order to investigate the possible kinetic benefits of this complex, CHO cells were incubated with Ad5GFP alone or BV^{CAR}-Ad5GFP complex at the same MOI in terms of Ad5GFP vector, and the number of cell-associated virions was determined at 10-min intervals during the first hour of virus-cell attachment, using real-time quantitative PCR. The number of Ad5 genome copies recovered per cell was found to be twofold higher for BV^{CAR}-Ad5GFP at all time points than for control Ad5GFP.

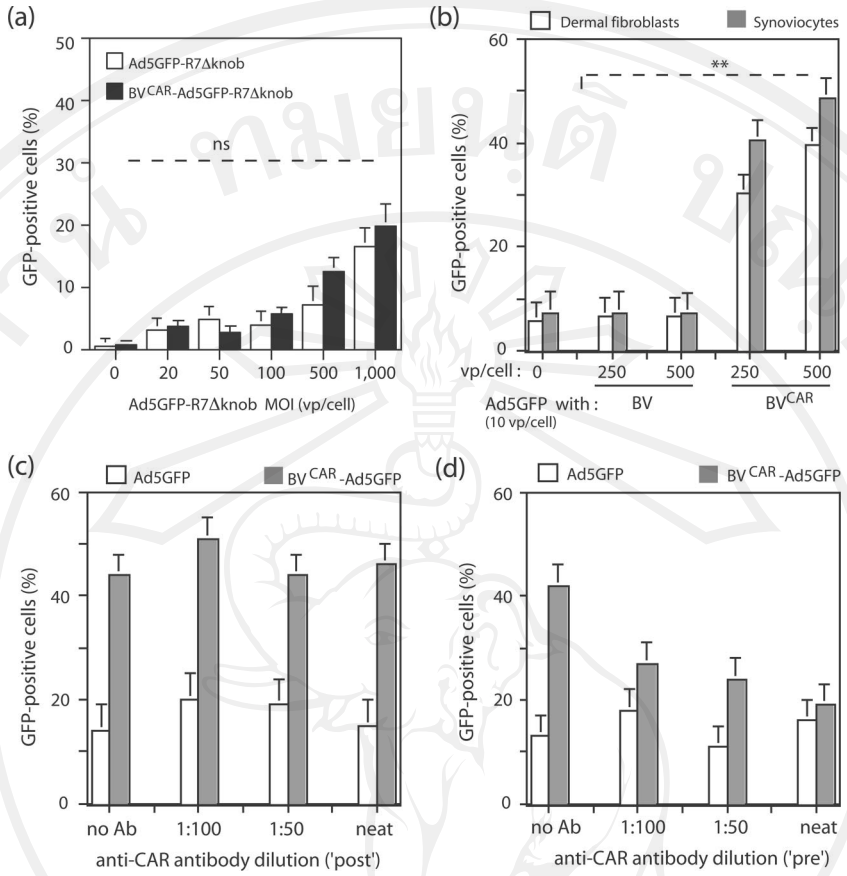

FIG. 9. Role of CAR and fiber knob in BV^{CAR}-Ad5GFP-mediated cell transduction. (a) Requirement for the fiber knob domain in Ad5GFP vector. Human dermal fibroblasts were transduced by Ad5GFP-R7ΔKnob alone at increasing MOIs or a mixture of BV^{CAR} at a constant MOI (500 vp/cell) and Ad5GFP-R7ΔKnob at increasing MOIs, as indicated on the *x* axis. (b) Requirement for CAR glycoprotein on the baculoviral membrane. Human dermal fibroblasts and synoviocytes were transduced by a mixture of Ad5GFP and BV^{CAR} or a mixture of Ad5GFP and nonpseudotyped BV (parental AcMNPV empty vector) at a constant MOI of Ad5GFP (10 vp/cell) and various BV or BV^{CAR} inputs at MOIs of 0, 250, and 500 vp/cell. (c and d) Requirement for CAR-fiber interaction. Human dermal fibroblasts were transduced by a mixture of BV^{CAR} (MOI of 250 vp/cell) and Ad5GFP (20 vp/cell), containing anti-CAR monoclonal antibody added at different dilutions. In panel c, anti-CAR antibody was added after complex formation, by premixing the two viruses followed by incubation for 1 h at 37°C ("post"). In panel d, anti-CAR antibody was added simultaneously with both viruses before complex formation ("pre"). Virus samples and antibody were further incubated for 1 h at 37°C. Controls consisted of Ad5GFP samples at the same MOI incubated with the same antibody dilutions. Results were expressed as the percentages of GFP-positive cells, assayed by flow cytometry (means of three separate experiments ± SEMs). **, $P < 0.01$; ns, no significant difference.

In addition, the slope of the curves of cell-bound viruses versus time indicated that the cellular uptake of Ad5GFP complexed with BV^{CAR} occurred at a significantly higher rate than that of Ad5GFP alone (twofold; Fig. 10a). In contrast, the cell binding kinetics of BV^{CAR} and the number of cell-associated baculoviral genome copies did not change significantly when BV^{CAR} was alone or in complex with Ad5 (Fig. 10b). These data suggested that the presence of BV^{CAR} in the complex provided significant kinetic benefits to Ad5GFP and not only an advantage in terms of cell tropism. Interestingly, the ratio of viral genomes recovered from BV^{CAR}-Ad5GFP-infected cells at 30 to 50 min p.i. (two Ad5GFP to 50 to 60 BV^{CAR}) corresponded to the ratio required for optimal cell transduction (Fig. 8c).

(ii) Role of baculoviral glycoprotein gp64. We next addressed the question of whether the envelope glycoprotein gp64 of BV^{CAR} was involved in the cell attachment and uptake of the BV^{CAR}-Ad5GFP complex, using dermal fibroblasts as the cellular target. We found that the BV^{CAR}-Ad5GFP-mediated gene transfer was inhibited in the presence of anti-gp64 monoclonal antibody in a dose-dependent manner, suggesting that gp64 was the major attachment protein of the complex (Fig. 10c). However, cell transduction was not totally inhibited, and the inhibitory effect plateaued at a residual value equivalent to twofold the basal level of transduction observed with Ad5GFP alone (Fig. 10c). This suggested that a baculoviral envelope glycoprotein(s) other than gp64 (e.g., CAR) might play a role in the cell attachment of BV^{CAR}-Ad5GFP and/or that the residual transduction was due to an alternative cell entry pathway, e.g., via macropinocytosis.

(iii) Influence of Ad5 virions on BV^{CAR}-Ad5GFP-mediated cell transduction: endosomal escape and cell entry. It is known that Ad5 is very efficient in endosomal escape, and this represents one of its advantages as a gene vector (14, 26, 65). In order to determine whether the adenoviral moiety of the BV^{CAR}-Ad5GFP complex was beneficial to the internalization of baculovirions, we used GFP-expressing BV vectors with or

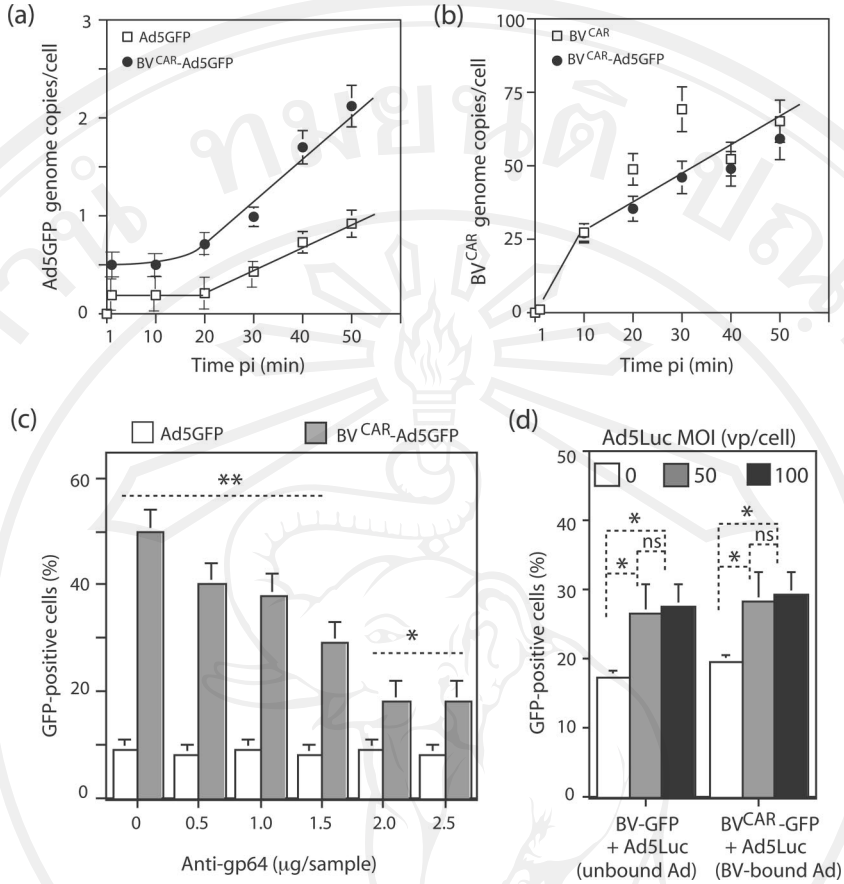

FIG. 10. Mechanism of cellular uptake of the BV^{CAR}-Ad5GFP complex. (a and b) Cell binding kinetics. Ad5GFP alone (open symbols), BV^{CAR} alone (open symbols), or BV^{CAR}-Ad5GFP complex (filled symbols) was incubated with CHO cells at 37°C for 50 min, and cell samples were withdrawn every 10 min p.i. After washing, cell-associated virions were assayed in cell lysates using real-time quantitative PCR. Results were expressed as the numbers of adenoviral and baculoviral genomes recovered per cell, using the beta-actin gene as an internal control. (a) Ad5GFP genomes: Ad5GFP alone ($y = 0.24x$, $R^2 = 0.993$) and BV^{CAR}-Ad5GFP complex ($y = 0.49x$, $R^2 = 0.977$). (b) BV^{CAR} genomes ($y = 10.5x$, $R^2 = 0.91$). (c) Role of baculoviral gp64. BV^{CAR}-Ad5GFP complex, at the BV^{CAR}/Ad5GFP MOI ratio of 500:20 vp/cell, was preincubated for 1 h at 37°C with different dilutions of anti-gp64 monoclonal antibody and added to monolayers of human dermal fibroblasts. (d) Role of the Ad5GFP moiety in cell internalization of BV^{CAR}-Ad5GFP complex. Human MSCs were transduced with a mixture of nonpseudotyped, GFP-expressing baculoviral vector BV-GFP and Ad5Luc (Ad5-unbound BV-GFP; leftmost bars) or a mixture of CAR-pseudotyped, GFP-expressing baculoviral vector BV^{CAR}GFP with Ad5Luc (Ad5-bound BV-GFP; rightmost bars). BV-GFP and BV^{CAR}GFP were used at constant MOIs each (MOI of 500), and Ad5Luc was used at different MOIs (0, 50, and 100). The transduction efficiency was expressed as the percentage of GFP-positive cells, assayed by flow cytometry (means of three separate experiments ± SEMs). *, $P < 0.05$; **, $P < 0.01$; ns, no significant difference.

without CAR pseudotyping, BV^{CAR}GFP and BV-GFP, respectively. BV^{CAR}GFP vector was incubated with Ad5Luc, an Ad5 vector expressing the firefly luciferase (27, 56). The BV^{CAR}GFP MOI was kept constant (500 vp/cell), while Ad5Luc MOI varied in the mix (MOI, 0, 50, or 100 vp/cell). Control samples consisted of (i) BV^{CAR}GFP alone without Ad5Luc and (ii) nonpseudotyped BV-GFP at the same constant dose (500 vp/cell) mixed with increasing MOIs of Ad5Luc. A modest but significant increase of GFP expression was detected in MSCs transduced by BV-GFP in the presence of Ad5Luc, compared to that with BV-GFP alone (50%; Fig. 10d, unbound Ad5). A similar level of enhancing effect was observed with BV^{CAR}GFP mixed with Ad5Luc (Fig. 10d; BV^{CAR}GFP-bound Ad5) compared to BV^{CAR}GFP alone. This indicated that Ad5 had only a discrete positive effect on the cellular internalization of the BV-GFP vector and that this effect did not require a physical bond between the baculovirion and the adenovirion.

(iv) Role of penton base-RGD-integrin recognition. To determine the contribution of RGD-dependent integrins in cell transduction by BV^{CAR}-Ad5GFP complex, we generated another baculoviral-adenoviral complex using the Ad5EGD-GFP mutant instead of the Ad5GFP vector. Due to its RGD-to-EGD alteration at position 340 in the penton base, the Ad5EGD-GFP mutant vector failed to recognize RGD-dependent integrins (26, 37, 67, 83). However, since the penton base mutation could mask or bias possible effects of BV^{CAR} in the BV^{CAR}-Ad5EGD-GFP complex, we first analyzed the intrinsic infectivity of Ad5EGD-GFP in permissive cells, in comparison to that of control Ad5GFP.

Ad5EGD-GFP stocks showed a range of infectivity indices (PFU/vp ratio) slightly inferior to that of control Ad5GFP vector grown in parallel, e.g., 1:108 versus 1:48, respectively, for the samples used in the present study. Ad5-permissive HEK-293 cells were infected by Ad5EGD-GFP or Ad5GFP at

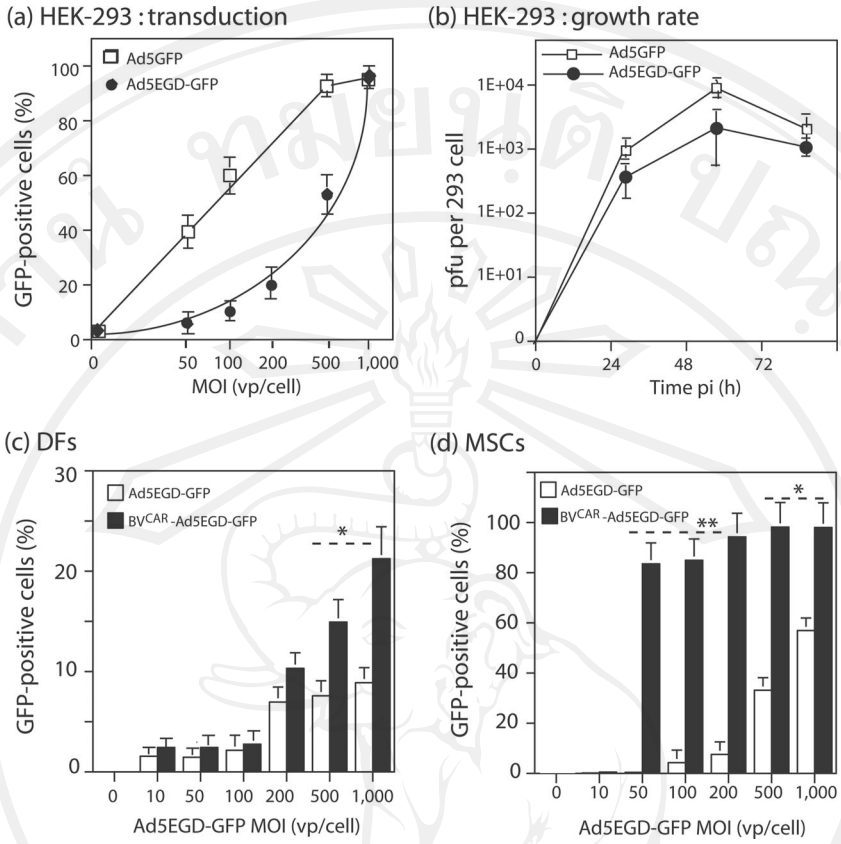

FIG. 11. Role of RGD-dependent integrins in BV^{CAR}-Ad5GFP-mediated transduction. (a) Efficiency of transduction of permissive cells by Ad5EGD-GFP mutant versus that by Ad5GFP. Aliquots of HEK-293 cells (1.75×10^5/well) were infected for 1 h with Ad5EGD-GFP or control vector Ad5GFP at different MOIs, as indicated on the *x* axis, and the percentage of GFP-positive cells was determined by flow cytometry at 48 h p.i. (means of three separate experiments ± SEMs). (b) Growth rate of Ad5EGD-GFP mutant versus that of Ad5GFP in permissive cells. Samples of 5×10^4 HEK-293 cells were infected at an MOI of 10 PFU/cell at 37°C for 1 h, rinsed once, and further incubated in culture medium at 37°C. Cells were harvested at 24, 48, and 72 h p.i. and lysed by freeze-thawing in 0.2 ml PBS, and titers of soluble supernatants were determined on HEK-293 cells. Titers were expressed as PFU/cell. (c and d) Efficiency of transduction by the BV^{CAR}-Ad5EGD-GFP complex. Dermal fibroblasts (DFs) (c) and MSCs (d) were transduced by Ad5EGD-GFP alone or a mixture of BV^{CAR} at a constant MOI (500 vp/cell) and Ad5EGD-GFP at increasing MOIs, as indicated on the *x* axis. The transduction efficiency was expressed as the percentage of GFP-positive cells, assayed by flow cytometry at 48 h p.i. (means of three separate experiments ± SEMs). *, $P < 0.05$; **, $P < 0.01$.

the same MOI (vp/cell), and the efficiency of infection and gene expression was determined by flow cytometric analysis of GFP-positive cells. The MOI required for 50% cell transduction (50% efficient transduction dose) was found to be 500 vp/cell for Ad5EGD-GFP, versus fivefold lower for Ad5GFP (50% efficient transduction dose = 100 vp/cell), and the maximum transduction was obtained at an MOI of 1,000 vp/cell for Ad5EGD-GFP, versus an MOI of 500 for Ad5GFP (Fig. 11a). These data showed that Ad5EGD-GFP infection was delayed compared to that by control vector Ad5GFP. Likewise, the growth rates were similar for the two vectors in HEK-293 cells, but the titer of infectious virus progeny recovered at 24, 48, and 72 h p.i. was three- to fourfold lower for Ad5EGD-GFP than for Ad5GFP (Fig. 11b). These data indicated that Ad5EGD-GFP was slightly but significantly impaired by its penton base mutation.

Taking into account the phenotype of Ad5EGD-GFP, we infected human dermal fibroblasts with Ad5EGD-GFP alone or BV^{CAR}-Ad5EGD-GFP complex at higher MOIs than those used previously with Ad5GFP and BV^{CAR}-Ad5GFP (Fig. 7 and 8). Of note, human dermal fibroblasts express alpha V integrins (21). Less than 10% of cells expressed GFP after transduction by Ad5EGD-GFP at an MOI of 1,000. With BV^{CAR}-Ad5EGD-GFP, however, a two- to threefold increase in transduction efficiency was observed at MOIs of 200 and higher (Fig. 11c). This moderate although significant augmentation was confirmed with other primary cells, MSCs. MSCs were transduced by BV^{CAR}-Ad5EGD-GFP with a 20-fold-higher efficiency at an MOI of 100 and a 10-fold-higher efficiency at an MOI of 200, compared to transduction with Ad5EGD-GFP alone (Fig. 11d). This implied that the integrity of penton base RGD motifs and their interaction with cellular integrins were not required for the BV^{CAR}-mediated augmentation of Ad5EGD-GFP transduction and that the BV^{CAR}-Ad5GFP complex could bypass the RGD-integrin endocytic pathway.

EM analysis of cell attachment and entry of BV^{CAR}-Ad5GFP complex into CAR-defective cells. CHO cells were incubated with BV^{CAR}-Ad5GFP complex for 1 h at 37°C, harvested at the end of this incubation period, fixed, and processed for EM

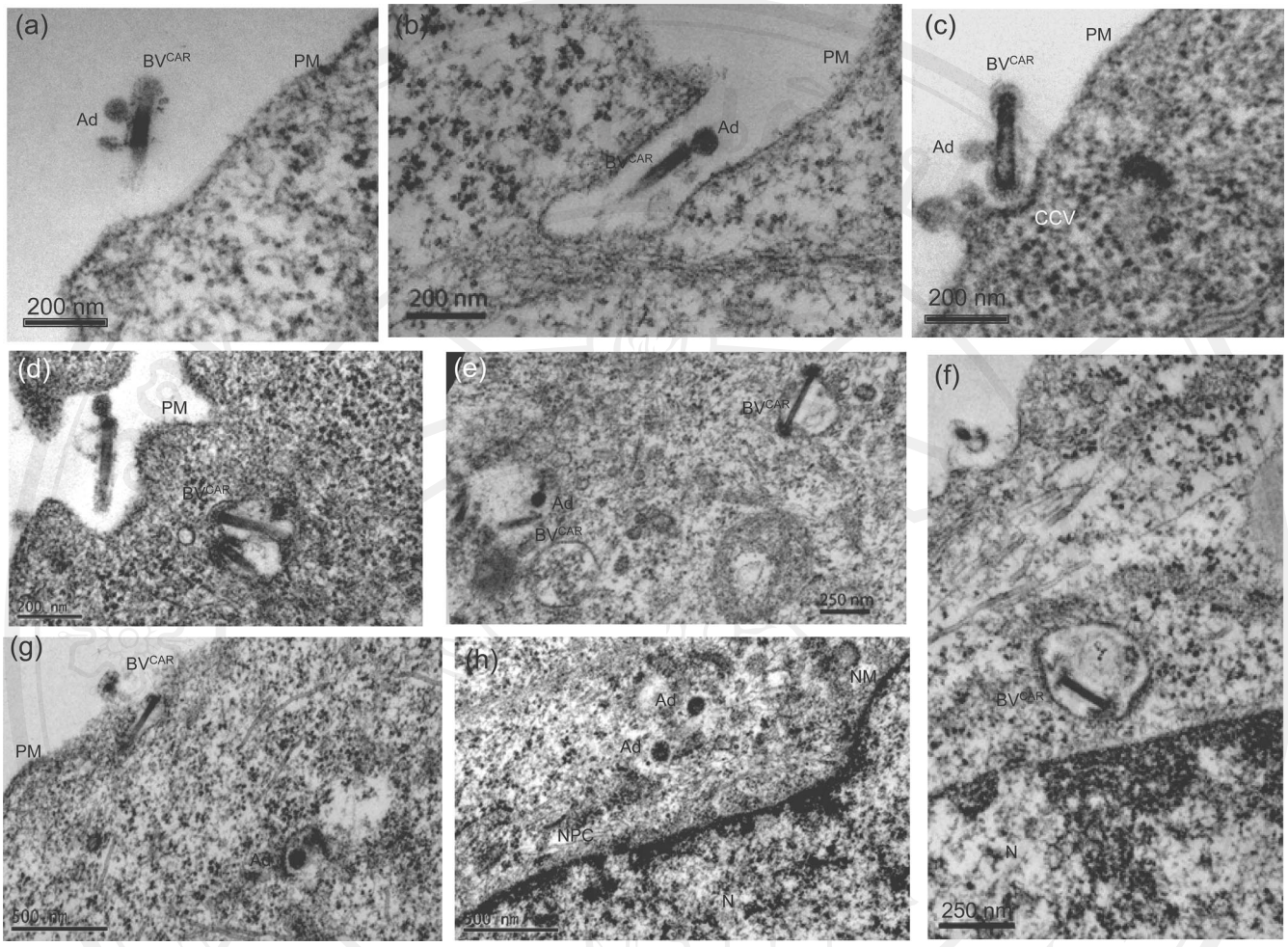

FIG. 12. EM analysis of the early steps of virus-cell interaction between BV^{CAR}-Ad5GFP complex and CAR-negative cells. Monolayers of CHO cells were incubated with BV^{CAR}-Ad5GFP (complex generated with an Ad5GFP-to-BV^{CAR} ratio of 1:25) for 1 h at 37°C, and cells were harvested and processed for EM analysis. Panels a to c show the steps of attachment of BV^{CAR}-Ad5GFP at the plasma membrane and formation of clathrin-coated vesicles (CCV). Panels d and e show coendocytosed virions of BV^{CAR} and Ad5GFP (Ad) within intracytoplasmic vesicles. In panel g, an adenovirion is seen in the process of vesicular escape. In panel h, two adenovirions are free within the cytoplasm, and electron-dense particles reminiscent of adenoviral cores are seen at the nuclear pore complex (NPC). Panel f shows an intravesicular BV^{CAR} nucleocapsid released from the baculoviral envelope. N, nucleus; PM, plasma membrane.

analysis. Complexes were seen at the cell surface, near or in close contact with the plasma membrane (Fig. 12a to d). At the point of BV^{CAR}-cell contact, a curvature of the plasma membrane with electron-dense material at its inner leaflet suggested the formation of a clathrin-coated pit (Fig. 12c), as previously reported (48). Coendocytosed baculovirions and adenovirions were observed within cytoplasmic vesicles (Fig. 12d and e). Adenovirions were occasionally seen in the process of vesicular escape with partial disruption of the endosomal membrane (Fig. 12g), or free within the cytoplasm, in the vicinity of nuclear pores (Fig. 12h). In contrast to Ad5 particles, baculoviral nucleocapsids were not observed within the cytoplasm and were still found within vesicles at 1 h p.i. (Fig. 12f). This suggested that adenovirions were released into the cytoplasm at a higher rate than were baculovirions. In none of the numerous cells examined did we observe a simultaneous endosomal escape of the two virions. This EM pattern was consistent with the relatively low rate of baculovirus release into the cytosol of mammalian cells (78) and supported the data for BV-bound and unbound Ad5Luc presented in Fig. 10d.

Biodistribution of BV^{CAR}-Ad5Luc complex in vivo in a mouse model. The preferential visceral localization of unmodified baculoviral vectors injected in the mouse tail vein has been reported to be, in decreasing order, heart, spleen, liver, kidney, lung, and brain (38). However, Ad5 vectors administered via the same way are in priority delivered to the liver (35, 61, 79, 81). It was therefore of interest to determine the viscerotropism of our BV^{CAR}-Ad5 complex and evaluate the respective influence of one or the other partner of the duo on the biodistribution of the complex in an animal model. To this aim, 5-week-old BALB/c nude mice received intravenously a bolus of 2×10^{10} vp of Ad5Luc or of BV^{CAR}-Ad5Luc complex (2×10^{10} vp of Ad5Luc and 3×10^{11} vp of BV^{CAR}, i.e., a ratio of BV^{CAR} to Ad5Luc vp of 15 to 1), and the level of luciferase expression was analyzed by noninvasive whole-body imaging at

days 2 and 4. The bioluminescent signal localized massively within the liver, and no qualitative difference could be detected between control mice receiving Ad5Luc alone and mice receiving the BV^{CAR}-Ad5Luc complex (not shown). Luciferase expression was then quantitatively assayed in different organs, and again the results showed that hepatic tissue was the preferential localization of both Ad5Luc alone and BV^{CAR}-Ad5Luc complex. In the other organs investigated, spleen, kidney, lung, brain, heart, and skeletal muscle, no significant difference in the levels of luciferase expression was found between Ad5Luc alone and the BV^{CAR}-Ad5Luc complex. The same organ distribution was observed when adenoviral genomes were quantitatively assayed using real-time quantitative PCR (data not shown). Of note, baculoviral genomes were recovered from the liver, as well as from the other tissues, and their relative distribution paralleled that of adenoviral genomes (data not shown). The change in tissue tropism of BV when complexed with Ad5 suggested that Ad5 carried the dominant determinants.

Influence of FX on BV^{CAR}-Ad5GFP-mediated transduction of CAR-negative cells in vitro. It has been shown recently that Ad5 hexon interacts with blood coagulation FX and to a lesser degree with FVII, FIX, and anticoagulant factor protein C (35, 61, 79, 81). The hexon-FX interaction is considered the major determinant of the preferential delivery of nonmodified Ad5 vectors to hepatocytes after in vivo administration. The next experiments were aimed at determining the possible role of FX in the hepatotropism of the BV^{CAR}-Ad5 complex, using an indirect, in vitro approach. Transduction of CHO cells by BV^{CAR}-Ad5GFP or Ad5GFP alone was performed in the presence or absence or FX. As expected from previous studies, a 20-fold increase in gene transfer efficiency was observed with Ad5GFP plus FX, compared to control Ad5GFP without FX: 42.6 ± 7.2 versus 1.9 ± 0.3 (mean $\pm$ standard error of the mean [SEM]; $n = 3$). However, when CHO cells were transduced with BV^{CAR}-Ad5GFP complex (generated with a suboptimal ratio of 10 BV^{CAR} to 1 Ad5GFP), no significant increase was observed: 26.1 ± 5.0 with FX versus 19.6 ± 1.5 without FX. This result suggested that FX had no direct effect on BV^{CAR}-Ad5GFP-mediated cell transduction in vitro.

DISCUSSION

The concept of BV display, i.e., exposing proteins or peptides of interest on the baculoviral envelope, is not novel and has been used to improve BV entry into different mammalian cell targets, including human cancer cells, by insertion of specific peptide ligands in the envelope glycoprotein gp64 (18, 39, 52–54, 75). This technology has also been used for immunization purposes (31, 32). The strategy described in the present study differed from conventional BV display methods in that it did not involve a gp64-fusion construct but consisted of the incorporation into the baculoviral envelope of a full-length glycoprotein normally exposed on the human cell plasma membrane and foreign to the virus. This fulfilled the criteria of virus pseudotyping. Such a pseudotyping of BV by, e.g., human hormone receptor (47) or vesicular stomatitis virus G (39), has been previously reported.

The originality of our strategy was to pseudotype BV with CAR (BV^{CAR}), the high-affinity receptor for Ad5 and several other Ad serotypes, to generate binary BV^{CAR}-Ad5 complexes via CAR-fiber knob interaction. BV^{CAR} was therefore used as a viral adapter to mediate cell entry of human Ad5 vector into Ad5-resistant cells. The rationale was based on two observations and implied two hypotheses. (i) It has been observed that BV has the capacity of entering a wide variety of cell types, including cells which are refractory to Ad5 infection, and to be internalized via a receptor-mediated pathway involving the early endosomal compartment (8, 32, 41, 73). (ii) The Ad5 fiber-CAR binding occurs with a high affinity, with a K_d (dissociation constant) range of 2 to 6 nM (27, 68, 85). We therefore hypothesized that (i) bridging Ad5 virions to BV^{CAR} via the strong interaction between adenoviral fiber and CAR glycoprotein inserted in the baculoviral envelope would result in the simultaneous cellular uptake of both Ad5 and BV^{CAR} into the same endocytic compartment and that (ii) the coendocytosed viruses would cooperate in the step of endosomolysis and contribute to a more efficient endosomal release and cell internalization.

We found that when Sf9 cells were infected with our recombinant BV expressing the human CAR glycoprotein under the control of the polyhedrin promoter, the BV progeny incorporated CAR molecules into the baculoviral envelope, resulting in a bona fide CAR-pseudotyped BV, abbreviated BV^{CAR}. EM analysis of BV^{CAR}-Ad5GFP complexes showed that the most frequent associations consisted of a stoichiometric ratio of one Ad5GFP per BV^{CAR} and less frequently two Ad5GFP per BV^{CAR}. EM observation of BV^{CAR}-Ad5GFP complexes and isolated BV^{CAR} virions immunogold labeled with anti-CAR or anti-gp64 antibodies revealed a gold grain topology different for gp64 and CAR molecules: gp64 localized at the head of the virus, whereas CAR molecules, free or engaged in bonds with Ad5 virions, preferentially localized along the stem.

We then exploited the capacity of BVs to transduce a wide repertoire of cell types. BV^{CAR} was used to piggyback Ad5GFP vector into cells which do not express CAR and were nonpermissive or poorly permissive to Ad5. We found that the transduction enhancement of CHO and MM39 cells using the BV^{CAR}-Ad5GFP complex was on the order of 30- to 40-fold, compared to Ad5GFP alone. For three human cancer cell lines, RD, SKOV3, and SKBR3, a significant augmentation of gene delivery (3- to 10-fold) was observed with BV^{CAR}-Ad5GFP. In the case of primary cells, dermal fibroblasts, synoviocytes, and MSCs, BV^{CAR}-Ad5GFP-mediated transduction increased by 1 order of magnitude and, more importantly, at a significantly low Ad5GFP input (MOI of 20 vp/cell). For cells of myeloid origin such as PBMCs and monocyte-derived DCs, the increase in BV^{CAR}-Ad5GFP-mediated transduction was less pronounced (only twofold) and observed only at high Ad5 vector doses of MOIs of 1,000 and 500, respectively. Not surprisingly, PBMCs and DCs have not been reported in the literature to efficiently internalize BVs.

We showed that the mechanism of augmentation of cell transduction of primary cells (e.g., dermal fibroblasts and synoviocytes) by BV^{CAR}-Ad5GFP in vitro, compared to Ad5GFP alone, required (i) the interaction of adenoviral fibers with CAR molecules inserted in the baculoviral envelope and (ii) the cell attachment of the BV^{CAR} partner via its gp64 peplomer; (iii) however, it did not depend on the interaction of penton base RGD motifs of the Ad5GFP partner with cellular

integrins; (iv) kinetic analysis of the virus-cell binding reaction showed that the presence of BV^{CAR} in the complex was beneficial to Ad5GFP, in terms of number of cell-bound virions and rate of cell attachment; (v) however, there was little reciprocity, as the benefit obtained by BV^{CAR} from its Ad5GFP partner in terms of rate of endosomal escape and cell internalization was modest.

Our data with control nonpseudotyped baculoviral vector BV-GFP, and BV-bound or unbound Ad5 vector, suggested that the helper function of BV^{CAR} toward Ad5GFP vector (2- to 40-fold-increased transduction in the various cell types tested) was much higher than that in the opposite scenario, when Ad5 was used as the helper of BV^{CAR}-GFP (only 50%). We assume that this was due to the mechanisms of vesicular escape, which differ for the two viruses. Both BVs and subgroup C Ads are endocytosed into early endosomes but are released into the cytosol by different mechanisms: Ads rapidly escape from endosomes by endosomolysis (30), while BVs use membrane fusion between baculoviral envelope glycoprotein and the endosomal membrane (32, 70). Our data indicated that the cell entry pathway and rate of endosomal escape of BV^{CAR} via gp64-mediated membrane fusion were not greatly affected by the presence of its Ad5GFP partner in the BV^{CAR}-Ad5GFP complex. However, both partners of the BV^{CAR}-Ad5GFP duo played their own part in one or the other step of the cell entry pathway, and cellular transduction benefited from the ensemble.

In vivo, after intravascular administration in BALB/c nude mice, the biodistribution of BV^{CAR}-Ad5Luc complex was unchanged compared to that of Ad5Luc alone, and the liver remained the preferred destination of the viral duo, as observed for unmodified Ad5 vectors in many laboratories (35, 61, 79, 81). Unmodified baculoviral vectors injected in the mouse tail vein also have intrinsic hepatotropism (6) but localize in smaller amounts in the liver, compared to heart and spleen (38). This suggested that Ad5 played the dominant role in the vector duo. Our in vitro experiments showed that BV^{CAR}-Ad5GFP-mediated transduction of CAR-negative cells was insensitive to blood coagulation FX and FX-hexon interaction (35, 61, 79, 81), in contrast to transduction by Ad5GFP alone, which was drastically enhanced in the presence of FX.

In conclusion, the advantages of using CAR-pseudotyped BV as a carrier of Ad5 vector(s) are multiple. (i) Many cells which are poorly permissive to Ad5 can be transduced at high MOIs of Ad5 vector, and up to 10^4 to 10^5 particles per cell are necessary to obtain a minimal level of transgene expression. Such high MOIs are hardly compatible with the cell physiology, and intrinsic vector cytotoxicity is likely to interfere with the biological function(s) of the transgene product(s). By comparison, our BV^{CAR}-Ad5 vector complex efficiently transduced Ad5-refractory cells at MOIs of 10 to 20. (ii) In the same line of arguments, Ad5 has an early cytopathic and cell-detaching effect, and the cell-detaching effect has been assigned to one of the major capsid proteins of incoming virions, the penton base and its integrin-binding motif RGD (4, 36, 37, 62). Results with penton base EGD mutant Ad5 suggested that our BV^{CAR}-Ad5 vector complex could bypass the RGD-integrin endocytic pathway. (iii) It is relatively easy to insert a gene of interest in the E1-deleted region of Ad5, and many commercial kits are available to generate recombinant Ad5. It is less easy, however, to modify the adenoviral capsid so as to redirect the Ad5 vector to a desired cell target via cell-specific ligands, while respecting the viability and the productivity of capsid-modified vectors (51). Our strategy of using BV^{CAR} as a macromolecular adapter of Ad5 vector, therefore, represents an alternative to hazardous Ad capsid modifications.

(iv) BV^{CAR}, and a fortiori our BV^{CAR}-Ad5 vector complex, could be redirected to cell targets by insertion of specific peptides or proteins in the envelope glycoprotein gp64 (18, 39, 52–54, 75). (v) Considering the last point (iv), it might be argued that there would be no need for a BV^{CAR}-Ad5 vector complex and that a recombinant BV vector expressing the gene of interest under the required promoter (31) and displaying a cell-targeting ligand would be sufficient for gene delivery to human cells nonpermissive to Ad5. However, our data indicated that our BV^{CAR}-Ad5GFP duo was significantly more efficient than BV^{CAR}-GFP alone in cell transduction of vertebrate cells. (vi) Given the possibility of transducing Ad-refractory cells belonging to the immune system by our BV^{CAR}-Ad5 vector complex, one could envisage delivering oncolytic Ads to tumors via cell carriers with specificity toward tumor cells. (vii) Although results of in vitro experiments could hardly be extrapolated to in vivo situations, our preliminary data suggested that the hepatotropism of the BV^{CAR}-Ad5GFP complex was independent of Ad5 hexon-FX interaction. (viii) Lastly, our system of coupling two viruses which are both vectors of gene transfer also offers the possibility of expressing several transgenes within the same target cell, while limiting the risk of interference between transgenes and promoters carried by a single recombinant genome.

ACKNOWLEDGMENTS

This work was supported by the French Cystic Fibrosis Foundation (Vaincre La Mucoviscidose, VLM contracts TG-0702 and TG-0801), the Centre National Recherche Scientifique (CNRS), the University of Lyon I, and the Hospices Civils de Lyon (HCL). O.G. was financially supported by a postdoctoral fellowship from VLM. K.K. was supported by the AMS-IRD URI-174 PHPT Franco-Thai Cooperation Program for High Education and Research and the Thai Higher Education Program. S.-S.H. is an INSERM scientist and the recipient of a Contrat d'Interface HCL-INSERM.

We are deeply grateful to Gérard Devauchelle (CNRS, St. Christolles-Ales, France) for his valuable advice on BV technology, to Kerstin Sollerbrant (Karolinska Institutet, Stockholm, Sweden) for her gift of plasmid pcDNA-hCAR1, to Norman Maitland (University of York Heslington, York, United Kingdom) for the baculoviral clone expressing GFP, to Frank Graham (University of Ontario, Hamilton, Ontario, Canada) for the Ad5Luc3 vector, and to Silvio Hemmi (University of Zurich, Zurich, Switzerland) for the monoclonal anti-CAR antibody. We also thank Elisabeth Errazuriz (Centre Commun d'Imagerie de Laennec), for her help with our electron microscopic studies; Blandine Deux, Olivier Peyruchaud, and Philippe Clezardin (INSERM U-664, Laennec School of Medicine, Lyon) for their significant contribution to our animal experiments; Gaelle Gonzalez for her valuable assistance in our quantitative PCR analyses; and Cathy Berthet for her efficient secretarial aid.

REFERENCES

1. **Ayres, M. D., S. C. Howard, J. Kuzio, M. Lopez-Ferber, and R. D. Possee.** 1994. The complete DNA sequence of *Autographa californica* nuclear polyhedrosis virus. Virology **202:**586–605.
2. **Belousova, N., G. Mikheeva, J. Gelovani, and V. Krasnykh.** 2008. Modification of adenovirus capsid with a designed protein ligand yields a gene vector targeted to a major molecular marker of cancer. J. Virol. **82:**630–637.
3. **Bergelson, J. M., J. A. Cunningham, G. Droguett, E. A. Kurt-Jones, A. Krithivas, J. S. Hong, M. S. Horwitz, R. L. Crowell, and R. W. Finberg.** 1997.

Isolation of a common receptor for Coxsackie B viruses and adenoviruses 2 and 5. Science **275:**1320–1323.
4. **Boudin, M.-L., M. Moncany, J.-C. D'Halluin, and P. Boulanger.** 1979. Isolation and characterization of adenovirus type 2 vertex capsomer (penton base). Virology **92:**125–138.
5. **Boulanger, P., and F. Puvion.** 1973. Large-scale preparation of soluble adenovirus hexon, penton and fiber antigens in highly purified form. Eur. J. Biochem. **39:**37–42.
6. **Boyce, F. M., and N. L. Bucher.** 1996. Baculovirus-mediated gene transfer into mammalian cells. Proc. Natl. Acad. Sci. USA **93:**2348–2352.
7. **Chorny, M., I. Fishbein, I. S. Alferiev, O. Nyanguile, R. Gaster, and R. J. Levy.** 2006. Adenoviral gene vector tethering to nanoparticle surfaces results in receptor-independent cell entry and increased transgene expression. Mol. Ther. **14:**382–391.
8. **Chuang, C.-K., L.-Y. Sung, S.-M. Hwang, W.-H. Lo, H.-C. Chen, and Y.-C. Hu.** 2007. Baculovirus as a new gene delivery vector for stem cell engineering and bone tissue engineering. Gene Ther. **14:**1417–1424.
9. **Corjon, S., A. Wortmann, T. Engler, N. van Rooijen, S. Kochanek, and F. Kreppel.** 2008. Targeting of adenovirus vectors to the LRP receptor family with the high-affinity ligand RAP via combined genetic and chemical modification of the pIX capsomer. Mol. Ther. **16:**1813–1824.
10. **DaFonseca, S., A. Blommaert, P. Coric, S. S. Hong, S. Bouaziz, and P. Boulanger.** 2007. The 3-O-(3′,3′-dimethylsuccinyl) derivative of betulinic acid (DSB) inhibits the assembly of virus-like particles in HIV-1 Gag precursor-expressing cells. Antivir. Ther. **12:**1185–1203.
11. **Dechecchi, M. C., P. Melotti, A. Bonizzato, M. Santacatterina, M. Chilosi, and G. Cabrini.** 2001. Heparan sulfate glycosaminoglycans are receptors sufficient to mediate the initial binding of adenovirus types 2 and 5. J. Virol. **75:**8772–8780.
12. **Dechecchi, M. C., A. Tamanini, A. Bonizzato, and G. Cabrini.** 2000. Heparan sulfate glycosaminoglycans are involved in adenovirus type 5 and 2-host cell interactions. Virology **268:**382–390.
13. **Franqueville, L., P. Henning, M. K. Magnusson, E. Vigne, G. Schoehn, M. E. Blair-Zajdel, N. Habib, L. Lindholm, G. E. Blair, S. S. Hong, and P. Boulanger.** 2008. Protein crystals in adenovirus type 5-infected cells: requirements for intranuclear crystallogenesis, structural and functional analysis. PLoS One **3:**e2894.
14. **Gaden, F., L. Franqueville, S. S. Hong, V. Legrand, C. Figarella, and P. Boulanger.** 2002. Mechanism of restriction of normal and cystic fibrosis transmembrane conductance regulator-deficient human tracheal gland cells to adenovirus (Ad) infection and Ad-mediated gene transfer. Am. J. Respir. Cell Mol. Biol. **27:**628–640.
15. **Gaden, F., L. Franqueville, M. K. Magnusson, S. S. Hong, M. D. Merten, L. Lindholm, and P. Boulanger.** 2004. Gene transduction and cell entry pathway of fiber-modified adenovirus type 5 vectors carrying novel endocytic peptide ligands selected on human tracheal glandular cells. J. Virol. **78:**7227–7247.
16. **Goujon, C., L. Jarrosson-Wuilleme, J. Bernaud, D. Rigal, J. L. Darlix, and A. Cimarelli.** 2003. Heterologous human immunodeficiency virus type 1 lentiviral vectors packaging a simian immunodeficiency virus-derived genome display a specific postentry transduction defect in dendritic cells. J. Virol. **77:**9295–9304.
17. **Granio, O., C. Norez, K. J. D. Asbourne Excoffon, P. Karpp, M. Lusky, F. Becq, P. Boulanger, J. Zabner, and S. S. Hong.** 2007. Cellular localization and activity of GFP-tagged CFTR transduced by adenovirus in CFTR-deficient cells. Am. J. Respir. Cell Mol. Biol. **37:**631–639.
18. **Guibinga, G. H., and T. Friedmann.** 2005. Baculovirus gp64-pseudotyped HIV-based lentivirus vectors are stabilized against complement inactivation by codisplay of decay accelerating factor (DAF) or of a gp64-DAF fusion protein. Mol. Ther. **11:**645–651.
19. **Hemmi, S., R. Geertsen, A. Mezzacasa, I. Peter, and R. Dummer.** 1998. The presence of human coxsackievirus and adenovirus receptor is associated with efficient adenovirus-mediated transgene expression in human melanoma cell cultures. Hum. Gene Ther. **9:**2363–2373.
20. **Henning, P., M. K. Magnusson, E. Gunneriusson, S. S. Hong, P. Boulanger, P. A. Nygren, and L. Lindholm.** 2002. Genetic modification of adenovirus 5 tropism by a novel class of ligands based on a three-helix bundle scaffold derived from staphylococcal protein A. Hum. Gene Ther. **13:**1427–1439.
21. **Hidaka, C., E. Milano, P. L. Leopold, J. M. Bergelson, N. R. Hackett, R. W. Finberg, T. J. Wickham, I. Kovesdi, P. Roelvink, and R. G. Crystal.** 1999. CAR-dependent and CAR-independent pathways of adenovirus vector-mediated gene transfer and expression in human fibroblasts. J. Clin. Investig. **103:**579–587.
22. **Hofmann, C., V. Sandig, G. Jennings, M. Rudolph, P. Schlag, and M. Strauss.** 1995. Efficient gene transfer into human hepatocytes by baculovirus vectors. Proc. Natl. Acad. Sci. USA **92:**10099–10103.
23. **Hofmann, C., and M. Strauss.** 1998. Baculovirus-mediated gene transfer in the presence of human serum or blood facilitated by inhibition of the complement system. Gene Ther. **5:**531–536.
24. **Honda, T., H. Saitoh, M. Masuko, T. Katagiri-Abe, K. Tominaga, I. Kozakai, K. Kobayashi, T. Kumanishi, Y. G. Watanabe, S. Odani, and R. Kuwano.** 2000. The coxsackievirus-adenovirus receptor protein as a cell adhesion molecule in the developing mouse brain. Brain Res. Mol. Brain Res. **77:**19–28.
25. **Hong, S. S., A. Galaup, R. Peytavi, N. Chazal, and P. Boulanger.** 1999. Enhancement of adenovirus-mediated gene delivery by use of an oligopeptide with dual binding specificity. Hum. Gene Ther. **10:**2577–2586.
26. **Hong, S. S., B. Gay, L. Karayan, M. C. Dabauvalle, and P. Boulanger.** 1999. Cellular uptake and nuclear delivery of recombinant adenovirus penton base. Virology **262:**163–177.
27. **Hong, S. S., L. Karayan, J. Tournier, D. T. Curiel, and P. Boulanger.** 1997. Adenovirus type 5 fiber knob binds to MHC class I alpha2 domain at the surface of human epithelial and B lymphoblastoid cells. EMBO J. **16:**2294–2306.
28. **Hong, S. S., M. K. Magnusson, P. Henning, L. Lindholm, and P. Boulanger.** 2003. Adenovirus stripping: a versatile method to generate adenovirus vectors with new cell target specificity. Mol. Ther. **7:**692–699.
29. **Hong, S. S., E. Szolajska, G. Schoehn, L. Franqueville, S. Myhre, L. Lindholm, R. W. Ruigrok, P. Boulanger, and J. Chroboczek.** 2005. The 100K-chaperone protein from adenovirus serotype 2 (subgroup C) assists in trimerization and nuclear localization of hexons from subgroups C and B adenoviruses. J. Mol. Biol. **352:**125–138.
30. **Horwitz, M. S.** 2001. Adenoviruses, p. 2301–2326. *In* D. M. Knipe, P. M. Howley, D. E. Griffin, R. A. Lamb, M. A. Martin, B. Roizman, and S. E. Straus (ed.), Fields virology, 4th ed. Lippincott Williams & Wilkins, Philadelphia, PA.
31. **Hu, Y. C.** 2008. Baculoviral vectors for gene delivery: a review. Curr. Gene Ther. **8:**54–65.
32. **Hu, Y. C.** 2006. Baculovirus vectors for gene therapy. Adv. Virus Res. **68:**287–320.
33. **Hüser, A., M. Rudolph, and C. Hofmann.** 2001. Incorporation of decay-accelerating factor into the baculovirus envelope generates complement-resistant gene transfer vectors. Nat. Biotechnol. **19:**451–455.
34. **Huvent, I., S. S. Hong, C. Fournier, B. Gay, J. Tournier, C. Carriere, M. Courcoul, R. Vigne, B. Spire, and P. Boulanger.** 1998. Interaction and co-encapsidation of HIV-1 Vif and Gag recombinant proteins. J. Gen. Virol. **79:**1069–1081.
35. **Kalyuzhniy, O., N. C. Di Paolo, M. Silvestry, S. E. Hofherr, M. A. Barry, P. L. Stewart, and D. M. Shayakhmetov.** 2008. Adenovirus serotype 5 hexon is critical for virus infection of hepatocytes in vivo. Proc. Natl. Acad. Sci. USA **105:**5483–5488.
36. **Karayan, L., B. Gay, J. Gerfaux, and P. Boulanger.** 1994. Oligomerization of recombinant penton base of adenovirus type 2 and its assembly with fiber in baculovirus-infected cells. Virology **202:**782–795.
37. **Karayan, L., S. S. Hong, B. Gay, J. Tournier, A. D. d'Angeac, and P. Boulanger.** 1997. Structural and functional determinants in adenovirus type 2 penton base recombinant protein. J. Virol. **71:**8678–8689.
38. **Kim, Y.-K., I.-K. Park, H.-L. Jiang, J.-Y. Choi, Y.-H. Je, H. Jin, H.-W. Kim, M.-H. Cho, and C.-S. Cho.** 2006. Regulation of transduction efficiency by pegylation of baculovirus vector in vitro and in vivo. J. Biotechnol. **125:**104–109.
39. **Kitagawa, Y., H. Tani, C. K. Limn, T. M. Matsunaga, K. Moriishi, and Y. Matsuura.** 2005. Ligand-directed gene targeting to mammalian cells by pseudotype baculoviruses. J. Virol. **79:**3639–3652.
40. **Korokhov, N., G. Mikheeva, A. Krendelshchikov, N. Belousova, V. Simonenko, V. Krendelshchikova, A. Pereboev, A. Kotov, O. Kotova, P. L. Triozzi, W. A. Aldrich, J. T. Douglas, K. M. Lo, P. T. Banerjee, S. D. Gillies, D. T. Curiel, and V. Krasnykh.** 2003. Targeting of adenovirus via genetic modification of the viral capsid combined with a protein bridge. J. Virol. **77:**12931–12940.
41. **Kost, T. A., and J. P. Condreay.** 2002. Recombinant baculoviruses as mammalian cell gene-delivery vectors. Trends Biotechnol. **20:**173–180.
42. **Kreppel, F., J. Gackowski, E. Schmidt, and S. Kochanek.** 2005. Combined genetic and chemical capsid modifications enabled flexible and efficient de- and retargeting of adenovirus vectors. Mol. Ther. **12:**107–117.
43. **Law, L. K., and B. L. Davidson.** 2005. What does it take to bind CAR? Mol. Ther. **12:**599–609.
44. **Lehtolainen, P., K. Tyynelä, J. Kannasto, K. J. Airenne, and S. Ylä-Herttuala.** 2002. Baculoviruses exhibit restricted cell type specificity in rat brain: a comparison of baculovirus- and adenovirus-mediated intracerebral gene transfer in vivo. Gene Ther. **9:**1693–1699.
45. **Leisy, D. J., T. D. Lewis, J.-A. C. Leong, and G. F. Rohrmann.** 2003. Transduction of cultured fish cells with recombinant baculoviruses. J. Gen. Virol. **84:**1173–1178.
46. **Li, Y. P., S. Paczesny, E. Lauret, S. Poirault, P. Bordigoni, F. Mekhloufi, O. Hequet, Y. Bertrand, J. P. Ou-Yang, J. F. Stoltz, P. Miossec, and A. Eljaafari.** 2008. Human mesenchymal stem cells license adult CD34+ hemopoietic progenitor cells to differentiate into regulatory dendritic cells through activation of the Notch pathway. J. Immunol. **180:**1598–1608.
47. **Loisel, T. P., H. Ansanay, S. St.-Onge, B. Gay, P. Boulanger, A. D. Strosberg, S. Marullo, and M. Bouvier.** 1997. Recovery of homogeneous and functional beta 2-adrenergic receptors from extracellular baculovirus particles. Nat. Biotechnol. **15:**1300–1304.
48. **Long, G., X. Pan, R. Kormelink, and J. M. Vlak.** 2006. Functional entry of

baculovirus into insect and mammalian cells is dependent on clathrin-mediated endocytosis. J. Virol. **80:**8830–8833.
49. **Magnusson, M. K., P. Henning, S. Myhre, M. Wikman, T. G. Uil, M. Friedman, K. M. Andersson, S. S. Hong, R. C. Hoeben, N. A. Habib, S. Stahl, P. Boulanger, and L. Lindholm.** 2007. Adenovirus 5 vector genetically retargeted by an Affibody molecule with specificity for tumor antigen HER2/neu. Cancer Gene Ther. **14:**468–479.
50. **Magnusson, M. K., S. S. Hong, P. Boulanger, and L. Lindholm.** 2001. Genetic retargeting of adenovirus: novel strategy employing "deknobbing" of the fiber. J. Virol. **75:**7280–7289.
51. **Magnusson, M. K., S. S. Hong, P. Henning, P. Boulanger, and L. Lindholm.** 2002. Genetic retargeting of adenovirus vectors: functionality of targeting ligands and their influence on virus viability. J. Gene Med. **4:**356–370.
52. **Mäkelä, A. R., J. Enbäck, J. P. Laakkonen, M. Vihinen-Ranta, P. Laakkonen, and C. Oker-Blom.** 2008. Tumor targeting of baculovirus displaying a lymphatic homing peptide. J. Gene Med. **10:**1019–1031.
53. **Mäkelä, A. R., H. Matilainen, D. J. White, E. Ruoslahti, and C. Oker-Blom.** 2006. Enhanced baculovirus-mediated transduction of human cancer cells by tumor-homing peptides. J. Virol. **80:**6603–6611.
54. **Mäkelä, A. R., and C. Oker-Blom.** 2006. Baculovirus display: a multifunctional technology for gene delivery and eukaryotic library development. Adv. Virus Res. **68:**91–112.
55. **Matthews, D. A., and W. C. Russell.** 1994. Adenovirus protein-protein interactions: hexon and protein VI. J. Gen. Virol. **75:**3365–3374.
56. **Mittal, S. K., M. R. McDermott, D. C. Johnson, L. Prevec, and F. L. Graham.** 1993. Monitoring foreign gene expression by a human adenovirus-based vector using the firefly luciferase gene as a reporter. Virus Res. **28:**67–90.
57. **Mizuguchi, H., and T. Hayakawa.** 2002. Adenovirus vectors containing chimeric type 5 and type 35 fiber proteins exhibit altered and expanded tropism and increase the size limit of foreign genes. Gene **285:**69–77.
58. **Molinier-Frenkel, V., R. Lengagne, F. Gaden, S. S. Hong, J. Choppin, H. Gahery-Segard, P. Boulanger, and J. G. Guillet.** 2002. Adenovirus hexon protein is a potent adjuvant for activation of a cellular immune response. J. Virol. **76:**127–135.
59. **Monsma, S. A., A. G. Oomens, and G. W. Blissard.** 1996. The GP64 envelope fusion protein is an essential baculovirus protein required for cell-to-cell transmission of infection. J. Virol. **70:**4607–4616.
60. **Novelli, A., and P. Boulanger.** 1991. Deletion analysis of functional domains in baculovirus-expressed adenovirus type 2 fiber. Virology **185:**365–376.
61. **Parker, A. L., S. N. Waddington, C. G. Nicol, D. M. Shayakhmetov, S. M. Buckley, L. Denby, G. Kemball-Cook, S. Ni, A. Lieber, J. H. McVey, S. A. Nicklin, and A. H. Baker.** 2006. Multiple vitamin K-dependent coagulation zymogens promote adenovirus-mediated delivery to hepatocytes. Blood **108:**2554–2561.
62. **Pereira, H. G.** 1958. A protein factor responsible for the early cytopathic effect of adenoviruses. Virology **6:**601–611.
63. **Peyruchaud, O., C. M. Serre, R. NicAmhlaoibh, P. Fournier, and P. Clezardin.** 2003. Angiostatin inhibits bone metastasis formation in nude mice through a direct anti-osteoclastic activity. J. Biol. Chem. **278:**45826–45832.
64. **Russell, W. C.** 2009. Adenoviruses: update on structure and function. J. Gen. Virol. **90:**1–20.
65. **Russell, W. C.** 2000. Update on adenovirus and its vectors. J. Gen. Virol. **81:**2573–2604.
66. **Russell, W. C., G. Patel, B. Precious, I. Sharp, and P. S. Gardner.** 1981. Monoclonal antibodies against adenovirus type 5: preparation and preliminary characterization. J. Gen. Virol. **56:**393–408.
67. **Salone, B., Y. Martina, S. Piersanti, E. Cundari, G. Cherubini, L. Franqueville, C. M. Failla, P. Boulanger, and I. Saggio.** 2003. Integrin $\alpha 3\beta 1$ is an alternative receptor for adenovirus serotype 5. J. Virol. **77:**13448–13454.
68. **Santis, G., V. Legrand, S. S. Hong, E. Davison, I. Kirby, J. L. Imler, R. W. Finberg, J. M. Bergelson, M. Mehtali, and P. Boulanger.** 1999. Molecular determinants of adenovirus serotype 5 fibre binding to its cellular receptor CAR. J. Gen. Virol. **80:**1519–1527.
69. **Sarkis, C., C. Serguera, S. Petres, D. Buchet, J.-L. Ridet, L. Edelman, and J. Mallet.** 2000. Efficient transduction of neural cells in vitro and in vivo by a baculovirus-derived vector. Proc. Natl. Acad. Sci. USA **97:**14638–14643.
70. **Slack, J., and B. M. Arif.** 2007. The baculoviruses occlusion-derived virus: virion structure and function. Adv. Virus Res. **69:**99–165.
71. **Sollerbrant, K., E. Raschperger, M. Mirza, U. Engstrom, L. Philipson, P. O. Ljungdahl, and R. F. Pettersson.** 2003. The Coxsackievirus and adenovirus receptor (CAR) forms a complex with the PDZ domain-containing protein ligand-of-numb protein-X (LNX). J. Biol. Chem. **278:**7439–7444.
72. **Songa, J., C. Lianga, and X. Chen.** 2006. Transduction of avian cells with recombinant baculovirus. J. Virol. Methods **135:**157–162.
73. **Stanbridge, L. J., V. Dussupt, and N. J. Maitland.** 2003. Baculoviruses as vectors for gene therapy against human prostate cancer. J. Biomed. Biotechnol. **2003:**79–91.
74. **Takayama, K., P. N. Reynolds, J. J. Short, Y. Kawakami, Y. Adachi, J. N. Glasgow, M. G. Rots, V. Krasnykh, J. T. Douglas, and D. T. Curiel.** 2003. A mosaic adenovirus possessing serotype Ad5 and serotype Ad3 knobs exhibits expanded tropism. Virology **309:**282–293.
75. **Tani, H., M. Nishijima, H. Ushijima, T. Miyamura, and Y. Matsuura.** 2001. Characterization of cell-surface determinants important for baculovirus infection. Virology **279:**343–353.
76. **Toh, M. L., S. S. Hong, F. van de Loo, L. Franqueville, L. Lindholm, W. van den Berg, P. Boulanger, and P. Miossec.** 2005. Enhancement of adenovirus-mediated gene delivery to rheumatoid arthritis synoviocytes and synovium by fiber modifications: role of arginine-glycine-aspartic acid (RGD)- and non-RGD-binding integrins. J. Immunol. **175:**7687–7698.
77. **Tomko, R. P., R. Xu, and L. Philipson.** 1997. HCAR and MCAR: the human and mouse cellular receptors for subgroup C adenoviruses and group B coxsackieviruses. Proc. Natl. Acad. Sci. USA **94:**3352–3356.
78. **van Loo, N. D., E. Fortunati, E. Ehlert, M. Rabelink, F. Grosveld, and B. J. Scholte.** 2001. Baculovirus infection of nondividing mammalian cells: mechanisms of entry and nuclear transport of capsids. J. Virol. **75:**961–970.
79. **Vigant, F., D. Descamps, B. Jullienne, S. Esselin, E. Connault, P. Opolon, T. Tordjmann, E. Vigne, M. Perricaudet, and K. Benihoud.** 2008. Substitution of hexon hypervariable region 5 of adenovirus serotype 5 abrogates blood factor binding and limits gene transfer to liver. Mol. Ther. **16:**1474–1480.
80. **Volkman, L. E., M. D. Summers, and C.-H. Hsieh.** 1976. Occluded and nonoccluded nuclear polyhedrosis virus grown in *Trichoplusia ni*: comparative neutralization, comparative infectivity, and in vitro growth studies. J. Virol. **19:**820–832.
81. **Waddington, S. N., J. H. McVey, D. Bhella, A. L. Parker, K. Barker, H. Atoda, R. Pink, S. M. Buckley, J. A. Greig, L. Denby, J. Custers, T. Morita, I. M. Francischetti, R. Q. Monteiro, D. H. Barouch, N. van Rooijen, C. Napoli, M. J. Havenga, S. A. Nicklin, and A. Baker.** 2008. Adenovirus serotype 5 hexon mediates liver gene transfer. Cell **132:**397–409.
82. **Walters, R. W., P. Freimuth, T. O. Moninger, I. Ganske, J. Zabner, and M. J. Welsh.** 2002. Adenovirus fiber disrupts CAR-mediated intercellular adhesion allowing virus escape. Cell **110:**789–799.
83. **Waszak, P., L. Franqueville, M.-L. Franco-Motoya, M. Rosa-Calatrava, O. Boucherat, L. Lindholm, C. Delacourt, and P. Boulanger.** 2007. Toxicity of fiber- and penton base-modified adenovirus type 5 vectors on lung development in newborn rats. Mol. Ther. **15:**2008–2016.
84. **Wickham, T. J., E. J. Filardo, D. A. Cheresh, and G. R. Nemerow.** 1994. Integrin alpha-v beta-5 selectively promotes adenovirus mediated cell membrane permeabilization. J. Cell Biol. **127:**257–264.
85. **Wickham, T. J., P. Mathias, D. A. Cheresh, and G. R. Nemerow.** 1993. Integrins alpha-v beta-3 and alpha-v beta-5 promote adenovirus internalization but not virus attachment. Cell **73:**309–319.
86. **Zabner, J., M. Chillon, T. Grunst, T. O. Moninger, B. L. Davidson, R. Gregory, and D. Armentano.** 1999. A chimeric type 2 adenovirus vector with a type 17 fiber enhances gene transfer to human airway epithelia. J. Virol. **73:**8689–8695.

Molecular Immunology 47 (2010) 982–990

Contents lists available at ScienceDirect

Molecular Immunology

journal homepage: www.elsevier.com/locate/molimm

Pairwise decomposition of residue interaction energies of single chain Fv with HIV-1 p17 epitope variants

Vannajan Sanghiran Lee[a,*], Panthip Tue-ngeun[a], Sawitree Nangola[b], Kuntida Kitidee[b], Jitrayut Jitonnom[a], Piyarat Nimmanpipug[a], Supat Jiranusornkul[c], Chatchai Tayapiwatana[b,d,**]

[a] Computational Simulation and Modeling Laboratory (CSML), Department of Chemistry and Center for Innovation in Chemistry, Chiang Mai University, Chiang Mai, 50200, Thailand
[b] Division of Clinical Immunology, Department of Medical Technology, Faculty of Associated Medical Sciences, Chiang Mai University, Chiang Mai, 50200, Thailand
[c] Department of Pharmaceutical Sciences, Faculty of Pharmacy, Chiang Mai University, Chiang Mai, 50200, Thailand
[d] Biomedical Technology Research Unit, National Center for Genetic Engineering and Biotechnology, National Science and Technology Development Agency at the Faculty of Associated Medical Sciences, Chiang Mai University, Chiang Mai, 50200, Thailand

ARTICLE INFO

Article history:
Received 27 October 2009
Received in revised form 7 November 2009
Accepted 13 November 2009
Available online 21 December 2009

Keywords:
HIV-1
p17
Epitope
Single chain Fv
Pairwise decomposition

ABSTRACT

Computational assisted modeling was carried out to investigate the importance of specific residues in the binding site of scFv. In this study, scFv against HIV-1 epitope at the C-terminal on p17 (scFv anti-p17) was used as a candidate molecule for evaluating the method. The wild-type p17 and its nine natural mutants were docked with scFv anti-p17. Potential mean force (PMF) scores predicted the most favorable binding interaction, and the correlation agreed well with the corresponding activity data from the peptide based ELISA. In the interaction with solvent molecules, the 3D structures of scFv anti-p17 and selected peptide epitopes were further investigated by molecular dynamics (MDs) simulation with the AMBER 9 program. Post-processing of the snapshot at equilibrium was performed to evaluate the binding free energy and pairwise decomposition or residue-based energy calculation of complexes in solution using the Molecular Mechanics Poisson–Boltzmann Surface Area (MM-PBSA) protocol. Our results demonstrated that the specific residues located in the complementary determining regions (CDRs) of scFv anti-p17, MET100, LYS101, ASN169, HIS228, and LEU229, play a crucial role in the effective binding interaction with the absolute relative decomposed energy more than 2.00 kcal/mol in comparison to the original substrate.

1. Introduction

The Gag p55 polyprotein of human immunodeficiency virus type 1 (HIV-1) plays a critical role in HIV-1 assembly and maturation. In the assembly step, the Gag polyprotein is directly targeted to the cell membrane to produce Gag dimerization or multimerization. Afterward, the viral-encoded protease cleaves the Gag precursor into the functional proteins: the matrix (MA or p17), capsid (CA or p24), nucleocapsid (NC) and p6 domains to form the infectious virus. The matrix protein (p17) is involved in many steps of the HIV life cycle, especially the assembly and maturation steps (Ganser-Pornillos et al., 2008; Bukrinskaya, 2004). Tewari and coworkers investigated an intrabody strategy using the single chain antibody fragment (scFv) derived from hybridoma-secreting anti-p17 antibody inside HIV-1 infected cells, which interfered with the viral replication process. This antibody specifically binds to the C-terminal epitope (DTGHSSQVSQNY) of the p17 domain (Tewari et al., 1998). The scFv platform can be expressed in both prokaryotic and eukaryotic systems and is able to be engineered in order to improve its functional affinity and stability (Quintero-Hernandez et al., 2007; Pavoni et al., 2006; Park et al., 2006). The potential applications of scFv have been explored in many areas of research, including diagnostics and gene therapy (Inui et al., 2009; Shen et al., 2008; Wang et al., 2008; Depetris et al., 2008; Stocks, 2005).

Computational approaches and protein structural analysis can provide relevant information about the functional roles of the scFv residues (Arcangeli et al., 2008). Fast protocols using force field based scoring functions and knowledge-based approaches for predicting binding affinities of protein-ligand complexes have been established. Some popular scoring functions for estimating binding affinities of protein–ligand complexes are DOCK (Ewing et al., 2001), AutoDock (Morris et al., 1998), PMF (Muegge and Martin,

* Corresponding author. Current address: Computational Simulation and Modelling Laboratory (CSML), Department of Chemistry and Center for Innovation in Chemistry, Faculty of Science, Chiang Mai University, Chiang Mai, 50200, Thailand. Tel.: +66891100216.
** Corresponding author. Current address: Division of Clinical Immunology, Department of Medical Technology, Faculty of Associated Medical Sciences, Chiang Mai University, Chiang Mai, 50200, Thailand. Tel. +66818845141.
E-mail addresses: vannajan@gmail.com (V.S. Lee), ptuengeun@gmail.com (P. Tue-ngeun), sawitree2727@hotmail.com (S. Nangola), kitidee_010@hotmail.com (K. Kitidee), jitrayut.018@gmail.com (J. Jitonnom), piyaratn@gmail.com (P. Nimmanpipug), supatjira@hotmail.com (S. Jiranusornkul), asimi002@hotmail.com (C. Tayapiwatana).

0161-5890/$ – see front matter © 2009 Elsevier Ltd. All rights reserved.
doi:10.1016/j.molimm.2009.11.021

1999), GOLD (Jones et al., 1997), LUDI (Bohm, 1998), FlexX (Rarey et al., 1996), and Ligscore (Krammer et al., 2005). Since most of the reactions of biological interest occur in water, the evaluation of the solvent effect represents an important aspect of the analytical and numerical molecular modeling approaches. Such computational approaches that consider the solvent as a part of a simulation system can be divided into several major groups: (i) continuum electrostatic methods, (ii) explicit solvent models with microscopic detail, and (iii) hybrids of the first two methods (Kollman, 1993; Smith and Pettitt, 1994; van Gunsteren et al., 1994; Tomasi and Persico, 1994; Leach, 1996; Gao, 1996; Levy and Gallicchio, 1998). An additional term is sometimes added to the force field to account for specific hydrogen bonding interactions. The more sophisticated methods have three-body nonadditive terms added. These methods include molecular dynamics (MD) (Pearlman et al., 1995; Brooks et al., 1983), Monte Carlo (MC) methods (Jorgensen, 1996), or a combination of these for sampling, and represent an advantage in terms of precision. These approaches can yield a reliable approximation method that allows one to (i) use a single trajectory of a complex between a receptor and a ligand; (ii) extract energies for the complex and all binding components by mapping their coordinates from the single trajectory; (iii) scan the sites of interest for the 'hot spots' in the receptor–ligand interface; and (iv) evaluate what the changes to the binding free energy would be upon modifications/mutations of the residues at the binding interface.

With the major advances in computer processing and clustering techniques, we are now able to perform molecular simulations of a large biomolecular system on a reasonable time scale. In this study, scFv anti-p17 was simulated based on molecular modeling of its homologue structure. The antibody-antigen complex models were generated using the flexible docking program incorporating binding activity data obtained from the peptide ELISA. The scFv anti-p17 structure with its epitopes at the C-terminal on the p17 fragment of HIV-1 and its natural mutant epitopes were analyzed in detail. In addition, the dynamic simulation method was applied to analyze the antibody–antigen interacting surface and to quantify the energetic nature of the complexes resulting from protein–ligand binding in water by applying the Molecular Mechanics–Poisson–Boltzmann Surface Area (MM-PBSA) protocol. The latter analysis can provide interesting information, such as electrostatic and van der Waals energies, solvation energies and entropic contributions at the binding interface. Our goal is to improve our understanding of the molecular basis of antigen recognition by scFv anti-p17.

2. Experimental

2.1. Computer assisted modeling

2.1.1. Homology modeling

The primary sequence of the scFv anti-p17 protein has previously been obtained by Tewari et al. (1998). The sequence of the light (VL) and heavy (VH) chain variable domains of scFv anti-p17 were compared with the primary sequences of all immunoglobulins deposited in the Protein Data Bank using the BLAST program (Altschul et al., 1997). The Complementary Determinant Region (CDR) definition of scFv anti-p17 variable domains was investigated using the Kabat method (Kabat et al., 1983).

The best match for the VH of scFv anti-p17 was the VH of idiotype-anti-idiotype Fab complex (pdb id:1iai), sharing 82% of sequence identity with the template, whereas the most homologous VL of scFv anti-p17 was the VL of the Fab fragment of a neutralizing antibody directed against an epitope of gp41 from HIV-1 (pdb id:1nld), sharing 96% of sequence identity with the template. These structures were used as templates for homology modeling of the 3D structure of scFv anti-p17 using the MODELLER program. The orientations of the VH and VL chains were generated by superposition using a crystal structure of the anti-DNA binding antibody (pdb id:2gki) as a scaffold template.

To minimize the steric clashes, the structure of scFv anti-p17 was subjected to energy minimization with 500 steps of steepest descent followed by 500 steps of conjugate gradient until the convergence criterion of 0.05 kcal/mol/Å was obtained, using the AMBER03 force field (Case et al., 2006). Structural validation of the scFv anti-p17 was checked using PROCHECK; more than 92% of the residues were in the most favored regions of the Ramachandran plot, and overall G-factors were inside the expected regions for structures with 2.0 Å resolutions. It is generally acknowledged that antigen binding occurs in a variety of ways, and thus leads to

Table 1
PMF scores and residues on CDR loops of scFv at 4.5 Å from each of four peptide epitopes. The common amino acids are in boldface type.

Peptide names	Peptide sequences	PMF score (kcal/mol)	Amino Acid in 4.5 Å from peptide epitope	
			Nonpolar hydrophobic	Polar hydrophilic
p17.1	^{121}DTGHSSQVSQNY^{132}	−902.11	GLY33 (H1), **TRP50 (H2)**, **MET100 (H3)**, **GLY226 (L3)**, **LEU229 (L3)**	**SER99 (H3)**, **SER103 (H3)**, **ASP163 (L1)**, **ASP190 (L2)**, **THR227 (L3)**
p17.2	^{121}DTGHS<u>N</u>QVSQNY^{132}	−899.18	**TRP50 (H2)**, **MET100 (H3)**, GLY161 (L1), LEU185 (L2), **GLY226 (L3)**, **LEU229 (L3)**	**THR59 (H2)**, **SER99 (H3)**, **LYS101 (H3)**, **SER103 (H3)**, SER162 (L1), **ASP163 (L1)**, **THR227 (L3)**, HIS228 (L3)
p17.3	^{121}DTGHSSQ<u>I</u>SQNY^{132}	−882.65	**TRP50 (H2)**, **MET100 (H3)**, PHE167 (L1), **GLY226 (L3)**, **LEU229 (L3)**	**SER99 (H3)**, **LYS101 (H3)**, **ASP163 (L1)**, TYR184, **ASP190 (L2)**, SER191, **THR227 (L3)**, GLN231 (L3)
p17.4	^{121}DTGH<u>N</u>SQVSQNY^{132}	−898.71	GLY33 (H1), **MET100 (H3)**, **GLY226 (L3)**, **LEU229 (L3)**	ASP31 (H1), TYR32 (H1), ASN52 (H2), **SER99 (H3)**, **LYS101 (H3)**, HIS228 (L3), GLN231 (L3)
p17.5	^{121}<u>N</u>TGHSSQVSQNY^{132}	−843.51	**TRP50 (H2)**, **MET100 (H3)**, **PHE167 (L1)**, LEU185 (L2), **LEU229 (L3)**	ASN35 (H1), **SER99 (H3)**, **LYS101 (H3)**, ASN169 (L1), TYR184, **ASP190 (L2)**, SER191, **THR227 (L3)**, **HIS228 (L3)**
p17.6	^{121}DTG<u>N</u>SSQVSQNY^{132}	−846.12	GLY33 (H1), **TRP50 (H2)**, **MET100 (H3)**, **LEU229 (L3)**	**SER99 (H3)**, **LYS101 (H3)**, LYS165 (L1), TYR184, SER191
p17.7	^{121}DTGHSSQ<u>A</u>SQNY^{132}	−829.94	**TRP50 (H2)**, **MET100 (H3)**, **PHE167 (L1)**, **GLY226 (L3)**	**THR59 (H2)**, **LYS101 (H3)**, LYS165 (L1), LYS188 (L2), **THR227 (L3)**, HIS228 (L3)
p17.8	^{121}DTGHS<u>K</u>QVSQNY^{132}	−926.79	**TRP50 (H2)**, **MET100 (H3)**, **PHE167 (L1)**, **GLY226 (L3)**, **LEU229 (L3)**	**THR59 (H2)**, **SER99 (H3)**, **LYS101 (H3)**, **SER103 (H3)**, SER162 (L1), **ASP163 (L1)**, **THR227 (L3)**
p17.9	^{121}DTG<u>NN</u>SQVSQNY^{132}	−841.02	**TRP50 (H2)**, **MET100 (H3)**, **PHE167 (L1)**, LEU185, **LEU229 (L3)**	**THR59 (H2)**, **SER99 (H3)**, **LYS101 (H3)**, LYS165, ASN169 (L1), TYR184, **ASP190 (L2)**, SER191, **HIS228 (L3)**

The underlined letters are the mutated residue in each sequence compared to the wild type.

a differing arrangement of antibody conformations. In scFv anti-p17, there are actually six unique hypervariable units. Each of the chains contains three of the six loops that form the binding groove. The hypervariable portions of the loops on the heavy chain are designated H1(31–35), H2(50–66) and H3(99–104) while those on the light chain are L1(154–169), L2(185–190), and L3(224–232) (Tewari et al., 1998). These regions are also known as complementary determining regions (CDRs), which have a higher binding affinity to the antigen.

2.1.2. Molecular docking

Nine peptides, an original HIV-1 epitope at the C-terminal (^{121}DTGHSSQVSQNY^{132}) on p17 and eight natural mutants (Table 1), were built partly based on a crystal structure from the Protein Databank (pdb id:1kj4). The initial structures of the nine modeled peptides were energy minimized (1000 steps of Adopted Basis Newton Raphson (ABNR)) using CHARMm force field with a RMS gradient of 0.01 kcal/(Å mol) in Discovery Studio 1.7. Structures of scFv anti-p17 (a homology model) complexed with the peptides were constructed using the docking procedure in the BioMedCaChe 2.0 (Fujitsu, Inc.) program, in which the CDR loops (L1–L3 and H1–H3) were defined as the potential binding sites. Both the peptides and the binding sites were set to be flexible during the docking simulation. Each of the docking complexes were energetically evaluated based on the potential of mean force (PMF) that describes the potential energies involving bond stretching, angle bending, torsional, and non-bonded interactions such as Amber van der Waals and hydrogen bond interactions of molecules (Muegge and Martin, 1999). The PMF scores of each peptide were evaluated by a genetic algorithm with a population size of 50, crossover rate of 0.80, elitism of 5, mutation rate of 0.2, and the maximum cycle generation was set to be 40,000. The size of the grid box was 30 × 30 × 30 Å. Finally, the complex structures were analyzed and the interaction energy between the peptides and antibody was calculated.

2.1.3. Molecular dynamics (MD) simulations and binding free energy calculation

MD simulations were carried out at the molecular mechanics level using the AMBER03 force field as implemented in the AMBER9 suite of programs (Case et al., 2005). Structures of antibody-peptide were solvated in a cubic box of TIP3P water extending at least 10 Å in each direction from the solute, and the cut-off distance was kept to 12 Å to compute the nonbonded interactions. All simulations were performed under periodic boundary conditions (Weber et al., 2000), and long-range electrostatics were treated by using the particle-mesh-Ewald method (Darden et al., 1993; Essmann et al., 1995). The time step was set to 1 fs and the trajectory was recorded every 0.1 ps.

Prior to MD simulations, the systems were relaxed by a series of steepest descent (SD) and conjugated gradient (CG) minimizations. The 2-ns MD simulations were performed based on each of the minimized systems by gradually heating over 60 ps from 0 to 310 K with the protein atoms fixed using a force constant of 5 kcal/mol/Å^2. Then, a 200 ps pressure-constant period (NPT) was applied to obtain an equilibrated density of the constrained protein atoms. The following step was a 40 ps-volume-constant period (NVT) at a force constant of 2.5 kcal/mol/Å^2 followed by 100 ps dynamics at a force constant of 1.25 kcal/mol/Å^2. Finally, a 1.6 ns unrestrained MD simulation (no force applied on any protein atoms) was performed for each fully flexible system in the NVT ensemble at a constant temperature of 310 K. A total of 500 snapshots were collected at 1 ps-intervals from the last 500 ps of MD for binding free energy analysis.

Based on the selected MD snapshots, the binding free energy for each antibody-peptide system could be estimated using MM-PBSA (Molecular Mechanics Poisson–Boltzmann Surface Area) (Kollman et al., 2000) and MM-GBSA (Molecular Mechanics Generalized Born Solvent Area) (Chong et al., 1999). The binding free energies ($\Delta G_{binding}$) were determined from the free energies of the complex, protein and peptide according to the equation:

$$\Delta G_{binding} = \Delta G_{water}(complex) - [\Delta G_{water}(protein) + \Delta G_{water}(peptide)]$$

The binding free energies for each species in turn were estimated from the absolute molecular mechanical energies (E_{MM}), the solvation free energies ($G_{PB/GB} + G_{nonpolar}$) and the vibration, rotation and translation entropies. Each of these terms was calculated as follows:

$$\Delta G_{water} = E_{MM} + \Delta G_{solvation} - T\Delta S;$$

$$G_{solvation} = G_{solvation-electrostatic} + G_{nonpolar};$$

$$E_{MM} = E_{internal} + E_{electrostatic} + E_{vdW};$$

$$E_{internal} = E_{bond} + E_{angle} - E_{torsion}$$

where the internal energy $E_{internal}$ has three contributions: E_{bond}, E_{angle}, and $E_{torsion}$, which represent the strain energy in bonds, angles and torsion angles caused by their deviation from the equilibrium values; $E_{electrostatic}$ and E_{vdW} are the electrostatic and van der Waals interaction energies, respectively; $-T\Delta S$ is the change of conformational entropy upon peptide binding, which is not considered here because of its high computational demand and relatively low accuracy of prediction (Hou et al., 2002). All energies are averaged along the MD trajectories.

E_{MM} was determined with the *sander* module of the AMBER suite with an infinite cut-off for all interactions. For the MM-PBSA calculations, ΔG_{PB} was calculated with a built-in module, the *pbsa* program in AMBER9 which solves the Poisson–Boltzmann equation. The grid size for the PB calculations was 0.5 Å. In the MM-GBSA calculations, ΔG_{GB} was calculated using the GB model with the parameters developed by Tsui and Case (2000). The values of the interior and exterior dielectric constants were set to 1 and 80, respectively. ΔG_{np} was estimated based on the solvent accessible surface area (SASA) as $\Delta G_{np} = 0.0072 \times SASA$, using the *molsurf* program (Kabat et al., 1983) and (Case et al., 2006). The scFv anti-p17/peptide interaction energy profiles were generated by decomposing the total binding free energies into residue-residue interaction pairs by the MM-GBSA decomposition process in the *mm_pbsa* program of AMBER9 (Gohlke et al., 2003; Hou et al., 2008).

2.2. Affinity determination

2.2.1. Vector construction

A vector for expressing scFv that specifically binds to the C-terminal epitope (^{121}DTGHSSQVSQNY^{132}) of the p17 fragment of HIV (scFv anti-p17) was constructed. Briefly, to generate the gene encoding scFv anti-p17 as described previously (Tewari et al., 1998), total RNA was extracted from hybridoma cells, MH-VM33C9/ATCC HB8975, using an RNeasy Mini kit (Qiagen, Hilden, Germany) and the first-strand cDNA was synthesized using a Transcriptor High Fidelity cDNA synthesis kit (Roch, Mannheim, Germany). The resulting cDNA was further amplified for the VH and VL fragments using specific primers, and the two fragments were linked together using Fw VHP17 and Rev VLP17 primers by overlapping PCR, which resulted in the completed fragment encoding scFv anti-p17. The fragment was treated with *Sfi*I restriction enzyme and cloned into *Sfi*I-treated pComb3X phagemid vector (a gift from Dr. C.F. Barbas, Scripps Research Institute, USA) resulting in the pComb3X-scFvp17 vector. The sequence of scFv anti-p17 was analyzed by standard sequencing methods (1st Base, Singapore).

The pComb3X-scFvp17 vector was subsequently transformed into the non-suppressor *Escherichia coli* strain HB2151.

The primers used for the amplification reactions were as follows: (1) Fw VHP17 (5′-ATATGCTAGCGGCCCAGGCGGCCCAGATC-CAGTTGGTGCAGT-3′), (2) Rev VHP17 (5′-CGACCCTCCACCGCG-GACCCGCCACCTCCAGACCCTCCGCCACCTGCA GAGACAGTGACC-AGAGTCCC-3′) for V_H fragment generation, (3) Fw VLP17 (5′-GGGTCCGGCGGTGGAGGGTCGGATGTTGTGATGACCCGACTCCA-3′) and 4) Rev VLP17 (5′-TATAAGCTTTCATTAAGCGTAGTCCGGAACGT-CGTACGGGTACTGGCCGCCCT GCCTTTGATTTCCAGCTTGGTACCTCC-3′) for V_L fragment generation.

2.2.2. Preparation of soluble scFv anti-p17

The soluble scFv anti-p17 was produced by expressing pComb3X-scFvp17 vector in the non-suppressor *E. coli* strain HB2151. The bacterial cells harboring the vector were grown in 10 ml of Terrific broth (1.2% (w/v) tryptone, 2.4% (w/v) yeast extract, 0.4% [w/v] glycerol, 17 mM KH_2PO_4, 72 mM K_2HPO_4) containing ampicillin (100 μg/ml) at 37 °C for 18 h with shaking. One hundred microliters of precultured bacteria were inoculated in 100 ml of the same medium containing 1% (w/v) glucose and ampicillin (100 μg/ml), with shaking continued at 37 °C until an optical density (OD) of 1.5 at 600 nm was reached. To induce the protein expression, IPTG was added to the culture at a final concentration of 1 mM. After induction, the bacteria were grown at 25 °C for 20 h. The culture supernatant containing extracellular soluble scFv anti-p17 was collected by centrifugation at 5000 × *g* for 30 min at 4 °C. Protein was precipitated with saturated $(NH_4)_2SO_4$ in an ice bath and concentrated with Amicon Ultra centrifugal filter units (Millipore, Cork, Ireland). Finally, the concentrated protein was reconstituted with 1.5 ml of 0.15 M PBS, pH 7.2. The concentrated protein was separated in 12% SDS-PAGE under reducing conditions, and transferred to a nitrocellulose membrane (GE Healthcare, Buckinghamshire, UK). The blotted membrane was blocked with 5% skimmed-milk in PBS for 1 h at room temperature (RT) with shaking and then treated with anti-HA antibody (Sigma–Aldrich, St. Louis, MO). After incubation, the membrane was washed 5 times with washing buffer (0.05% Tween-20 in PBS) and peroxidase-conjugated goat anti-mouse immunoglobulin antibodies were added to the membranes. The peroxidase reaction was visualized using a SuperSignal West Pico Substrate (Pierce, Rockford, USA).

2.2.3. Evaluation of the binding activity of scFv anti-p17 by ELISA

To evaluate the binding activity of scFv anti-p17 with mutant peptides, four peptides were synthesized (GenScript, Piscataway, New Jersey, USA) and tested with the scFv protein using a standard ELISA procedure. Peptide p17.1 represented the wild-type epitope while another peptide represented the mutant peptides. The amino acid sequences of all synthetic peptides are shown in Table 1. Briefly, 100 μl of 50 μg/ml of each peptide in coating buffer (0.1 M $NaHCO_3$, pH 8.6) were added to microtiter plates (NUNC, Roskilde, Denmark) and incubated overnight at 4 °C. The coated wells were then blocked with 200 μl of blocking buffer (2% BSA in TBS) for 1 h at RT. The wells were washed five times with washing buffer (0.05% Tween-20 in TBS). 100 μl of 200 μg/ml of scFv anti-p17 protein in blocking buffer were added to each well and incubated for 1 h at RT. After incubation, the excess antibody was eliminated by washing. Subsequently, the wells were incubated for 1 h at RT with 100 μl of HRP-conjugated goat anti-mouse IgS antibody (KPL, Maryland, USA) diluted 1/3000 in blocking solution. Wells were then washed again prior to adding 100 μl of 3,3′,5,5′-tetramethyl-benzidine (TMB) substrate. The optical densities (OD) at 450 nm were measured by an ELISA plate reader (TECAN, Austria) after adding 100 μl of 1 N HCl.

To assess the binding affinity between scFv anti-p17 and mutant peptides, a peptide competitive ELISA was performed. The same procedure was followed as described for the peptide ELISA; the scFv protein was mixed with 100 ng/ml of each mutant peptide and incubated for 1 h at RT. 100 μl of the mixture were applied into individual peptide p17.1 pre-coated wells and incubated for 1 h at RT. After washing the wells, the bound scFv anti-p17 was monitored by adding 100 μl of HRP-conjugated goat anti-mouse IgS antibody. Wells were then washed again and 100 μl of TMB substrate were subsequently added for 45 min. The enzymatic reaction was stopped by adding 100 μl of 1N HCl. The OD at 450 nm was measured by an ELISA plate reader. The OD values were converted to percentage inhibition values (PI) by using the following formula:

$PI = 100 - \left(\left(\frac{B}{B_0}\right) \times 100\right)$ B and B_0 are the OD values of scFv with peptide inhibitor and without peptide inhibitor respectively.

3. Discussion

3.1. Homology modeling of scFv and complex model

We selected VH and VL fragments of anti-p17 antibody from hybridoma cells MH-VM33C9/ATCC HB8975 for analysis. We had also prepared recombinant scFv anti-p17 by cloning the gene encoding VH and VL into a prokaryotic expression vector. For the homology modeling, the scFv antibody with the peptide epi-

(a)

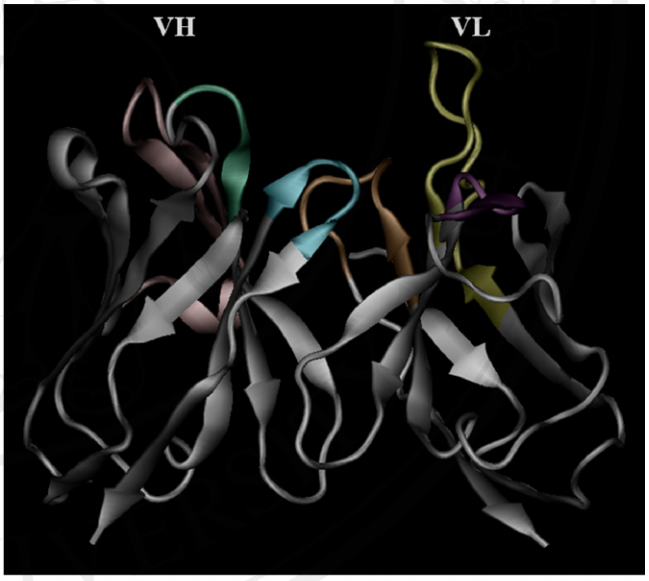

(b) VH sequence

CDR H1
QIQLVQSGPELKKPGETVEISCKASGYTFTDYGMNWMKQAPGKSLKWMGW 50
CDR H2
INTYTGEPTYADEFKGRFAFSLETSASTAYLQINNLKSEDMATYFCSRSM 100
CDR H3
KGSYWGQGTLVTVSA 115

VL sequence

CDR L1
DVVMTQTPLTLSVTIGQPASISCKSSQSLLGSDGKTFLNWLLQRPGQSPK 50
CDR L2 CDR L3
RLIYLVSKLDSGVPDRFTGSGSGTDFTLKISRVEAEDLGVYYCWQGTXLP 100

QTFGGGTKLEIK 112

Fig. 1. Molecular models of scFv anti-p17. (a) 3D structural model for scFv anti-p17. VH and VL domains are colored *white*. The hypervariable binding loops are colored *green* (H1), *pink* (H2), *cyan* (H3), *yellow* (L1), *purple* (L2), and *orange* (L3). (b) Amino acid sequences of the hypervariable binding VH (1–114) and VL (131–241) domains of scFv anti-p17 and an artificial linker shown in bold $(GGGGS)_3$; the loops in the heavy chain (CDRH1: 31–35, CDRH2: 50–66, and CDRH3: 99–104), and the loops in the light chain (CDRL1: 154–169, CDRL2: 185-190, and CDRL3: 224–232) of the scFv antibody. (For interpretation of the references to color in this figure legend, the reader is referred to the web version of the article.).

Table 2
Relationship between the binding activities from competitive ELISA and those from MM-PBSA methodology at 310 K.

Method	Contribution	Peptide Names				CD147
		p17.1	p17.3	p17.7	p17.8	
MM	Δ(L(	−227.32	−174.34	−169.29	−91.34	
	ΔVDW	−72.28	−55.46	−48.01	−68.95	
	ΔGAS	−299.60	−229.81	−217.30	−160.29	
PBSA	ΔPB_{SUL}	−11.02	−9.73	−8.54	−10.56	
	ΔPB_{CAL}	280.63	230.71	217.07	144.47	
	ΔPB_{SOL}	269.61	220.99	208.53	133.91	
	ΔPB_{ELE}	53.31	56.37	47.78	53.13	
	ΔPB_{TOT}	−29.98	−8.82	−8.77	−26.38	
GBSA	ΔGB_{SUL}	−11.02	−9.73	−8.54	−10.56	
	ΔGB_{CAL}	273.07	220.02	207.41	136.89	
	ΔGB_{SOL}	262.05	210.29	198.87	126.33	
	ΔGB_{ELE}	45.75	45.68	38.12	45.55	
	ΔGB_{TOT}	−37.55	−19.52	−18.43	−33.97	
	Experimental value[a]	75.94	55.25	44.60	79.46	7.94

ELE, electrostatic interactions; VDW, van der Waals interactions between the fragments; GAS, addition ELE + VDW + INT being the binding enthalpic contributions in vacuo; PB_{SUR}, nonpolar contribution to solvation; PB_{CAL}, polar contribution of solvation; PB_{SOL}, the PB_{SUR} + PB_{CAL}; PB_{ELE}, PB_{CAL} + ELE addition; PB_{TOT}, total binding free energy calculated by the MM-PBSA method.

[a] Competitive ELISA: PI (%)

tope was assembled and modeled based on a homology modeling approach. The three dimensional structure and the amino acid sequence of scFv anti-p17 are shown in Fig. 1. The models of scFv, nine peptide epitopes, and the scFv-peptide complexes were generated separately. The sequences of mutated peptides that were obtained from the GenBank database comprised the following positions: the single mutation of S126N, V128I, S125N D121N, H124N, V128A, S126K, and the double mutation of H124N and S125N. The sequences of all peptide epitopes that were initially positioned outside the binding region were docked against scFv in the same manner. The PMF scores (Table 1) of the complex structures were calculated with the BioMedCaChe 2.0 (Fujitsu, Inc.) program, where flexible peptide epitopes were docked into flexible side chain proteins. The peptide epitopes and the side chains of the amino acids of the CDR domains were kept flexible during the docking simulation. The PMF scores were in the range of −829.939 to −926.793 kcal/mol. The peptides bound in two orientations, where the N-terminal (p17.1, p17.2, p17.4–p17.6, and p17.8) and the C-terminal (p17.3, p17.7, and p17.9) of peptide sequences were directed toward the binding pocket. All interactions of the optimum docking structures reflected the negative binding energies in all models, indicating favorable binding in all complexes. Less favorable binding of peptide 17.3 and p17.9 to scFv was due to their inverted binding of the N-terminal to the outside of the binding pocket. The C-terminal sequences of p17.3 and p17.9 had better fits in the binding pocket. A similar binding pattern as for the substrate with the N-terminal sequence towards the inside of the pocket was also observed, but had higher binding energy scores. Interestingly, we found that mutation of a particular epitope at S125K of peptide p17.8 caused the maximum enhancement of the binding energy. The interacting amino acids of scFv within 4.5 Å from an individual docked peptide are listed in Table 1. The common binding residues of scFv are composed of the combination of hydrophilic and hydrophobic amino acids: Trp50 (H2), Thr59 (H2), Ser99 (H3), Met100 (H3), Lys101 (H3), Ser103 (H3), Asp163 (L1), Phe167 (L1) Asp190 (L2), Gly226 (L3), Thr227 (L3), His228 (L3), and Leu229 (L3), as indicated in boldface type.

3.2. Comparison of calculated binding free energy with experimental data

The DNA encoding scFv fragment of anti-p17 was successfully generated and cloned into a pComb3X phagemid vector, resulting in the pComb3X-scFvp17 vector. This vector was subsequently transformed in non-suppressor *E. coli* (HB2151) for soluble expression of scFv anti-p17. The bacterial cells harboring pComb3X-scFvp17 vector were cultured and induced with 1 mM IPTG. The soluble protein in the culture supernatant was precipitated by ammonium precipitation and concentrated with an Amicon Ultra centrifuge filter. The scFv anti-p17 was expressed in its soluble form by induction, secreted into culture supernatant and revealed by western immunoblotting. A band with a molecular weight of approximately 30 kDa, corresponding to the molecular size of scFv, was detected in the concentrated protein (data not shown).

In order to investigate protein binding efficiency, peptide ELISA was employed to demonstrate the binding activity of scFv anti-p17 to its target peptide (p17.1), and the chosen mutant peptides (p17.3, p17.7 and p17.8) (Fig. 2). Positive signals were observed in all peptide coated wells, indicating that this recombinant scFv could bind to all mutant peptides. Peptide p17.8 gave the highest signal followed by p17.1, p17.3 and p17.7, respectively. All soluble mutant peptides were able to inhibit the binding between the scFv and immobilized p17.1 peptide (Table 2), as revealed by the percentage inhibition value (PI), but the CD147 peptide had no significant inhibitory effect. Peptides p17.1 and p17.8 exhibited the highest

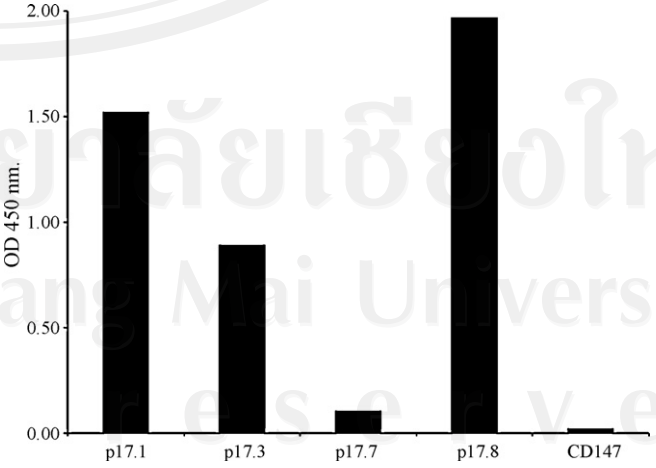

Fig. 2. The binding activity of soluble scFv anti-p17 from peptide ELISA.

inhibitory effects compared to the other two peptides, p17.3 and p17.7, at the same concentration.

Comparison of experimental activities with the results derived from MM-PBSA and MM-GBSA calculations suggested that the experimental value for MM-PBSA had a nearby correlation ($r^2 = 0.88$) with the calculated binding free energy of MM-GBSA ($r^2 = 0.90$), as shown in Table 2. Initially, favorable configurations for forming a scFv anti-p17–antigen complex system were built by molecular docking. The binding structures of the ligand to its receptor were analyzed based on the energy of the ligand or receptor. From the PMF scores, we selected four peptide epitopes consisting of one wild-type peptide (p17.1) and three mutated peptides (p17.3, p17.7, and p17.8) for further investigation by MDs and peptide ELISA. Peptide p17.7 had the lowest score and p17.8 had the highest score, whereas p17.3 had very similar score to that of the wild-type peptide. To understand the binding interaction in water, the binding free energies of those complexes were simulated by molecular dynamics simulations (MDs), and the Molecular Mechanics Poisson–Boltzmann Surface Area methodology was applied to calculate the binding free energy of all residues of the complexes. Table 2 lists the terms that contributed the calculation of binding free energy for the selected complex. The value of PB_{TOT} was used to compare the simulation with the experimental results. The more negative the value, the more favorable the binding. The binding energies identified by the MM-PBSA protocol were ranked as follows: peptide p17.1 < p17.8 < p17.3 < p17.7 with the values of −29.98, −26.38, −8.82, −8.77, and kcal/mol, respectively. The results were consistent with PMF scores from molecular docking data, which divided the mutants into two groups of high and low activities. The binding free energy indicated highly favorable binding of scFv with peptides p17.1 and p17.8, about 18 kcal/mol more negative than p17.3. Consequently, we identified the p17.3, p17.4, p17.5, p17.6, p17.7 and p17.9 as the low affinity binding peptides, whereas the p17.1, p17.2, and p17.8 were identified as the high affinity binding peptides with our scFv.

The major contributions to the binding free energy arise from the electrostatic energy, as calculated by the molecular mechanic (MM) force field (ELE); from the electrostatic contribution to the solvation free energy, as calculated by PB (PB_{CAL}); and van der Waals contribution from MM (VDW). For the four binding peptides, both van der Waals and electrostatic energies were quite varied among the low and high activities groups, indicating that both terms are factors determining the binding activity. Peptide p17.8 had a somewhat lower electrostatic contribution (−91.34 kcal/mol). Among the other sequences, however, the combination with VDW and the sum of nonpolar and polar contributions to solvation (PB_{SOL}) resulted in a total negative binding free energy. This supported a favorable scFv–peptide complex in pure water. The result does not equal the real binding free energy since we did not estimate the entropy contribution to binding in this study.

3.3. Decomposition of energy on the amino acid residues in CRD loops and specific contact upon binding

The interpretation of macroscopic data in terms of microscopic interactions of scFv with a peptide binding sequence can be done by decomposing the calculated binding free energies as a sum of components that correspond to the contributions of different energy terms or different parts of the system. Therefore, important residues of anti-HIV p17 scFv will show strong interactions in association with its antigen. To gain further insight into the key residue interactions, the overall agreement between the calculated and experimental values for the ligands obtained by the MM-PBSA approach allows us to be optimistic of the results when estimating protein–ligand interactions. Table 3 and Fig. 3 illustrate the results of this analysis, plotting the relative decomposed energies versus common amino acids on the CDR loops of scFv anti-p17 and each of four peptide epitopes. All amino acids in the scFv sequences were found to exhibit positive or negative influences on binding to the substrate molecules. Several residues of the wild-type

Table 3
Common interacting residues found among the natural peptide sequences in the docking study.

Residue	Loop	Decomposed energy (kcal/mol)			
		p17.1	p17.3	p17.7	p17.8
ASP31	H1	0.26	0.35 (0.09)	0.28 (0.02)	0.24 (−0.02)
TYR32	H1	0.04	−0.05 (−0.09)	0.03 (−0.01)	0.01 (−0.03)
GLY33	H1	0.01	−0.08 (−0.09)	−0.02 (−0.03)	−0.11 (−0.12)
ASN35	H1	0.14	−0.14 (−0.28)	−0.09 (−0.23)	−0.34 (−0.48)
TRP50	H2	−1.73	**−3.76 (−2.03)**	−2.05 (−0.32)	**−4.90 (−3.17)**
ASN52	H2	0.03	−0.25 (−0.28)	−0.05 (−0.08)	−0.84 (−0.87)
THR59	H2	0.04	−0.56 (−0.60)	−0.57 (−0.61)	−0.61 (−0.65)
SER99	H3	−0.18	−0.17 (0.01)	0.09 (0.27)	−0.62 (−0.44)
MET100	H3	−3.80	**−1.02 (2.78)**	−3.27 (0.53)	−3.59 (0.21)
LYS101	H3	−2.91	**−0.56 (2.35)**	−1.10 (1.81)	**4.24 (7.15)**
SER103	H3	−0.11	0.06 (0.17)	0.03 (0.14)	−1.31 (−1.2)
GLY161	L1	0.01	−0.01 (−0.02)	−0.07 (−0.08)	−0.02 (−0.03)
SER162	L1	0.11	0.03 (−0.08)	−0.07 (−0.18)	0.20 (0.09)
ASP163	L1	0.40	0.28 (−0.12)	0.39 (−0.01)	−0.27 (−0.67)
LYS165	L1	−0.50	−0.16 (0.34)	−0.26 (0.24)	0.46 (0.96)
PHE167	L1	−2.26	−3.14 (−0.88)	−1.59 (0.67)	**−4.87 (−2.61)**
ASN169	L1	−2.66	**0.00 (2.66)**	**0.09 (2.75)**	**−0.22 (2.44)**
TYR184	–	−2.41	−2.06 (0.35)	−1.44 (0.97)	−1.79 (0.62)
LEU185	L2	−0.07	−1.24 (−1.17)	−1.13 (−1.06)	−2.06 (−1.99)
LYS188	L2	−0.14	−0.07 (0.07)	−0.30 (−0.16)	0.02 (0.16)
ASP190	L2	0.26	−0.37 (−0.63)	0.20 (−0.06)	−0.10 (−0.36)
SER191	–	−0.03	0.00 (0.03)	0.00 (0.03)	0.01 (0.04)
GLY226	L3	−0.18	−0.57 (−0.39)	−0.07 (0.11)	−1.29 (−1.11)
THR227	L3	−0.30	−0.32 (−0.02)	−1.85 (−1.55)	**−2.90 (−2.6)**
HIS228	L3	−3.93	**0.14 (4.07)**	**−0.42 (3.51)**	**−1.12 (2.81)**
LEU229	L3	−4.53	**−0.70 (3.83)**	**−1.15 (3.38)**	**−2.07 (2.46)**
GLN231	L3	−0.52	**−2.75 (−2.23)**	−1.20 (−0.68)	0.14 (0.66)

Relative energy to p17.1 is in parenthesis. The amino acids which have significant contribution with the absolute relative energy larger than 2 Kcal/mol are indicated in bold letters.

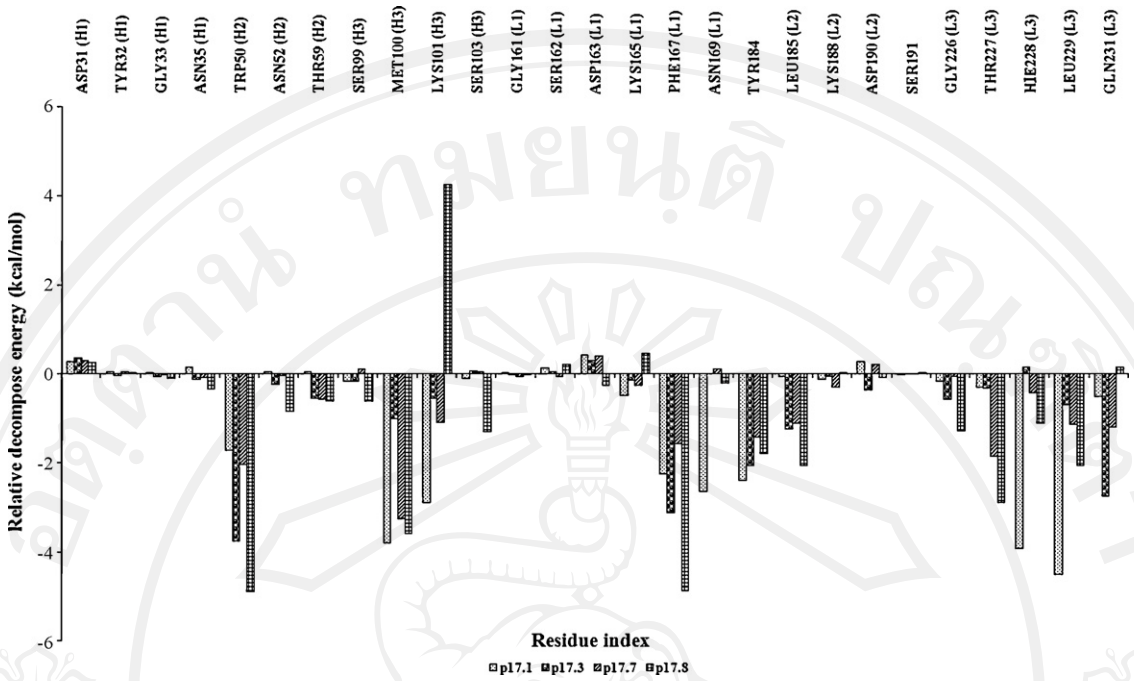

Fig. 3. List of the decomposed energies of the common amino acids in CDR loops of scFv.

p17.1 (Trp50, Met100, Lys101, Phe167, Asn169, Thr227, His228, Leu229 and Gln231) were verified to have significant effective contributions with the absolute relative energy larger than 2 kcal/mol for the stabilization energy as highlighted in Table 3. There was strong interdependence of the effects of the individual residues in the epitope sequences. Among three mutated peptides, poor binding and/or weak interaction, with relative energy above 2 kcal/mol in comparison with wild-type p17.1, was obtained from Met100, Lys101, Asn169, His228, and Leu229 of scFv. Better binding was indicated by the lower decomposed energy with the absolute relative energy below 2 kcal/mol. The difference between high and low affinity binding depends on the interaction of each sequence with the amino acids in the CDR region of scFV. The Trp50 of scFv exhibited more binding interaction with both p17.3 (V128I) and p17.8 (S125K) than the wild-type peptide. Sequence p17.1 shows the strongest binding among all sequences, with Met100, Lys101, Asn169, His228, and Leu229, whereas sequence p17.8 exhibited the strongest binding with different amino acids such as Try50, Phe167 and Thr227. This is compared to only one strong binding interaction among other sequences with Gln231 as observed in sequence 17.3 and no strong binding interaction with 17.7 resulted in a low binding affinity. These interactions make a significant contribution to the overall binding. As mentioned in the previous section, the decomposed energies of some residues in scFv have positive values with peptide epitopes. A particularly strong case, with decomposed energy of 4.24 kcal/mol, was observed for p17.8 binding with Lys101. However, the sum of all those energy terms resulted in favorable binding. Overall we found that Met100(H3), Lys101(H3),

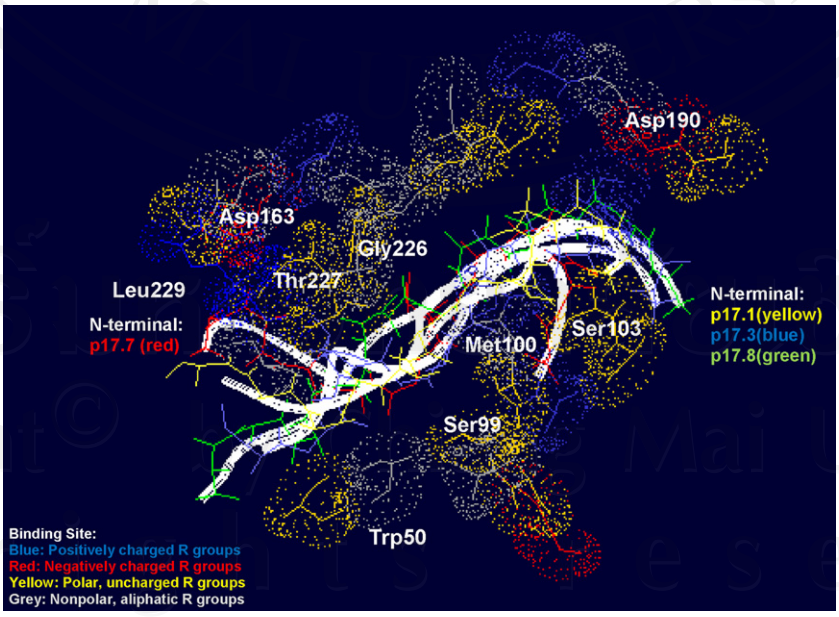

Fig. 4. The residues interaction of the final MD complex structures between scFv anti-p17 and four peptide epitopes.

Asn169(L1), His228(L3), and Leu229(L3) exhibited strong interactions with peptide p.17.1. From the MD structure in the last 500 ps, we also observed strong hydrogen bonding interactions with more than 95% occupancy for R181 in L2 with D121 and Q127 of the substrate sequence.

Further analysis of the final MD complex structures is shown in Fig. 4. As expected, p17.3 bound in different patterns among other sequences since its C-terminal has binding sites oriented toward the inside of the pocket instead of the N-terminal. Our study using pairwise decomposition of residue interaction energies has allowed us to gain insight into the interactions between anti-p17 single chain Fv with its peptide epitopes for HIV-1.

4. Conclusions

Computer models were combined with laboratory experiments for the efficient determination and the identification of the most important residues for scFv in binding with natural peptide substrates. ScFv anti-p17 was built from its X-ray structure homologue, and the complexes of scFv anti-p17 with its natural epitope were generated using a flexible docking method. The efficacy of combining the scFv antibody with peptide epitopes according to the potential mean force scoring correlated well with peptide ELISA results. Molecular dynamics simulations were performed on selected peptides to evaluate their interaction in water. Overall structural changes of binding peptides in response to enzyme binding in water were investigated by the root mean square displacement. Poorly binding peptides exhibit a larger root mean square displacement than do tightly binding peptides. MM-PBSA and pairwise decomposition energies were calculated from post-analysis of molecular dynamics structures. The calculated binding free energies concurred well with experimentally determined high binding affinity (decomposed energy >2 kcal/mol) and low binding affinity of investigated peptides to anti-p17 scFv. Several amino acids, MET100, LYS101, ASN169, HIS228, and LEU229, in the complementary determining regions (CDRs) were defined for their major contribution to the binding efficiency of natural HIV epitope at the C-terminal on p17. This technique could be applied to elucidate the most important amino acids involved in the binding of scFv with its target molecules. Moreover, the identified amino acids can be modified for improving the binding activity.

Acknowledgements

The authors would like to express grateful acknowledgement the financial support from the Thailand Research Fund (TRF), the Research Chair Grant of National Sciences and Technology Development Agency (Thailand), the Center for Innovation in Chemistry (PERCH-CIC), Commission on Higher Education, Ministry of Education of Thailand, and the Computational Nanoscience Consortium (CNC), the National Nanotechnology Center (NANOTEC) and National Science and Technology Development Agency (NSTDA), Thailand for the access to Discovery Studio Version 1.7 program package. The authors would also like to thank Dr. Dale Taneyhill for proofreading the manuscript.

Contributors: SN, KK, CT contributed with experimental design, performance of all experiments, and writing of the manuscript. VSL and PT participated in all calculations and JJ assisted with the antibody modeling building. VSL, PN, SJ, and CT contributed with supervising and writing of the manuscript. All authors read and approved the final manuscript.

References

Altschul, S.F., Madden, T.L., Schäffer, A.A., Zhang, J., Zhang, Z., Miller, W., Lipman, D.J., 1997. Gapped BLAST and PSI-BLAST: a new generation of protein database search programs. Nucleic Acids Res. 25, 3389–3402.

Arcangeli, C., Cantale, C., Galeffi, P., Rosato, V., 2008. Structure and dynamics of the anti-AMCV scFv(F8): effects of selected mutations on the antigen combining site. J. Struct. Biol. 164, 119–133.

Bohm, H.J., 1998. Prediction of binding constants of protein-ligands: a fast method for the prioritization of hits obtained from de novo design or 3D database search programs. J. Comput. Aided Mol. Des. 12, 309–323.

Brooks, B.R., Bruccoleri, R.E., Olafson, B.D., States, D.J., Swaminathan, S., Karplus, M., 1983. CHARMM: A program for macromolecular energy, minimization, and dynamics calculations. J. Comput. Chem. 4, 187–217.

Bukrinskaya, A.G., 2004. HIV-1 assembly and maturation. Arch. Virol. 149, 1067–1082.

Case, D.A., Cheatham III, T.E., Darden, T., Gohlke, H., Luo, R., Merz, J.K.M., Onufriev, A., Simmerling, C., Wang, B., Woods, R.J., 2005. The Amber biomolecular simulation programs. J. Comput. Chem. 26, 1668–1688.

Case, D.A., Darden, T.A., Cheatham III, T.E., Simmerling, C.L., Wang, J., Duke, R.E., Luo, R., Merz, K.M., Pearlman, D.A., Crowley, M., 2006. AMBER 9. University of California, San Francisco, CA.

Chong, L.T., Duan, Y., Wang, L., Massova, I., Kollman, P.A., 1999. Molecular dynamics and free-energy calculations applied to affinity maturation in antibody 48G7. Proc. Natl. Acad. Sci. U.S.A. 96, 14330–14335.

Darden, T., York, D., Pedersen, L., 1993. Particle mesh Ewald: an N log(*N*) method for Ewald sums in large systems. J. Chem. Phys. 98, 10089–10092.

Depetris, M., Casalis, P., Kratje, R., Etcheverrigaray, M., Oggero, M., 2008. A scFv antibody fragment as a therapeutic candidate to neutralize a broad diversity of human IFN-alpha subtypes. J. Immunol. Methods 334, 104–113.

Essmann, U., Perera, L., Berkowitz, M.L., Darden, T., Lee, H., Pedersen, L., 1995. A smooth particle mesh ewald potential. J. Chem. Phys. 103, 8577–8592.

Ewing, T.J.A., Makino, S., Skillman, A.G., Kuntz, I.D., 2001. DOCK 4.0: Search strategies for automated molecular docking of flexible molecule database. J. Comput. Aided Mol. Des. 15, 411–428.

Ganser-Pornillos, B.K., Yeager, M., Sundquist, W.I., 2008. The structural biology of HIV assembly. Curr. Opin. Struct. Biol. 18, 203–217.

Gao, J., 1996. Hybrid quantum mechanical/molecular mechanical simulations: an alternative avenue to solvent effects in organic chemistry. Acc. Chem. Res. 29, 298–305.

Gohlke, H., Kiel, C., Case, D., 2003. Insights into protein-protein binding by binding free energy calculation and free energy decomposition for the Ras-Raf and Ras-RalGDS complexes. J. Mol. Biol. 330, 891–913.

Hou, T., Guo, S., Xu, X., 2002. Predictions of binding of a diverse set of ligands to gelatinase-A by a combination of molecular dynamics and continuum solvent models. J. Phys. Chem. B 106, 5527–5535.

Hou, T., Zhang, W., Case, D.A., Wang, W., 2008. Characterization of domain–peptide interaction interface: a case study on the amphiphysin-1 SH3 domain. J. Mol. Biol. 376, 1201–1214.

Inui, H., Takehara, A., Doi, F., Nishi, K., Takai, M., Miyake, S., Ohkawa, H., 2009. A scFv antibody-based immunoaffinity chromatography column for clean-up of bisphenol A-contaminated water samples. J. Agric. Food. Chem. 57, 353–358.

Jones, G., Willett, P., Glen, R.C., Leach, A.R., Taylor, R., 1997. Development and validation of a genetic algorithm for flexible docking. J. Mol. Biol. 267, 727–748.

Jorgensen, W.L., 1996. BOSS 3. 6. Yale University, New Haven, CT.

Kabat, E.A., Wu, T.T., Bilofsky, H., Reid-Milner, M., Perry, H., 1983. Sequences of Proteins of Immunological Interest. NIH Publications No. 369–847, Bethesda, MD.

Kollman, P.A., 1993. Free energy calculations: applications to chemical and biochemical phenomena. Chem. Rev. 93, 2395–2417.

Kollman, P.A., Massova, I., Reyes, C., Kuhn, B., Huo, S., Chong, L., Lee, M., Lee, T., Duan, Y., Wang, W., Donini, O., Cieplak, P., Srinivasan, J., Case, D.A., Cheatham 3rd., T.E., 2000. Calculating structures and free energies of complex molecules: combining molecular mechanics and continuum models. Acc. Chem. Res. 33, 889–897.

Krammer, A., Kirchhoff, P.D., Jiang, X., Venkatachalam, C.M., Waldman, M., 2005. LigScore: a novel scoring function for predicting binding affinities. J. Mol. Graph. Model. 23, 395–407.

Leach, A.R., 1996. Molecular Modelling: Principles and Applications. Addison Wesley Longman Ltd., Singapore.

Levy, R.M., Gallicchio, E., 1998. Computer simulations with explicit solvent: recent progress in the thermodynamic decomposition of free energies and in modeling electrostatic effects. Annu. Rev. Phys. Chem. 49, 531–567.

Morris, G.M., Goodsell, D.S., Halliday, R., Huey, R., Hart, W.E., Belew, R.K., Olson, A.J., 1998. Automated docking using a Lamarckian genetic algorithm and an empirical binding free energy function. J. Comput. Chem. 19, 1639–1662.

Muegge, I., Martin, Y.C., 1999. A general and fast scoring function for protein-ligand interactions: a simplified potential approach. J. Med. Chem. 42, 791–804.

Park, S.G., Jung, Y.J., Lee, Y.Y., Yang, C.M., Kim, I.J., Chung, J.H., Kim, I.S., Lee, Y.J., Park, S.J., Lee, J.N., Seo, S.K., Park, Y.H., Choi, I.H., 2006. Improvement of neutralizing activity of human scFv antibodies against hepatitis B virus binding using CDR3 V(H) mutant library. Viral. Immunol. 19, 115–123.

Pavoni, E., Flego, M., Dupuis, M.L., Barca, S., Petronzelli, F., Anastasi, A.M., D'Alessio, V., Pelliccia, A., Vaccaro, P., Monteriu, G., Ascione, A., De Santis, R., Felici, F., Cianfriglia, M., Minenkova, O., 2006. Selection, affinity maturation, and characterization of a human scFv antibody against CEA protein. BMC Cancer 6, 41.

Pearlman, D.A., Case, D.A., Caldwell, J.W., Ross, W.R., Cheatham, T.E., Ferguson, D.M., Seibel, G.L., Singh, U.C., Weiner, P., Kollman, P.A., 1995. AMBER4.1 (UCSF). University of California, San Francisco, CA.

Quintero-Hernandez, V., Juarez-Gonzalez, V.R., Ortiz-Leon, M., Sanchez, R., Possani, L.D., Becerril, B., 2007. The change of the scFv into the Fab format improves the

stability and in vivo toxin neutralization capacity of recombinant antibodies. Mol. Immunol. 44, 1307–1315.
Rarey, M., Kramer, B., Lengauer, T., Klebe, G., 1996. A fast flexible docking method using an incremental construction algorithm. J. Mol. Biol. 261, 470–489.
Shen, Z., Yan, H., Zhang, Y., Mernaugh, R.L., Zeng, X., 2008. Engineering peptide linkers for scFv immunosensors. Anal. Chem. 80, 1910–1917.
Smith, P.E., Pettitt, B.M., 1994. Modeling solvent in biomolecular systems. J. Phys. Chem. 98, 9700–9711.
Stocks, M., 2005. Intrabodies as drug discovery tools and therapeutics. Curr. Opin. Chem. Biol. 9, 359–365.
Tewari, D., Goldstein, S.L., Notkins, A.L., Zhou, P., 1998. cDNA encoding a single-chain antibody to HIV p17 with cytoplasmic or nuclear retention signals inhibits HIV-1 replication. J. Immunol. 161, 2642–2647.
Tomasi, J., Persico, M., 1994. Molecular interactions in solution: an overview of methods based on continuous distributions of the solvent. Chem. Rev. 94, 2027–2094.
Tsui, V., Case, D.A., 2000. Molecular dynamics simulations of nucleic acids with a generalized Born solvation model. J. Am. Chem. Soc. 122, 2489–2498.
van Gunsteren, W.F., Luque, F.J., Timms, D., Torda, A.E., 1994. Molecular mechanics in biology: from structure to function, taking account of solvation. Annu. Rev. Biophys. Biomol. Struct. 23, 847.
Wang, G.P., Qi, Z.H., Chen, F.P., 2008. Treatment of acute myeloid leukemia by directly targeting both leukemia stem cells and oncogenic molecule with specific scFv-immunolipoplexes as a deliverer. Med. Hypotheses 70, 122–127.
Weber, W., Hünenberger, P., McCammon, J., 2000. Molecular dynamics simulations of a polyalanine octapeptide under Ewald boundary conditions: influence of artificial periodicity on peptide conformation. J. Phys. Chem. B 104, 3668–4575.